

**SANDIA NATIONAL LABORATORIES
WASTE ISOLATION PILOT PLANT**

**ANALYSIS PACKAGE FOR SALADO FLOW IN THE 2019
COMPLIANCE RECERTIFICATION APPLICATION
PERFORMANCE ASSESSMENT (CRA-2019 PA)**

REVISION 0

Author: Brad Day  9/3/19
Print Signature Date

Technical
Reviewer: James Bethune Sarah Brunell for 9/4/2019
Print Signature Date

QA
Reviewer: Shelly Nielsen Shelly R. Nielsen 9-4-19
Print Signature Date

Management
Reviewer: Chris Camphouse Chris Camphouse for 9/4/2019
Print Signature Date

**ERMS #571368
SEPTEMBER 2019
WIPP:4.2.1:PA:QA-L:571155**

Information Only

This page intentionally left blank.

TABLE OF CONTENTS

EXECUTIVE SUMMARY	IX
1.0 INTRODUCTION.....	11
1.1 Changes Since the CRA-2014	12
1.1.1 Abandonment of Panel Closures in the South and No Waste in Panel 9	13
1.1.2 Additional Shaft and Associated Drifts.....	14
1.1.3 Addition of Brine Radiolysis to Gas Generation.....	15
1.1.4 Refinement to the Corrosion Rates of Steel	16
1.1.5 Refinement to Colloid Enhancement Parameters.....	17
1.1.6 Refinement to the Hydromagnesite to Magnesite Conversion Rate	17
1.1.7 Removal of Iron Sulfidation Reactions	18
1.1.8 Correction to Length of Northernmost Panel Closure Representation.....	18
1.1.9 Updates to WIPP Waste Inventory Parameters	19
1.1.10 Updates to Radionuclide Solubilities	20
1.1.11 Correction to the Relative Permeability and Capillary Pressure Model Applied to an Open Borehole.....	20
1.1.12 Introduction of New Materials Names	21
1.1.13 Computational code updates to BRAGFLO and PREBRAG	25
2.0 CONCEPTUAL APPROACH FOR THE CRA-2019	27
2.1 Repository Representation in BRAGFLO	27
2.2 Initial Conditions	31
2.3 Boundary Conditions	32
3.0 SALADO FLOW MODELING METHODOLOGY.....	33
3.1 Modeling Scenarios	34
3.2 Material Maps	34
3.2.1 Scenario S1-BF (Undisturbed Conditions).....	35
3.2.2 Scenario S2-BF (E1 intrusion at 350 years).....	35
3.2.3 Scenario S3-BF (E1 intrusion at 1000 years).....	36
3.2.4 Scenario S4-BF (E2 intrusion at 350 years).....	36
3.2.5 Scenario S5-BF (E2 intrusion at 1000 years).....	37
3.2.6 Scenario S6-BF (E2 intrusion at 1000 years, E1 intrusion at 2000 years).....	37
3.3 Code Execution and Run Control	51

4.0 RESULTS	53
4.1 Pressure	53
4.2 Brine Saturation	67
4.3 Gas Saturation.....	81
4.4 Gas Generation.....	81
4.5 Brine and Gas Flows.....	89
5.0 SUMMARY	101
6.0 REFERENCES.....	103

LIST OF TABLES

Table 1 – Southernmost Panel Closure Properties for CRA19.....	14
Table 2 – BRAGFLO Grid Cell X- and Z-Dimensions for Shaft Representation (CRA14 and CRA19).....	15
Table 3 – BRAGFLO Grid Dimensions for Experimental Area (CRA14 and CRA19)	15
Table 4 – Radionuclide Radiolysis and Decay Parameters for CRA19.....	16
Table 5 – Iron Corrosion Parameters for CRA19	17
Table 6 – Hydromagnesite to Magnesite Conversion Rate Parameter (CRA19)	18
Table 7 – Iron Sulfidation Stoichiometric Parameters (CRA19).....	18
Table 8 – BRAGFLO Grid Cell X-Dimensions for Northernmost Panel Closure Representation (CRA14 and CRA19).....	19
Table 9 – Iron and CPR Inventories (CRA14 and CRA19).....	20
Table 10 – Nitrate and Sulfate Inventories (CRA14 and CRA19)	20
Table 11 – Open Borehole Relative Permeability and Capillary Pressure Model Parameter (CRA19).....	21
Table 12 – DRZ_OE_0 and DRZ_OE_1 Parameter Values (CRA19).....	23
Table 13 – DRZ_PC_0 and DRZ_PC_1 Parameter Values (CRA19).....	24
Table 14 – CAVITY_5 Parameter Values (CRA19)	24
Table 15 – BRAGFLO Modeling Scenarios.....	34
Table 16 – Time Period Associations Between Material Map Figures and BRAGFLO Scenarios	39
Table 17 – Pressure Statistics on Overall Means for CRA14 and CRA19.....	65
Table 18 – Pressure Statistics on Individual Vectors for CRA14 and CRA19.....	66
Table 19 – Brine Saturation Statistics on Overall Means for CRA14 and CRA19	79
Table 20 – Brine Saturation Statistics on Individual Vectors for CRA14 and CRA19	80
Table 21 – Gas Generation Statistics on Overall Means for CRA14 and CRA19	87
Table 22 – Gas Generation Statistics on Individual Vectors for CRA14 and CRA19	88
Table 23 – Brine Flow Statistics on Overall Means for CRA14 and CRA19	99
Table 24 – Brine Flow Statistics on Individual Vectors for CRA14 and CRA19	100

LIST OF FIGURES

Figure 1 – Generic CRA-2014 PA BRAGFLO Grid with Modeled Area Descriptions	29
Figure 2 – Generic CRA-2019 PA BRAGFLO Grid with Modeled Area Descriptions	30
Figure 3 – CRA-2019 PA BRAGFLO Grid and Material Map; Years -5 to 0 [Scenarios S1-BF through S6-BF]	40
Figure 4 – CRA-2019 PA BRAGFLO Grid and Material Map; Years 0 to 100 [Scenarios S1-BF through S6-BF]	41
Figure 5 – CRA-2019 PA BRAGFLO Grid and Material Map; Years 100 to 200 [Scenarios S1-BF through S6-BF]	42
Figure 6 – CRA-2019 PA BRAGFLO Grid and Material Map; Years 200 to 10000 [Scenario S1-BF], Years 200 to Time of E1 or E2 Intrusion [Scenarios S2-BF through S6-BF]	43
Figure 7 – CRA-2019 PA BRAGFLO Grid and Material Map; Time of E2 Intrusion to Time of E2 Intrusion Plus 200 Years [Scenarios S4-BF through S6-BF]	44
Figure 8 – CRA-2019 PA BRAGFLO Grid and Material Map; Time of E2 Intrusion Plus 200 Years to 10000 Years [Scenarios S4-BF and S5-BF], Time of E2 Intrusion Plus 200 Years to Time of E1 Intrusion [Scenario S6-BF]	45
Figure 9 – CRA-2019 PA BRAGFLO Grid and Material Map; Time of E1 Intrusion to Time of E1 Intrusion Plus 200 Years [Scenarios S2-BF and S3-BF]	46
Figure 10 – CRA-2019 PA BRAGFLO Grid and Material Map; Time of E1 Intrusion to Time of E1 Intrusion Plus 200 Years [Scenario S6-BF]	47
Figure 11 – CRA-2019 PA BRAGFLO Grid and Material Map; Time of E1 Intrusion Plus 200 Years to Time of E1 Intrusion Plus 1200 Years [Scenarios S2-BF, S3-BF, and S6-BF]	48
Figure 12 – CRA-2019 PA BRAGFLO Grid and Material Map; Time of E1 Intrusion Plus 1200 Years to 10000 Years [Scenarios S2-BF, S3-BF, and S6-BF]	49
Figure 13 – Salado Flow Run Control Diagram	52
Figure 14 – Pressure Means for the Experimental Area, Scenario S1-BF	55
Figure 15 – Pressure Means for the Experimental Area, Scenario S2-BF	55
Figure 16 – Pressure Means for the Experimental Area, Scenario S4-BF	56
Figure 17 – Pressure Means for the Experimental Area, Scenario S6-BF	56
Figure 18 – Pressure Means for the Operations Area, Scenario S1-BF	57
Figure 19 – Pressure Means for the Operations Area, Scenario S2-BF	57
Figure 20 – Pressure Means for the Operations Area, Scenario S4-BF	58
Figure 21 – Pressure Means for the Operations Area, Scenario S6-BF	58
Figure 22 – Pressure Means for the North Rest-of-Repository, Scenario S1-BF	59
Figure 23 – Pressure Means for the North Rest-of-Repository, Scenario S2-BF	59

Figure 24 – Pressure Means for the North Rest-of-Repository, Scenario S4-BF	60
Figure 25 – Pressure Means for the North Rest-of-Repository, Scenario S6-BF	60
Figure 26 – Pressure Means for the South Rest-of-Repository, Scenario S1-BF	61
Figure 27 – Pressure Means for the South Rest-of-Repository, Scenario S2-BF	61
Figure 28 – Pressure Means for the South Rest-of-Repository, Scenario S4-BF	62
Figure 29 – Pressure Means for the South Rest-of-Repository, Scenario S6-BF	62
Figure 30 – Pressure Means for the Waste Panel, Scenario S1-BF	63
Figure 31 – Pressure Means for the Waste Panel, Scenario S2-BF	63
Figure 32 – Pressure Means for the Waste Panel, Scenario S4-BF	64
Figure 33 – Pressure Means for the Waste Panel, Scenario S6-BF	64
Figure 34 – Brine Saturation Means for the Experimental Area, Scenario S1-BF	68
Figure 35 – Brine Saturation Means for the Experimental Area, Scenario S2-BF	68
Figure 36 – Brine Saturation Means for the Experimental Area, Scenario S4-BF	69
Figure 37 – Brine Saturation Means for the Experimental Area, Scenario S6-BF	69
Figure 38 – Brine Saturation Means for the Operations Area, Scenario S1-BF	70
Figure 39 – Brine Saturation Means for the Operations Area, Scenario S2-BF	70
Figure 40 – Brine Saturation Means for the Operations Area, Scenario S4-BF	71
Figure 41 – Brine Saturation Means for the Operations Area, Scenario S6-BF	71
Figure 42 – Brine Saturation Means for the North Rest-of-Repository, Scenario S1-BF	72
Figure 43 – Brine Saturation Means for the North Rest-of-Repository, Scenario S2-BF	72
Figure 44 – Brine Saturation Means for the North Rest-of-Repository, Scenario S4-BF	73
Figure 45 – Brine Saturation Means for the North Rest-of-Repository, Scenario S6-BF	73
Figure 46 – Brine Saturation Means for the South Rest-of-Repository, Scenario S1-BF	74
Figure 47 – Brine Saturation Means for the South Rest-of-Repository, Scenario S2-BF	74
Figure 48 – Brine Saturation Means for the South Rest-of-Repository, Scenario S4-BF	75
Figure 49 – Brine Saturation Means for the South Rest-of-Repository, Scenario S6-BF	75
Figure 50 – Brine Saturation Means for the Waste Panel, Scenario S1-BF	76
Figure 51 – Brine Saturation Means for the Waste Panel, Scenario S2-BF	76
Figure 52 – Brine Saturation Means for the Waste Panel, Scenario S4-BF	77
Figure 53 – Brine Saturation Means for the Waste Panel, Scenario S6-BF	77
Figure 54 – Gas Generation from Corrosion and Biodegradation, Scenario S1-BF	82
Figure 55 – Gas Generation from Corrosion and Biodegradation, Scenario S2-BF	82

Figure 56 – Gas Generation from Corrosion and Biodegradation, Scenario S4-BF83

Figure 57 – Gas Generation from Corrosion and Biodegradation, Scenario S6-BF83

Figure 58 – CRA19 Moles of Gas Generated by All Sources, Scenario S1-BF84

Figure 59 – CRA19 Moles of Gas Generated by All Sources, Scenario S2-BF84

Figure 60 – CRA19 Moles of Gas Generated by All Sources, Scenario S4-BF85

Figure 61 – CRA19 Moles of Gas Generated by All Sources, Scenario S6-BF85

Figure 62 – Brine Flow Means into Repository, Scenario S1-BF91

Figure 63 – Brine Flow Means into Repository, Scenario S2-BF91

Figure 64 – Brine Flow Means into Repository, Scenario S4-BF92

Figure 65 – Brine Flow Means into Repository, Scenario S6-BF92

Figure 66 – Brine Flow Means into Experimental Area, Scenario S1-BF93

Figure 67 – Brine Flow Means up the Shaft, Scenario S1-BF93

Figure 68 – Brine Flow Means up the Shaft, Scenario S2-BF94

Figure 69 – Brine Flow Means up the Shaft, Scenario S4-BF94

Figure 70 – Brine Flow Means up the Shaft, Scenario S6-BF95

Figure 71 – Brine Flow Means up the Borehole, Scenario S2-BF95

Figure 72 – Brine Flow Means up the Borehole, Scenario S4-BF96

Figure 73 – Brine Flow Means up the Borehole, Scenario S6-BF96

Figure 74 – CRA19 Brine Flow up the Borehole; Comparison of Brine Flow, Waste Panel Brine Saturation, and Pressure Overall Means to Top 15 Borehole Brine Flow Vector Means, Scenario S4-BF97

Figure 75 – Gas Flow Means out of South Rest-of-Repository (South to North) Across the Panel Closure Plane, Scenario S2-BF98

Figure 76 – Gas Flow Means out of North Rest-of-Repository (South to North) Across the Panel Closure Plane, Scenario S2-BF98

Executive Summary

The Land Withdrawal Act requires that the U.S. Department of Energy (DOE) apply for recertification of the Waste Isolation Pilot Plant (WIPP) every five years following the initial 1999 waste shipment. The 2019 Compliance Recertification Application (CRA-2019) is the fourth WIPP recertification application submitted for approval by the U.S. Environmental Protection Agency. A performance assessment (PA) has been executed by Sandia National Laboratories in support of the DOE submittal of the CRA-2019. Results found in the CRA-2019 PA are compared to those obtained in the 2014 Compliance Recertification Application (CRA-2014) to assess repository performance in terms of the current regulatory baseline. This package documents the Salado flow analysis component of the CRA-2019 PA. Changes incorporated into the CRA-2019 PA include repository planned changes, parameter updates, and refinements to PA implementation. Changes included in the CRA-2019 PA that were observed to most substantially affect Salado flow results as compared to the CRA-2014 PA are:

- The lack of ROMPCS emplacement between Panels 3, 4, 5, 6, and 9, modeled as the southernmost panel closure area, which allows greater communication between the waste panel and the south rest-of-repository.
- Increase in the inundated steel corrosion rates and the addition of brine radiolysis which results in an increase in hydrogen gas generation.
- Addition of 5th shaft and associated access drift volume in the experimental area which increases the cross-sectional area of the shaft and increases void space in the experimental area.
- Updates to WIPP waste inventory parameters, including increased iron and cellulose mass, which contributes to increased associated corrosion and biodegradation gas generation.

Overall, the primary impacts of changes for the CRA-2019 PA in comparison to the CRA-2014 PA baseline are substantially increased waste area brine pressures and saturations for intrusion scenarios that intersect a hypothetical brine reservoir that underlies the repository. These scenarios are greatly influenced by increased total gas generation due to the availability of brine within the waste panel and south rest-of-repository that flows from the Castile brine reservoir, up the intrusion borehole, to the waste panel, and across the abandoned panel closure area to the south rest-of-repository. Undisturbed and non-Castile intruded scenarios are generally less impacted by changes, but the CRA-2019 PA results under these scenarios generally experience increased brine pressures and reduced brine saturations within the waste areas due to the increased gas generation and brine consumption induced by the associated process model and parameter modifications in comparison to the CRA-2014 PA.

This page intentionally left blank.

1.0 INTRODUCTION

The Waste Isolation Pilot Plant (WIPP), located in southeastern New Mexico, has been developed by the U.S. Department of Energy (DOE) for the geologic (deep underground) disposal of transuranic (TRU) waste. Containment of TRU waste at the WIPP is regulated by the U.S. Environmental Protection Agency (EPA) according to the regulations set forth in Title 40 of the Code of Federal Regulations (CFR), Part 191. The DOE demonstrates compliance with the containment requirements according to the Certification Criteria in Title 40 CFR Part 194 by means of performance assessment (PA) calculations performed by Sandia National Laboratories (SNL). WIPP PA calculations estimate the probability and consequence of potential radionuclide releases from the repository to the accessible environment for a regulatory period of 10,000 years after facility closure. The models used in PA are maintained and updated with new information as part of an ongoing process. Improved information regarding important WIPP features, events, and processes typically results in refinements and modifications to PA models and the parameters used in them. Planned changes to the repository and/or the components therein also result in updates to WIPP PA models. WIPP PA models are used to support the repository recertification process that occurs at five-year intervals following the receipt of the first waste shipment at the site in 1999.

PA calculations were included in the 1996 Compliance Certification Application (CCA) (U.S. DOE 1996), and in a subsequent Performance Assessment Verification Test (PAVT) (MacKinnon and Freeze 1997a, 1997b and 1997c). Based in part on the CCA and PAVT PA calculations, the EPA certified that the WIPP met the regulatory containment criteria. The facility was approved for disposal of transuranic waste in May 1998 (U.S. EPA 1998). PA calculations were an integral part of the 2004 Compliance Recertification Application (CRA-2004) (U.S. DOE 2004). During their review of the CRA-2004, the EPA requested an additional PA calculation, referred to as the CRA-2004 Performance Assessment Baseline Calculation (PABC) (Leigh et al. 2005), be conducted with modified assumptions and parameter values (Cotsworth 2005). Following review of the CRA-2004 and the CRA-2004 PABC, the EPA recertified the WIPP in March 2006 (U.S. EPA 2006).

PA calculations were completed for the second WIPP recertification and documented in the 2009 Compliance Recertification Application (CRA-2009). The CRA-2009 PA resulted from continued review of the CRA-2004 PABC, including several technical changes and corrections, as well as updates to parameters and improvements to the PA computer codes (Clayton et al. 2008). To incorporate additional information which was received after the CRA-2009 PA was completed, but before the submittal of the CRA-2009, the EPA requested an additional PA calculation, referred to as the 2009 Compliance Recertification Application Performance Assessment Baseline Calculation (PABC-2009) (Clayton et al. 2010), be undertaken which included updated information (Cotsworth 2009). Following the completion and submission of the PABC-2009, the WIPP was recertified in 2010 (U.S. EPA 2010).

PA calculations were completed for the third WIPP recertification and documented in the 2014 Compliance Recertification Application (CRA-2014). Following the completion and submission of the CRA-2014, the WIPP was recertified in 2017 (U.S. EPA 2017a).

The Land Withdrawal Act (U.S. Congress 1992) requires that the DOE apply for WIPP recertification every five years following the initial 1999 waste shipment. The 2019 Compliance Recertification Application (CRA-2019) is the fourth WIPP recertification application submitted by the DOE for EPA approval. The PA executed by SNL in support of the CRA-2019 is detailed in AP-181 (Zeitler 2019a). The CRA-2019 PA includes repository planned changes, parameter updates, and refinements to PA implementation. Results found in the CRA-2019 PA are compared to those obtained in the CRA-2014 PA to assess repository performance in terms of the current regulatory baseline. This analysis package documents the Salado flow component of the CRA-2019 PA analysis.

1.1 Changes Since the CRA-2014

Several changes are incorporated in the CRA-2019 PA relative to the CRA-2014 PA that potentially impact Salado flow results. The changes are:

- Inclusion of an approach to accommodate the operational decisions to not emplace panel closures in Panels 3, 4, 5, and 6 and to not emplace waste in Panel 9.
- Inclusion of an approach to accommodate an additional shaft connecting the repository to the surface, as well as an additional mined region in the repository north end to accommodate drifts that lead to the new shaft.
- Refinement of the gas generation process model to include brine radiolysis.
- Refinement to the corrosion rates of steel under humid and inundated conditions.
- Refinement to colloid enhancement parameters associated with actinide mobilization.
- Refinement to the hydromagnesite to magnesite conversion rate.
- Removal of two chemical reactions associated with iron sulfidation.
- Correction to the length of the northernmost panel closure representation in the BRAGFLO grid.
- Updates to WIPP waste inventory parameters.
- Updates to radionuclide solubilities and their associated uncertainty.
- An update to the relative permeability and capillary pressure model applied to an open borehole.
- Introduction of new material names to define equivalent material properties in disturbed rock zone areas.
- Computational code updates to BRAGFLO and PREBRAG.

Changes listed above are discussed in more detail in the sections that follow with all Salado flow parameter values implemented for the CRA-2019 PA analysis (CRA19) detailed in Kim and Feng (2019).

1.1.1 Abandonment of Panel Closures in the South and No Waste in Panel 9

As outlined in the CRA-2019 analysis plan (Zeitler 2019a), operational considerations have prompted the need to abandon plans for placement of run-of-mine salt panel closures (ROMPCS) in Panels 3, 4, 5, and 6 and to emplace waste in Panel 9. An approach to modeling the impacts of the operational changes was developed through the Abandonment of Panel Closures in South End of Repository (APCS) analysis described in Zeitler et al. (2017). The APCS approach was formally presented to the EPA and agreed upon as the methodology for implementation in the CRA-2019 PA (Peake 2018). The aspects of the APCS approach that are impactful to the Salado flow results are the replacement of the ROMPCS in the southernmost panel closure area with a new material, PCS_NO, and treatment of the DRZ regions surrounding the abandoned panel closure area. PCS_NO adopts material properties that are utilized for other excavated areas within the repository such as the operations (OPS_AREA) and experimental (EXP_AREA) that do not contain waste as shown in Table 1. For consistency, the DRZ above and below the abandoned southernmost panel closure are the same as above and below the waste areas and operations and experimental areas (i.e., the DRZ_PCS, S_ANH_AB and MB_139 materials do not replace the DRZ_1 material above and below the abandoned southernmost panel closure area). Finally, emplacement of waste in Panel 9 was unchanged with the APCS approach as it was demonstrated that emplacement of waste in Panel 9 is an appropriate surrogate to represent placement of Panel 9 waste in an alternate panel location farther to the north.

Table 1 – Southernmost Panel Closure Properties for CRA19

Material	Property	Description	Units	Value
PCS_NO	CAP_MOD	Model number, capillary pressure model	(-)	1
PCS_NO	COMP_RCK	Bulk Compressibility	Pa ⁻¹	0
PCS_NO	KPT	Flag for Permeability Determined Threshold	(-)	0
PCS_NO	PCT_A	Threshold Pressure Linear Parameter	Pa	0
PCS_NO	PCT_EXP	Threshold pressure exponential parameter	(-)	0
PCS_NO	PC_MAX	Maximum allowable capillary pressure	Pa	1.0E8
PCS_NO	PORE_DIS	Brooks-Corey pore distribution parameter	(-)	0.7
PCS_NO	POROSITY	Effective porosity	(-)	0.18
PCS_NO	PO_MIN	Minimum brine pressure for capillary model KPC=3	Pa	101325
PCS_NO	PRESSURE	Brine far-field pore pressure	Pa	101325
PCS_NO	PRMX_LOG	Log of intrinsic permeability, X-direction	log(m ²)	-11
PCS_NO	PRMY_LOG	Log of intrinsic permeability, Y-direction	log(m ²)	-11
PCS_NO	PRMZ_LOG	Log of intrinsic permeability, Z-direction	log(m ²)	-11
PCS_NO	RELP_MOD	Model number, relative permeability model	(-)	11
PCS_NO	SAT_IBRN	Initial Brine Saturation	(-)	0
PCS_NO	SAT_RBRN	Residual Brine Saturation	(-)	0
PCS_NO	SAT_RGAS	Residual Gas Saturation	(-)	0

1.1.2 Additional Shaft and Associated Drifts

In the wake of the 2014 radiological release event at the WIPP site, a modified ventilation system is planned that will provide sufficient airflow necessary for the resumption of increased-rate disposal operations in the future. The primary components of the modified ventilation system are an additional shaft in the north end of the repository and associated drifts to connect the additional shaft to the experimental area of the repository.

There are four shafts currently located in the repository north end, namely a salt handling shaft, an exhaust shaft, a waste shaft, and an air intake shaft. In WIPP PA, these shafts are combined into a single shaft that captures the combined impacts of all of them. The additional, planned shaft will be combined with the four existing shafts in the CRA-2019 PA. Additionally, mined volume in the repository north end is modified in the repository representation to include the additional drifts created to access the new shaft. A similar approach was employed for the SHFT14 analysis that accompanied a planned change notice (PCN) submitted to the EPA in 2017 (Camphouse 2014). That analysis showed minimum impact to the long-term repository

performance from representing the additional shaft and drifts. The shaft and drift dimensions assumed for the SHFT14 analysis were based on a preliminary design, while the dimensions assumed for the CRA-2019 PA are based on a more recent design. Updated model dimensions for the shaft and experimental area representations used in the BRAGFLO Salado grid were derived by Zeitler (2019b) and are summarized below in Table 2 and Table 3.

Table 2 – BRAGFLO Grid Cell X- and Z-Dimensions for Shaft Representation (CRA14 and CRA19)

Analysis	X-Dim (m)	Z-Dim (m)	Area (m ²)	Length (m)	Volume (m ³)
CRA14	10	9.5	95	658.56	62563
CRA19	12.6933	12.0586	153.06	658.56	100802

Table 3 – BRAGFLO Grid Dimensions for Experimental Area (CRA14 and CRA19)

Analysis	One-Cell Dimension			Full Dimension			Volume (m ³)
	X-Dim (m)	Y-Dim (m)	Z-Dim (m)	X-Dim (m)	Y-Dim (m)	Z-Dim (m)	
CRA14	361.65	1.32	51.68 ^a	723.3	3.96	51.68 ^a	148011
CRA19	361.65	1.32	67.05	723.3	3.96	67.05	192053

^a – Three EXP cells in the CRA-2014 PA had a z-dimension of 51.68 m and three had z-dimension of 51.67 m.

1.1.3 Addition of Brine Radiolysis to Gas Generation

A recent scoping analysis has identified a need to include radiolytic gas generation in WIPP PA as it is no longer considered an insignificant source in comparison to other gas generation mechanism (Day 2019). Therefore, brine radiolysis is included in the CRA-2019 PA as part of the gas generation process model. The implementation and associated assumptions are described in detail in Day (2019) and parameterization implications are summarized below.

The total radiolytic H₂ generation rate is due to contributions from one or more decaying radionuclides in the repository waste areas. The hydrogen generation rate due to radiolysis of radionuclides in solution and due to a fractional contribution from the wetted solid form of the radionuclides is dependent upon the following variables:

- GDEPFAC* = energy deposition probability for wetted solid radionuclides [-]
- DECAYNRG* = disintegration energy of radionuclide [MeV]
- GH2AVG* = average “G” value for H₂ [molecule/eV]
- SRADO2* = stoichiometric coefficient for O₂ from radiolysis [mol O₂/mol H₂]

An inventory assessment as part of the CRA-2019 PA (Kicker 2019) determined which radionuclides are considered to participate in radiolysis based on the relative amount of decay heats compared to the overall inventory heat production. For those five selected radionuclides, new DECAYNRG parameters (Table 4) are implemented in CRA-2019 PA to support the radiolysis and decay calculations. The source for the GLOBAL:GH2AVG parameter is an experimentally-derived value from Reed et al. (1993). Justifications for the GLOBAL:GDEPFAC and GLOBAL:SRADO2 parameter recommendations are provided by Day (2019).

Table 4 – Radionuclide Radiolysis and Decay Parameters for CRA19

Material	Property	Description	Units	Value
AM241	DECAYNRG	Radionuclide disintegration energy	MeV	5.6379
PU238				5.5930
PU239				5.2442
PU240				5.2559
PU242				4.9855
GLOBAL	GH2AVG	Average G-value for H ₂	molecules/eV	0.014
GLOBAL	GDEPFAC	Energy deposition probability for wetted solid radionuclides	(-)	Uniform Distribution from [0 - 0.5]
GLOBAL	SRADO2	Stoichiometric coefficient for O ₂ from radiolysis	mol O ₂ /mol H ₂	0

1.1.4 Refinement to the Corrosion Rates of Steel

The interaction of steel in the WIPP with repository brines will result in the formation of H₂ gas due to anoxic corrosion of the metal. Two steel corrosion rates are updated for the CRA-2019 PA, STEEL:CORRMCO2 (hereafter CORRMCO2) and STEEL:HUMCORR (hereafter HUMCORR).

For the CRA-2014 PA, experimental results from Roselle (2013) were used to determine an updated parameter distribution for CORRMCO2, which represents the anoxic steel corrosion rate for brine-inundated steel in the absence of microbially produced CO₂. Subsequent to the submittal of the CRA-2014, the EPA requested that the DOE reconsider the subset of the Roselle data to be included in the CORRMCO2 distribution. As a result, a new, cumulative distribution for CORRMCO2 was developed (Zeitler and Hansen 2015a). Later, in their technical support document (TSD) on chemistry-related issues, the EPA recommended an adjustment of the Zeitler and Hansen (2015a) distribution for the CRA-2019 PA via an increase by a factor of two (U.S. EPA 2017b) and the DOE has agreed to the adjustment by a factor of two. The resulting cumulative distribution for CORRMCO2 is described in detail in Zeitler (2018a) and is used in the CRA-2019 PA (Table 5).

For the CRA-2014 PA, experimental results from Roselle (2013) were used to determine that HUMCORR, which represents the humid corrosion rate of steel should maintain a value of zero. Subsequent to the submittal of the CRA-2014, the EPA requested that the DOE reconsider the subset of the Roselle data to be used for development of the STEEL:HUMCORR parameter. As a result, a cumulative distribution for HUMCORR was developed (Zeitler and Hansen 2015b) and later revised based on an updated estimate of the CO₂ level expected in the repository, which itself is recalculated each time the thermodynamic database is revised (Zeitler and Hansen 2015c). In order to avoid recalculation of the HUMCORR distribution each time the thermodynamic database is revised in the future, a CO₂ level that is expected to bound future predicted CO₂ levels was selected and used to again revise the HUMCORR distribution (Zeitler 2018b). The cumulative distribution described in Zeitler (2018b) is used in the CRA-2019 PA (Table 5).

Table 5 – Iron Corrosion Parameters for CRA19

Material	Property	Description	Units	Value
STEEL	CORRMCO2	Inundated corrosion rate for steel without CO ₂ present ^a	m/s	Cumulative distribution as summarized in Zeitler (2018a)
STEEL	HUMCORR	Humid corrosion rate for steel	m/s	Cumulative distribution as summarized in Zeitler (2018b)

^a – The original description of STEEL:CORRMCO2 identified that the property value did not consider the presence of CO₂. The definition was and cannot be changed but, for clarity, the new cumulative distribution does consider CO₂.

1.1.5 Refinement to Colloid Enhancement Parameters

Refinements to the colloid enhancement parameters are summarized in Section 1.1.3 of Sarathi (2019) and potentially impact the Salado flow solution through the inclusion of brine radiolysis which is in part dependent upon the concentration of each contributing radionuclide in the waste area brine.

1.1.6 Refinement to the Hydromagnesite to Magnesite Conversion Rate

For the CRA-2014 PA, the reaction of hydromagnesite to form magnesite was included along with an associated reaction rate, parameterized as WAS_AREA:HYMAGCON (hereafter HYMAGCON), derived by Clayton (2013). Subsequent to the submittal of the CRA-2014, the EPA requested that the DOE revise the distribution for HYMAGCON. A revised distribution was provided to the EPA by the DOE, but the EPA recommended a different distribution for the CRA-2019 PA (U.S. EPA 2017b). The uniform distribution used for HYMAGCON in the CRA-2019 PA is described in U.S. EPA (2017b) and summarized in Zeitler (2019c) (Table 6).

Table 6 – Hydromagnesite to Magnesite Conversion Rate Parameter (CRA19)

Material	Property	Description	Units	Value
WAS_AREA	HYMAGCON	Rate of conversion of hydromagnesite to magnesite	mol kg ⁻¹ sec ⁻¹	Uniform distribution as summarized in Zeitler (2019c)

1.1.7 Removal of Iron Sulfidation Reactions

For the CRA-2014 PA, the sulfidation reactions with iron and iron hydroxide were included as part of the repository brine and gas production/consumption calculations. Subsequent to the submittal of the CRA-2014, the EPA requested that the DOE remove these chemical reactions from WIPP PA by setting the appropriate stoichiometric coefficients (i.e., REFCON:STCO_31, REFCON:STCO_32, REFCON: STCO_35, REFCON:STCO_36, REFCON:STCO_43, and REFCON:STCO_46) to zero. The request to remove iron sulfidation reactions from WIPP PA and the impact to WIPP PA parameters for the CRA-2019 PA is described in U.S. EPA (2017b) and summarized in Zeitler (2019c) (Table 7).

Table 7 – Iron Sulfidation Stoichiometric Parameters (CRA19)

Material	Properties	Description	Units	Value
REFCON	STCO_31, STCO_32, STCO_35, STCO_36, STCO_43, STCO_46	FeOH ₂ and metallic Fe sulfidation stoichiometric coefficients	(-)	0

1.1.8 Correction to Length of Northernmost Panel Closure Representation

Three separate panel closure areas are modeled in BRAGFLO. The “northernmost” panel closure area separates the operations area from the “north rest-of -repository” (NROR) waste area, the “middle” panel closure separates the NROR from the “south rest-of-repository” (SROR), and the “southernmost” panel closure separates the SROR from the waste panel.

As part of the DOE/EPA completeness determination discussions for CRA-2014, an error in the length of the northernmost panel closure was identified by the DOE – the northernmost panel closure in the BRAGFLO grid should represent the length of two panel closures. This is done to represent the combined resistance to flow corresponding to the set of panel closures directly north of Panel 10 in addition to the set of closures between the operations and experimental areas. Thus, the northernmost panel closure should have been 200 ft. (60.96 m) long, rather than 100 ft. (30.48 m) long, as had been used in the BRAGFLO model for the CRA-2014 PA (DOE

2015). A PA calculation was done to examine the impact of doubling the length of the northernmost panel closure and negligible changes to the pressures and saturations in the waste areas were found (Zeitler 2015d). The correction to the BRAGFLO grid was made for the CRA-2019 PA via changes in grid cell *x*-dimensions for the two columns of cells that contain the representation of the northernmost panel closures (Table 8).

Table 8 – BRAGFLO Grid Cell X-Dimensions for Northernmost Panel Closure Representation (CRA14 and CRA19)

Analysis	One-Cell Length (m)	Full Length (m)
CRA14	15.24	30.48
CRA19	30.48	60.96

1.1.9 Updates to WIPP Waste Inventory Parameters

The Performance Assessment Inventory Report (PAIR) – 2018 (Van Soest 2018) was released on December 20, 2018. The PAIR – 2018 contains updated estimates to the radionuclide content and waste material parameters, scaled to a full repository, based on inventory information collected up to December 31, 2017. The waste inventory detailed in the PAIR – 2018 is used in the CRA-2019 PA.

Waste inventory changes in the PAIR – 2018 potentially impact gas generation results for Salado flow calculations. Specifically, changes to iron and CPR (cellulose, plastic, and rubber) content in the waste inventory can alter the gas production that occurs when these materials come in contact with brine. The PAIR – 2018 contains updated information for iron and CPR content in the repository. Inventory masses of these materials are compared to their CRA-2014 counterparts in Table 9. Values shown in that table for CRA14 are calculated using Table 6-3 and 6-4 of the PAIR – 2012 and for CRA19 are calculated using Table 6-3 and Table 6-5 of the PAIR – 2018. Iron and CPR mass values given in the PAIR – 2018 for CH (contact-handled) and RH (remote-handled) waste and packaging materials are added to the corresponding emplacement material masses, yielding the values shown in Table 9.

Microbial degradation of CPR consumes nitrate (NO_3^-) and sulfate (SO_4^{2-}) in the repository. Emplacements of these ions are updated in the CRA-2019 PA, with values shown in Table 10. Values shown in that table for the baseline analysis (CRA14) are taken from Table C-5 of Kicker and Zeitler (2013) and Table D-5 of Kicker (2019) provides values for CRA19.

Table 9 – Iron and CPR Inventories (CRA14 and CRA19)

Material	CRA14 (kg)	CRA19 (kg)
Iron	4.91E+07	6.30E+07
Cellulose	4.65E+06	5.97E+06
Plastics	9.51E+06	1.06E+07
Rubber	1.25E+06	1.22E+06
Total CPR	1.54E+07	1.78E+07

Table 10 – Nitrate and Sulfate Inventories (CRA14 and CRA19)

Material	CRA14 (moles)	CRA19 (moles)
Nitrate	2.74E+07	2.72E+07
Sulfate	4.91E+06	4.73E+06

1.1.10 Updates to Radionuclide Solubilities

Refinements to the radionuclide solubilities are summarized in Section 1.1.2 of Sarathi (2019) and potentially impact the Salado flow solution through the inclusion of brine radiolysis which is in part dependent upon the concentration of each contributing radionuclide in the waste area brine.

1.1.11 Correction to the Relative Permeability and Capillary Pressure Model Applied to an Open Borehole

Three minor errors in the BRAGFLO code related to the calculation of capillary pressure were discovered, as detailed in software problem report (SPR) 18-002, and determined to have an insignificant effect on repository performance results (Day 2018). One of the SPR 18-002 corrections also prompted the necessity to revise a BRAGFLO input parameter for the relative permeability and capillary pressure function that is used to model an open borehole (BH_OPEN:RELP_MOD). The RELP_MOD parameter was revised from 5 (the value used in the CRA-2014 PA) to 11 for the CRA-2019 PA to resolve the issue where the code correction resulted in a positive capillary pressure within the open borehole under RELP_MOD=5, which is both physically unrealistic and numerically unstable. The use of RELP_MOD = 11 for the BH_OPEN material is consistent with the relative permeability and (zero) capillary pressure implemented for other “open” repository areas such as the operations and experimental areas (Table 11).

Table 11 – Open Borehole Relative Permeability and Capillary Pressure Model Parameter (CRA19)

Material	Property	Description	Units	Value
BH_OPEN	RELP_MOD	Model number, relative permeability model	(-)	11

1.1.12 Introduction of New Materials Names

As part of the review of the CRA-2014, the EPA directed multiple sensitivity studies that investigated impacts of parameter changes to the OPS, EXP, and panel closure areas and their associated disturbed-rock zones (DRZs), while leaving the DRZ surrounding the waste panel unchanged. To facilitate those analyses, new material names were used that introduced flexibility in specifying material properties independently across areas for which material properties in the CRA-2014 PA were identical. The flexibility of managing material properties by using these new material names is preserved in the CRA-2019 PA. This subsection describes the new materials (DRZ_OE_0, DRZ_OE_1, DRZ_PC_1, DRZ_PC_0, and CAVITY_5) and the sources for the associated property values that already exist in the PAPDB due to their use in the sensitivity studies. To be clear, while material names representing these areas of the BRAGFLO grid have changed since the CRA 2014 PA, properties for those areas have not changed. One unrelated exception is the DRZ surrounding the abandoned southernmost panel closure area, which will have DRZ_0 and DRZ_1 properties as discussed in Section 1.1.1.

In the CRA-2014 PA, the DRZ surrounding the waste, OPS, and EXP areas were given identical properties in BRAGFLO calculations via the DRZ_0 and DRZ_1 materials. In the CRA14_SEN2 study (Day 2016), to isolate the parameter modifications for the DRZ surrounding the OPS and EXP areas, the new materials DRZ_OE_0 and DRZ_OE_1 were introduced to represent the DRZ surrounding only the OPS and EXP areas in the -5 to 0 year and 0 to 10,000 year timeframes, respectively (the DRZ_0 and DRZ_1 materials continued to represent the DRZ surrounding the waste areas). In the CRA14_SEN4 sensitivity study (Zeitler and Day 2016), the properties of the DRZ surrounding the OPS and EXP areas were not changed from the CRA-2014 PA values, but the flexibility of isolating potential changes to the DRZ surrounding the OPS and EXP areas was preserved by maintaining the DRZ_OE_0 and DRZ_OE_1 materials and assigning values used in the CRA-2014 PA for the DRZ_0 and DRZ_1 materials, respectively.

For the CRA-2019 PA, the DRZ_OE_0 and DRZ_OE_1 materials are used with parameter values equal to those used in the CRA-2014 PA for the DRZ_0 and DRZ_1 materials, respectively. Because the DRZ_OE_0 and DRZ_OE_1 materials did not exist for the CRA-2014 PA, the CRA-2019 PA will use the values defined in the sensitivity studies, as described above and summarized in Table 12.

In the CRA14_SEN3 study (Day and Zeitler 2016), to isolate the parameter modifications for the DRZ surrounding the panel closure areas, the new materials DRZ_PC_0 and DRZ_PC_1 were introduced that represented the DRZ surrounding panel closure areas in the -5 to 0 year and 0 to 10,000-year timeframes, respectively. In the CRA14_SEN4 sensitivity study (Zeitler and Day

2016), the properties of the DRZ surrounding the panel closure areas were not changed from the CRA-2014 PA values, but the flexibility of isolating potential changes to the DRZ surrounding the panel closure areas was preserved by maintaining the DRZ_PC_0 and DRZ_PC_1 materials and assigning values used in the CRA-2014 PA for the DRZ_0 and DRZ_1 materials, respectively.

For the CRA-2019 PA, the DRZ_PC_0 and DRZ_PC_1 (0 to 200 y timeframe) materials are with parameter values equal to those used in the CRA-2014 PA for the DRZ_0 and DRZ_1 materials, respectively. Because the DRZ_PC_0 and DRZ_PC_1 materials did not exist for the CRA-2014 PA, the CRA-2019 PA uses the values defined in the sensitivity studies, as described above and summarized in Table 13.

The CRA14_SEN3 sensitivity study (Day and Zeitler 2016) investigated changes to panel closure properties. For the CRA-2014 PA, the panel closure system was, along with the shaft area, part of the CAVITY_4 material used in the -5 to 0-year time frame, but was separated from CAVITY_4 for the CRA14_SEN3 analysis. The startup material used for the panel closure system was a new material, CAVITY_5, and that material will continue to be used for the CRA-2019 PA, in order to preserve flexibility in assigning startup material properties to panel closure areas independently of the shaft area. For the CRA14_SEN3 analysis, the CAVITY_4 and CAVITY_5 materials had different property values, but for the CRA-2019, the property values for these two materials are identical. Because the CAVITY_5 material did not exist for the CRA-2014 PA, the CRA-2019 PA uses the values defined in the sensitivity studies, as described above and summarized in Table 14.

Table 12 – DRZ_OE_0 and DRZ_OE_1 Parameter Values (CRA19)

Material	Material for which Property Values are Equivalent (CRA14 and CRA19)	Properties	Analysis from which Defined Property Values are Used
DRZ_OE_0	DRZ_0	KPT, PC_MAX, PO_MIN, PORE_DIS, RELP_MOD	CRA14_SEN2
DRZ_OE_0	DRZ_0	CAP_MOD, COMP_RCK, PCT_A, PCT_EXP, POROSITY, PRMX_LOG, PRMY_LOG, PRMZ_LOG, SAT_IBRN, SAT_RBRN, SAT_RGAS	CRA14_SEN4
DRZ_OE_1	DRZ_1	KPT, PC_MAX, PO_MIN, PORE_DIS, RELP_MOD	CRA14_SEN2
DRZ_OE_1	DRZ_1	CAP_MOD, COMP_RCK, PCT_A, PCT_EXP, POROSITY, PRMX_LOG, PRMY_LOG, PRMZ_LOG, SAT_IBRN, SAT_RBRN, SAT_RGAS	CRA14_SEN4

Table 13 – DRZ_PC_0 and DRZ_PC_1 Parameter Values (CRA19)

Material	Material for which Property Values are Equivalent (CRA14 and CRA19)	Properties	Analysis from which Defined Property Values are Used
DRZ_PC_0	DRZ_0 (-5 to 0 yr.)	KPT, PC_MAX, PO_MIN, PORE_DIS, RELP_MOD	CRA14_SEN3
DRZ_PC_0	DRZ_0 (-5 to 0 yr.)	CAP_MOD, COMP_RCK, PCT_A, PCT_EXP, POROSITY, PRMX_LOG, PRMY_LOG, PRMZ_LOG, SAT_IBRN, SAT_RBRN, SAT_RGAS	CRA14_SEN4
DRZ_PC_1	DRZ_1 (0 to 200 yr.)	KPT, PC_MAX, PO_MIN, PORE_DIS, RELP_MOD	CRA14_SEN3
DRZ_PC_1	DRZ_1 (0 to 200 yr.)	CAP_MOD, COMP_RCK, PCT_A, PCT_EXP, POROSITY, PRMX_LOG, PRMY_LOG, PRMZ_LOG, SAT_IBRN, SAT_RBRN, SAT_RGAS	CRA14_SEN4

Table 14 – CAVITY_5 Parameter Values (CRA19)

Material	Material for which Property Values are Equivalent (CRA14 and CRA19)	Properties	Analysis from which Defined Property Values are Used
CAVITY_5	CAVITY_4	KPT, PC_MAX, PO_MIN, PORE_DIS, PRESSURE	CRA14_SEN3
CAVITY_5	CAVITY_4	CAP_MOD, COMP_RCK, PCT_A, PCT_EXP, POROSITY, PRMX_LOG, PRMY_LOG, PRMZ_LOG, RELP_MOD, SAT_IBRN, SAT_RBRN, SAT_RGAS	CRA14_SEN4

1.1.13 Computational code updates to BRAGFLO and PREBRAG

As a result of SPR 18-002 discussed in Section 1.1.11 and primarily to implement brine radiolysis into the BRAGFLO gas generation process model discussed in Section 1.1.3, BRAGFLO was revised from version 6.03 to 7.00 and PREBRAG was revised from version 8.03 to 9.00.

The BRAGFLO version 7.00 revision invoked the addition of two additional software requirements, listed below, that were subject to validation and verification (WIPP PA 2018a) through an additional test case:

- Allow for the calculation of mass for up to five radionuclides in up to two waste areas by accounting for radioactive decay. Note: The ability to model two waste areas within BRAGFLO is applied to cover the three waste areas modeled within the Salado flow grid through the application of the 2nd waste area material properties (REPOSIT) to both the south rest-of-repository and the north rest-of-repository grid cells.
- Allow for the calculation of radiolysis (the radiolytic breakdown of water/brine into hydrogen and oxygen) resulting from up to five inventory radionuclides. Radiolysis can result from radionuclides dissolved in brine and, optionally, from the remaining inventory of solid (precipitated) radionuclides that are in contact with brine (wetted). The fraction of disintegration energy from the solid radionuclides that contributes to radiolysis can be specified.

The PREBRAG version 9.00 revision invoked the addition of an additional software requirement, listed below, that was subject to validation and verification (WIPP PA 2018b) through an additional test case:

- Output radiolysis and radionuclide decay data obtained from the CAMDAT file or through the PREBRAG input control file.

Both the PREBRAG version 9.00 and BRAGFLO version 7.00 code revisions are used for the CRA-2019 PA.

This page intentionally left blank.

2.0 CONCEPTUAL APPROACH FOR THE CRA-2019

The conceptual models implemented in the BRAGFLO simulations for the CRA-2019 PA are unchanged from those used in the CRA-2014 PA. However, implementing aspects of the repository fluid flow conceptual model have been adjusted to address the addition of a 5th shaft and associated shaft access drifts; abandonment of ROMPCS in Panels 3, 4, 5, 6, and 9; continued use of Panel 9 as a surrogate for equivalent waste emplacement in an alternate panel farther north; extension of the length of the ROMPCS above Panel 10 to represent the combined effects of the northernmost panel closure and the panel closure between the operations and experimental area; and inclusion of brine radiolysis as a gas generation mechanism due to the decay of radionuclides in solution in addition to the wetted-solid form of radionuclides in the waste areas. A summary of modifications to the computational grid, material map, and input parameters having the potential to impact repository performance through the Salado flow simulation results are summarized in Section 1.1 and selectively further discussed below.

2.1 Repository Representation in BRAGFLO

The computational grid and associated material map used by BRAGFLO is altered for the CRA-2019 PA in order to implement the use of new and equivalent material names to represent the DRZ above and below emplaced panel closures and the operations and experimental area, correct for the length of the northernmost panel closure, add the additional mined volume in the repository experimental region associated with new access drifts for the 5th shaft, increase the cross-sectional area of the modeled composite shaft to accommodate the 5th shaft geometry, and accommodate modifications to the southernmost panel closure area and associated DRZ to represent the abandonment of plans to emplace ROMPCS between Panel 3, 4, 5, 6, and 9. Otherwise, the computational grid used in the CRA-2019 PA is the same as that used in the CRA-2014 PA.

The generic BRAGFLO computational grids with modeled area descriptions and cell dimensions for the CRA-2014 and CRA-2019 PA are shown in Figure 1 and Figure 2, where the cell dimension changes indicated in red are associated with the northernmost panel closure extension, increased composite shaft cross-sectional area, and depth increase to accommodate the 5th shaft access drift volume in the experimental area. Also shown are the material area changes in the DRZ areas above and below and within the southernmost panel closure area which has been abandoned for the CRA-2014 PA. Detailed material maps associated with the six modeling scenarios are further defined in Section 3.2 for the CRA-2019 PA.

This page intentionally left blank.

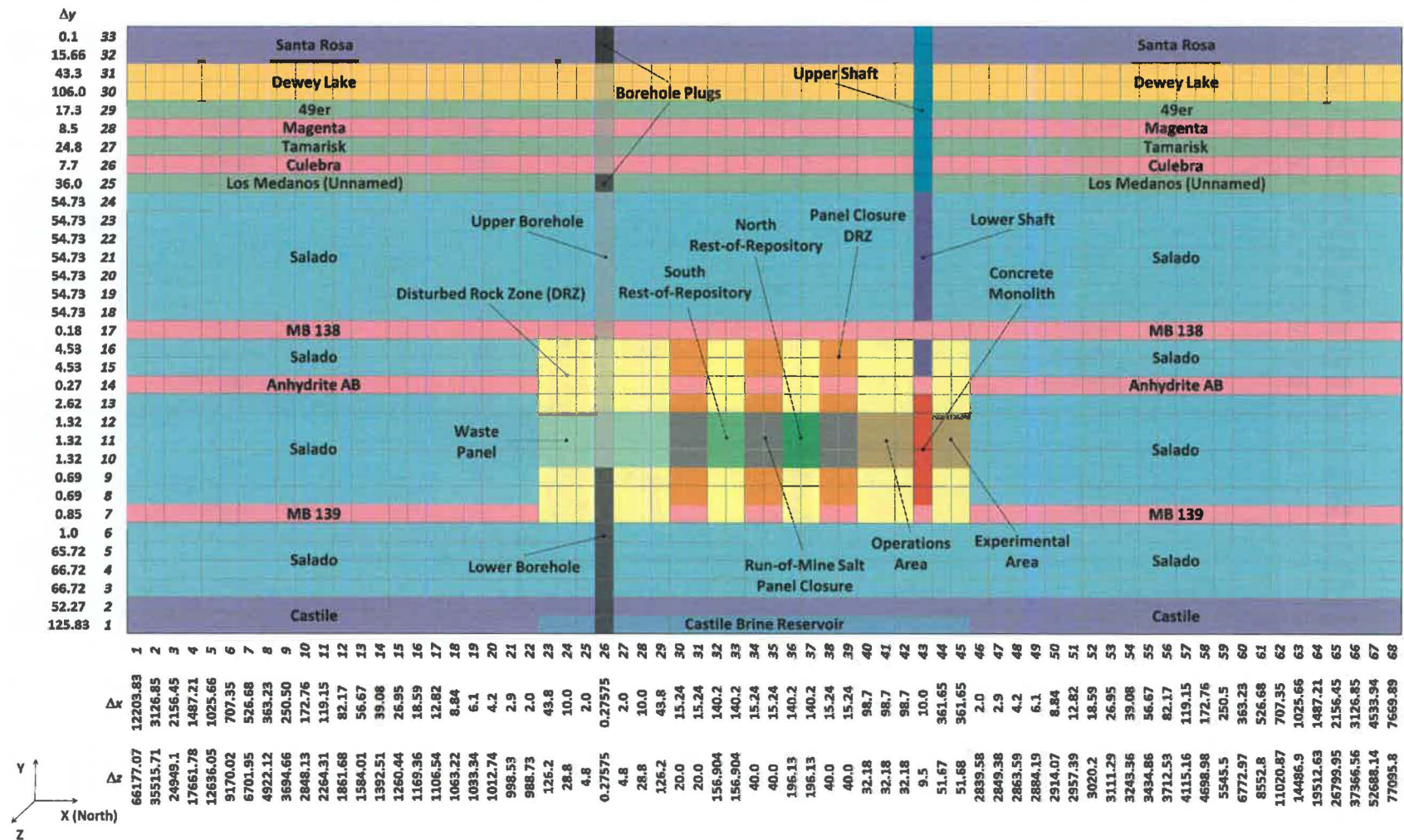


Figure 1 – Generic CRA-2014 PA BRAGFLO Grid with Modeled Area Descriptions

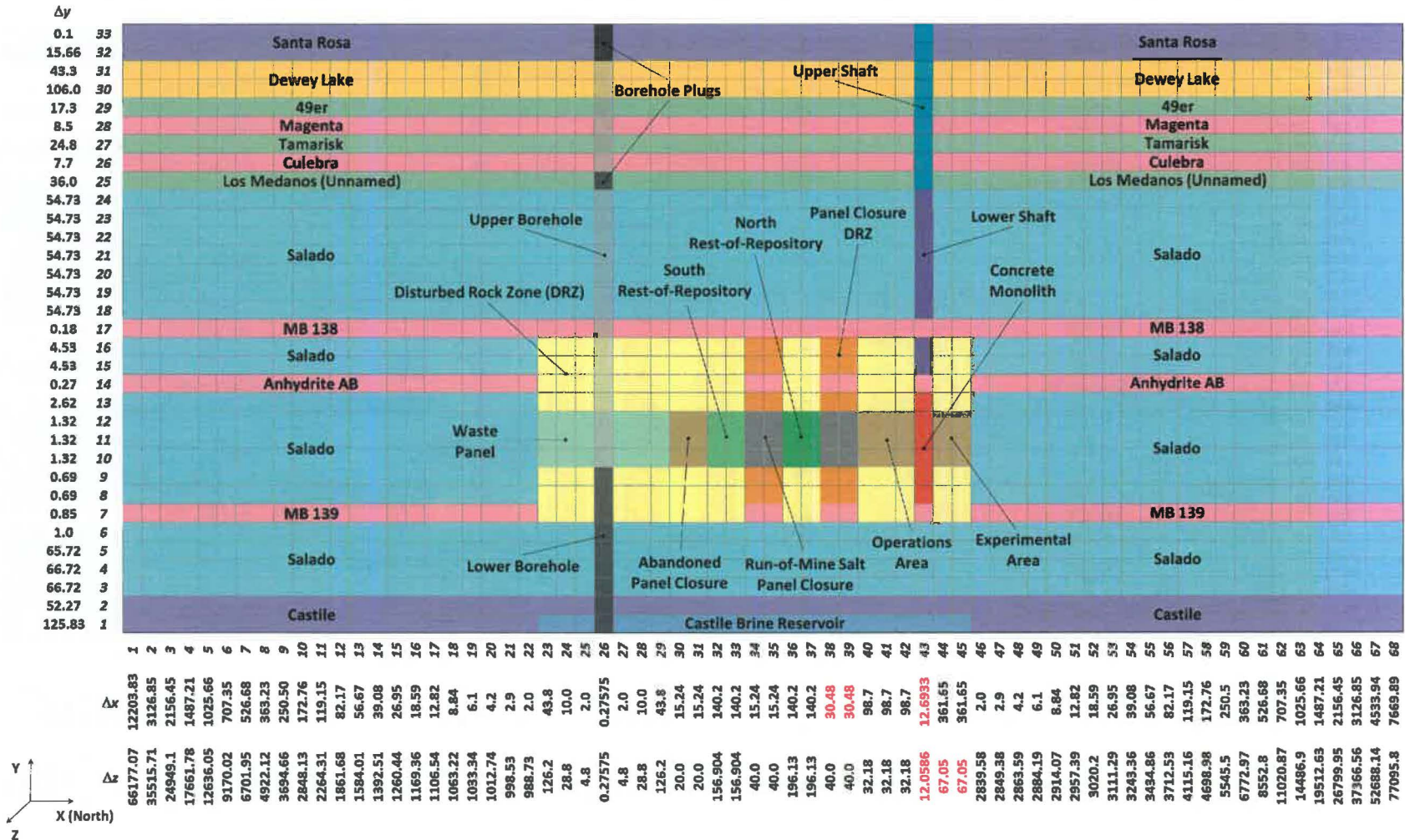


Figure 2 – Generic CRA-2019 PA BRAGFLO Grid with Modeled Area Descriptions

2.2 Initial Conditions

BRAGFLO simulations require the assignment of initial conditions including brine pressure, brine saturation, grid block center elevations, quantities for all radionuclides participating in radiolysis, and concentrations of iron, magnesium oxide, and biodegradable material in the waste areas. These initial conditions are provided to BRAGFLO through various pre-processing steps in which values are retrieved from the WIPP PA Performance Assessment Parameter Database or sampled as appropriate.

At the beginning of each BRAGFLO run, the model simulates a short period of time representing disposal operations. This portion of the run is called the initialization period and lasts for 5 years (from $t = -5$ to 0 years), corresponding to the time a typical waste panel is expected to be open during disposal operations. All grid blocks require initial pressure and saturation at the beginning of the run ($t = -5$ years). At the beginning of the regulatory period (0 to 10,000 years), BRAGFLO resets initial conditions within the excavated regions and in the shaft.

The initial conditions specified for BRAGFLO modeling are listed below:

- Brine pressure in all non-excavated regions is equal to lithostatic pressure. This pressure is sampled at a single location and assumed hydrostatic at all other locations. Note that brine pressure in all non-excavated regions is alternatively set equal to one atmosphere (1.01325×10^5 Pa) for any location above the water table.
- Pressure within all excavated regions is set to one atmosphere (1.01325×10^5 Pa) at $t = -5$ years.
- Pressure within the excavated waste regions at $t = 0$ years is increased to 1.28039×10^5 Pa in order to account for the pressure increase (0.26714×10^5 Pa) associated with microbial gas produced at short times (Nemer et al. 2005).
- Brine saturation within the non-excavated regions is set to 1.0 at $t = -5$ years.
- Brine saturation within the excavated regions is set to a value of 0 at $t = -5$ years.
- Brine saturation in the excavated regions at $t = 0$ years is prescribed the following values:
 - 0.015 for the excavated waste regions.
 - 0.0 for the operations and experimental areas.
 - 0.9999999 for the shaft (upper, lower, and concrete monolith).
 - Sampled value for the emplaced panel closures from a cumulative distribution with a minimum of 0.0, a mean of 0.25, and a maximum of 0.6.
 - 0.0 for the abandoned panel closure.
- Brine saturation in the Santa Rosa and the upper Dewey Lake is set to 0.08363 at $t = -5$ years.

During the initialization period brine tends to flow into the excavated areas and the shaft, resulting in decreased pressure and saturation in the rock immediately adjacent to the

excavations. At time $t = 0$ years, the pressure and saturation in all the excavations is reset to initial conditions for the materials used to represent these regions for the regulatory period. This practice is intended to capture the effect of evaporation of brine inflow during the operational period and the transport of this brine up the shaft ventilation system, as well as the depressurization of the surrounding rock formations due to excavation.

The initial conditions for radionuclide quantities are applied by equally distributing the sum of radiolysis-contributing contact-handled (CH) and remote-handled (RH) radionuclide inventory on a volumetric basis over all waste areas of the repository.

2.3 Boundary Conditions

The boundary conditions assigned for the BRAGFLO calculations in the CRA-2019 PA are the same as those for the CRA-2014 PA as follows:

- Constant pressure at the north and south ends of the Culebra and Magenta dolomites.
- Constant pressure (1.01325×10^5 Pa) and saturation (0.08363) conditions at the land surface boundary of the grid, except for saturation at the shaft cell on the land surface boundary (Vaughn 1996).
- No-flow conditions at all other grid boundaries.

3.0 SALADO FLOW MODELING METHODOLOGY

The BRAGFLO numerical code calculates the flow of brine and gas in the vicinity of the WIPP repository over a 10,000-year regulatory compliance period. The results of these calculations are used by other codes to calculate potential radionuclide releases to the accessible environment. Some of the specific processes included in the BRAGFLO calculations include:

- Two-phase, immiscible, brine and gas flow.
- Pressure-induced fracture of the host rock.
- Creep closure of the waste filled regions within the repository.
- Pressure-dependent increase in permeability (i.e., Klinkenberg effect).
- Brine and gas consumption and/or generation due to chemical processes (e.g., iron corrosion, cellulose biodegradation, MgO hydration and carbonation, brine radiolysis) within the waste.

There is significant uncertainty associated with characterizing the physical properties of geologic materials that influence these processes. WIPP PA addresses these uncertainties in two ways. Properties such as permeability and porosity are usually measured indirectly and vary significantly depending upon location. The uncertainty in particular physical property values is called subjective (epistemic) uncertainty. Subjective uncertainty can, in theory, be reduced by further study of the system. Subjective uncertainty is addressed within Salado flow modeling by the use of probability distributions for subjectively uncertain parameters. Multiple flow realizations are performed in which the values of uncertain parameters are sampled from their respective distributions. For subjectively uncertain, spatially distributed quantities, e.g. the permeability of the DRZ, one sampled value is used to specify a particular parameter value over its entire spatial extent in a single realization. To reduce the number of realizations required and to ensure that low probability (and possibly high consequence) combinations are represented, Latin Hypercube Sampling (LHS) is used to create the realizations. For the WIPP PA, the LHS software (WIPP PA 2005) is used to create a “replicate” of 100 distinct parameter sets (“vectors”) that are sampled from the full range of parameter uncertainty. To ensure that the Latin Hypercube replicates are representative, a total of three replicates are run for a total of 300 separate vectors.

Another type of uncertainty encountered in WIPP PA is that of stochastic (aleatory) uncertainty associated with incomplete knowledge of future events. Unlike subjective uncertainty, stochastic uncertainty cannot be reduced by further study. WIPP PA addresses stochastic uncertainty by employing a Monte Carlo sampling technique on random futures. In this context, a future is defined as one possible sequence of events. During BRAGFLO calculations, stochastic uncertainty is addressed by defining a set of six scenarios for which brine and gas flow is calculated for each of the vectors generated by the LHS software. The total number of BRAGFLO simulations that have to be run for a WIPP PA calculation is 300 vectors times 6 scenarios equaling 1,800 BRAGFLO simulations.

3.1 Modeling Scenarios

The six scenarios used in the CRA-2019 PA are unchanged from those used for the CRA-2014 PA. Results obtained in the six scenarios from BRAGFLO are used to initialize flow and material properties in subsequent codes in the PA computational suite, e.g. in the calculation of direct brine release volumes. The intrusion types specified in PA code calculations subsequent to BRAGFLO are the same as those implemented in BRAGFLO. The intrusion times, however, are not always equal. To avoid confusion resulting from the use of identical scenario notation for scenarios with unequal intrusion times in the various PA codes, the scenarios in BRAGFLO are denoted as S1-BF to S6-BF. The scenarios include one undisturbed scenario (S1-BF), four scenarios that include a single inadvertent future drilling intrusion into the repository during the 10,000-year regulatory period (S2-BF to S5-BF), and one scenario investigating the effect of two intrusions into a single waste panel (S6-BF). Two types of intrusions, denoted as E1 and E2, are considered. An E1 intrusion assumes the borehole passes through a waste-filled panel and into a region of pressurized brine that may exist under the repository in the Castile formation. An E2 intrusion assumes that the borehole passes through the repository but does not encounter pressurized brine. Scenarios S2-BF and S3-BF model the effect of an E1 intrusion occurring at 350 years and 1000 years, respectively, after the repository is closed. Scenarios S4-BF and S5-BF model the effect of an E2 intrusion at 350 and 1000 years. Scenario S6-BF models an E2 intrusion occurring at 1000 years, followed by an E1 intrusion into the same panel at 2000 years. BRAGFLO results obtained in Scenario S6-BF are used to calculate transport releases to the Culebra. Table 15 summarizes the six scenarios used in WIPP PA Salado flow analyses.

Table 15 – BRAGFLO Modeling Scenarios

Scenario	Description
S1-BF	Undisturbed Repository
S2-BF	E1 intrusion at 350 years
S3-BF	E1 intrusion at 1,000 years
S4-BF	E2 intrusion at 350 years
S5-BF	E2 intrusion at 1,000 years
S6-BF	E2 intrusion at 1,000 years; E1 intrusion at 2,000 years.

The primary event mechanics of each scenario and the associated material property maps are given in Section 3.2. Note that the ROMPCS implemented in the CRA-2019 PA, as well as materials used to represent the shaft, attain their long-term permeability values at 200 years, well before the occurrence of any of the waste panel intrusions in scenarios S2-BF to S6-BF.

3.2 Material Maps

Implementation of the BRAGFLO scenarios necessitates the modification of the grid material maps at different times. Figure 3 through Figure 12 show material maps associated with the BRAGFLO grid for all BRAGFLO scenarios across all time periods (-5 to 10,000 years). Associations between the material maps and BRAGFLO scenarios are summarized in Table 16.

3.2.1 Scenario S1-BF (Undisturbed Conditions)

- **-5 years:** Initialization phase with open waste areas, panel closures, and shaft. (Figure 3)
- **0 years:** Waste, panel closures, and shaft are emplaced. ROMPCS represented by material PCS_T1 with no healing of the DRZ above and below the panel closure and abandoned panel closure represented by material PCS_NO. (Figure 4)
- **100 years:** ROMPCS material transitions from PCS_T1 to PCS_T2 with no healing of the DRZ above and below the panel closure. (Figure 5)
- **200 years:** ROMPCS material transitions from PCS_T2 to PCS_T3 with healed regions of DRZ above and below the panel closure represented by material DRZ_PCS. Lower shaft material transitions from SHFTL_T1 to SHFTL_T2. (Figure 6)

3.2.2 Scenario S2-BF (E1 intrusion at 350 years)

- **-5 years:** Initialization phase with open waste areas, panel closures, and shaft. (Figure 3)
- **0 years:** Waste, panel closures, and shaft are emplaced. ROMPCS represented by material PCS_T1 with no healing of the DRZ above and below the panel closure and abandoned panel closure represented by material PCS_NO. (Figure 4)
- **100 years:** ROMPCS material transitions from PCS_T1 to PCS_T2 with no healing of the DRZ above and below the panel closure. (Figure 5)
- **200 years:** ROMPCS material transitions from PCS_T2 to PCS_T3 with healed regions of DRZ above and below the panel closure represented by material DRZ_PCS. Lower shaft material transitions from SHFTL_T1 to SHFTL_T2. (Figure 6)
- **350 years:** Borehole intrusion through the Waste Panel and into a hypothetical pressurized brine region in the underlying Castile Formation, with the borehole represented by material BH_OPEN. Concrete borehole plugs, represented by material CONC_PLG, immediately emplaced in the borehole below the Culebra and at the surface. (Figure 9)
- **550 years:** Borehole plugs fail, and the entire borehole is modeled as having properties equivalent to sand. The borehole, bottom to top, is represented by material BH_SAND. (Figure 11)
- **1550 years:** The permeability of the borehole between the repository and the Castile brine region decreases due to creep closure of the salt. The lower borehole is represented by material BH_CREEP. (Figure 12)

3.2.3 Scenario S3-BF (E1 intrusion at 1000 years)

- **-5 years:** Initialization phase with open waste areas, panel closures, and shaft. (Figure 3)
- **0 years:** Waste, panel closures, and shaft are emplaced. ROMPCS represented by material PCS_T1 with no healing of the DRZ above and below the panel closure and abandoned panel closure represented by material PCS_NO. (Figure 4)
- **100 years:** ROMPCS material transitions from PCS_T1 to PCS_T2 with no healing of the DRZ above and below the panel closure. (Figure 5)
- **200 years:** ROMPCS material transitions from PCS_T2 to PCS_T3 with healed regions of DRZ above and below the panel closure represented by material DRZ_PCS. Lower shaft material transitions from SHFTL_T1 to SHFTL_T2. (Figure 6)
- **1000 years:** Borehole intrusion through the Waste Panel and into a hypothetical pressurized brine region in the underlying Castile Formation, with the borehole represented by material BH_OPEN. Concrete borehole plugs, represented by material CONC_PLG, immediately emplaced in the borehole below the Culebra and at the surface. (Figure 9)
- **1200 years:** Borehole plugs fail, and the entire borehole is modeled as having properties equivalent to sand. The borehole, bottom to top, is represented by material BH_SAND. (Figure 11)
- **2200 years:** The permeability of the borehole between the repository and the Castile brine region decreases due to creep closure of the salt. The lower borehole is represented by material BH_CREEP. (Figure 12)

3.2.4 Scenario S4-BF (E2 intrusion at 350 years)

- **-5 years:** Initialization phase with open waste areas, panel closures, and shaft. (Figure 3)
- **0 years:** Waste, panel closures, and shaft are emplaced. ROMPCS represented by material PCS_T1 with no healing of the DRZ above and below the panel closure and abandoned panel closure represented by material PCS_NO. (Figure 4)
- **100 years:** ROMPCS material transitions from PCS_T1 to PCS_T2 with no healing of the DRZ above and below the panel closure. (Figure 5)
- **200 years:** ROMPCS material transitions from PCS_T2 to PCS_T3 with healed regions of DRZ above and below the panel closure represented by material DRZ_PCS. Lower shaft material transitions from SHFTL_T1 to SHFTL_T2. (Figure 6)
- **350 years:** Borehole intrusion terminating at the floor of the Waste Panel, with the borehole represented by material BH_OPEN. Concrete borehole plugs,

represented by material CONC_PLG, immediately emplaced in the borehole below the Culebra and at the surface. (Figure 7)

- **550 years:** Borehole plugs fail, and the entire borehole is modeled as having properties equivalent to sand. The borehole, bottom to top, is represented by material BH_SAND. (Figure 8)

3.2.5 Scenario S5-BF (E2 intrusion at 1000 years)

- **-5 years:** Initialization phase with open waste areas, panel closures, and shaft. (Figure 3)
- **0 years:** Waste, panel closures, and shaft are emplaced. ROMPCS represented by material PCS_T1 with no healing of the DRZ above and below the panel closure and abandoned panel closure represented by material PCS_NO. (Figure 4)
- **100 years:** ROMPCS material transitions from PCS_T1 to PCS_T2 with no healing of the DRZ above and below the panel closure. (Figure 5)
- **200 years:** ROMPCS material transitions from PCS_T2 to PCS_T3 with healed regions of DRZ above and below the panel closure represented by material DRZ_PCS. Lower shaft material transitions from SHFTL_T1 to SHFTL_T2. (Figure 6)
- **1000 years:** Borehole intrusion terminating at the floor of the Waste Panel, with the borehole represented by material BH_OPEN. Concrete borehole plugs, represented by material CONC_PLG, immediately emplaced in the borehole below the Culebra and at the surface. (Figure 7)
- **1200 years:** Borehole plugs fail, and the entire borehole is modeled as having properties equivalent to sand. The borehole, bottom to top, is represented by material BH_SAND. (Figure 8)

3.2.6 Scenario S6-BF (E2 intrusion at 1000 years, E1 intrusion at 2000 years)

- **-5 years:** Initialization phase with open waste areas, panel closures, and shaft. (Figure 3)
- **0 years:** Waste, panel closures, and shaft are emplaced. ROMPCS represented by material PCS_T1 with no healing of the DRZ above and below the panel closure and abandoned panel closure represented by material PCS_NO. (Figure 4)
- **100 years:** ROMPCS material transitions from PCS_T1 to PCS_T2 with no healing of the DRZ above and below the panel closure. (Figure 5)
- **200 years:** ROMPCS material transitions from PCS_T2 to PCS_T3 with healed regions of DRZ above and below the panel closure represented by material DRZ_PCS. Lower shaft material transitions from SHFTL_T1 to SHFTL_T2. (Figure 6)

- **1000 years:** Borehole intrusion terminating at the floor of the Waste Panel, with the borehole represented by material BH_OPEN. Concrete borehole plugs, represented by material CONC_PLG, immediately emplaced in the borehole below the Culebra and at the surface. (Figure 7)
- **1200 years:** Borehole plugs fail, and the entire borehole is modeled as having properties equivalent to sand. The borehole, bottom to top, is represented by material BH_SAND. (Figure 8)
- **2000 years:** A second borehole intrusion connects the waste panel to a hypothetical pressurized brine region in the underlying Castile Formation. The lower borehole is represented by material BH_OPEN. (Figure 10)
- **2200 years:** The lower borehole is modeled as having properties equivalent to sand and is represented by material BH_SAND. (Figure 11)
- **3200 years:** The permeability of the borehole between the repository and the Castile brine region decreases due to creep closure of the salt. The lower borehole is represented by material BH_CREEP. (Figure 12)

Table 16 – Time Period Associations Between Material Map Figures and BRAGFLO Scenarios

Scenario	Material Map Figure Number and Associated Time Period (year)									
	Figure 3	Figure 4	Figure 5	Figure 6	Figure 7	Figure 8	Figure 9	Figure 10	Figure 11	Figure 12
S1-BF	-5 - 0	0 - 100	100 - 200	200 -10000	-	-	-	-	-	-
S2-BF	-5 - 0	0 - 100	100 - 200	200 - 350	-	-	350-550	-	550 - 1550	1550 - 10000
S3-BF	-5 - 0	0 - 100	100 - 200	200 - 1000	-	-	1000 - 1200	-	1200 - 2200	2200 - 10000
S4-BF	-5 - 0	0 - 100	100 - 200	200 - 350	350 - 550	550 - 10000	-	-	-	-
S5-BF	-5 - 0	0 - 100	100 - 200	200 - 1000	1000 - 1200	1200 - 10000	-	-	-	-
S6-BF	-5 - 0	0 - 100	100 - 200	200 - 1000	1000 - 1200	1200 - 2000	-	2000 - 2200	2200 - 3200	3200 - 10000

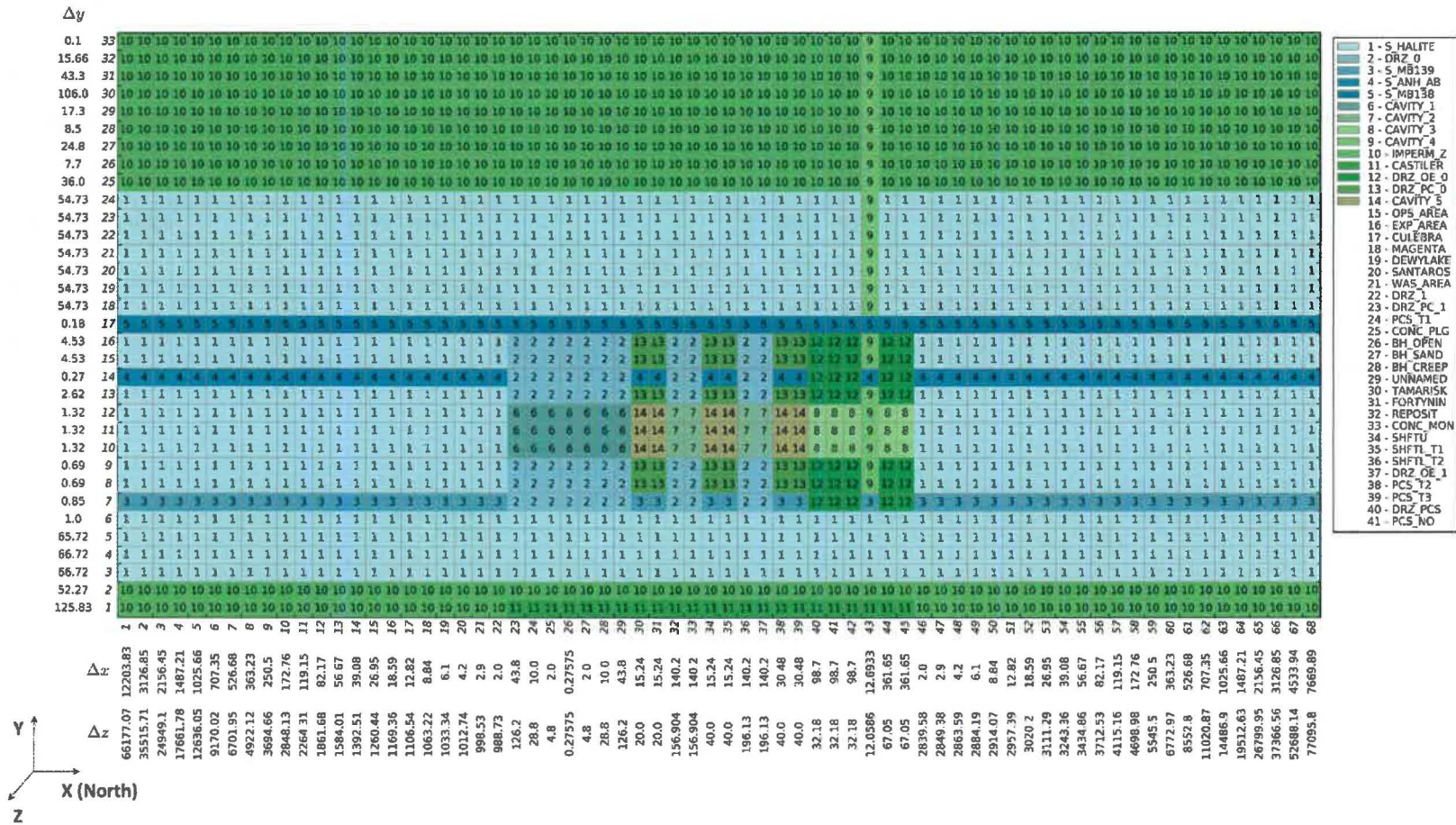


Figure 3 – CRA-2019 PA BRAGFLO Grid and Material Map; Years -5 to 0 [Scenarios S1-BF through S6-BF]

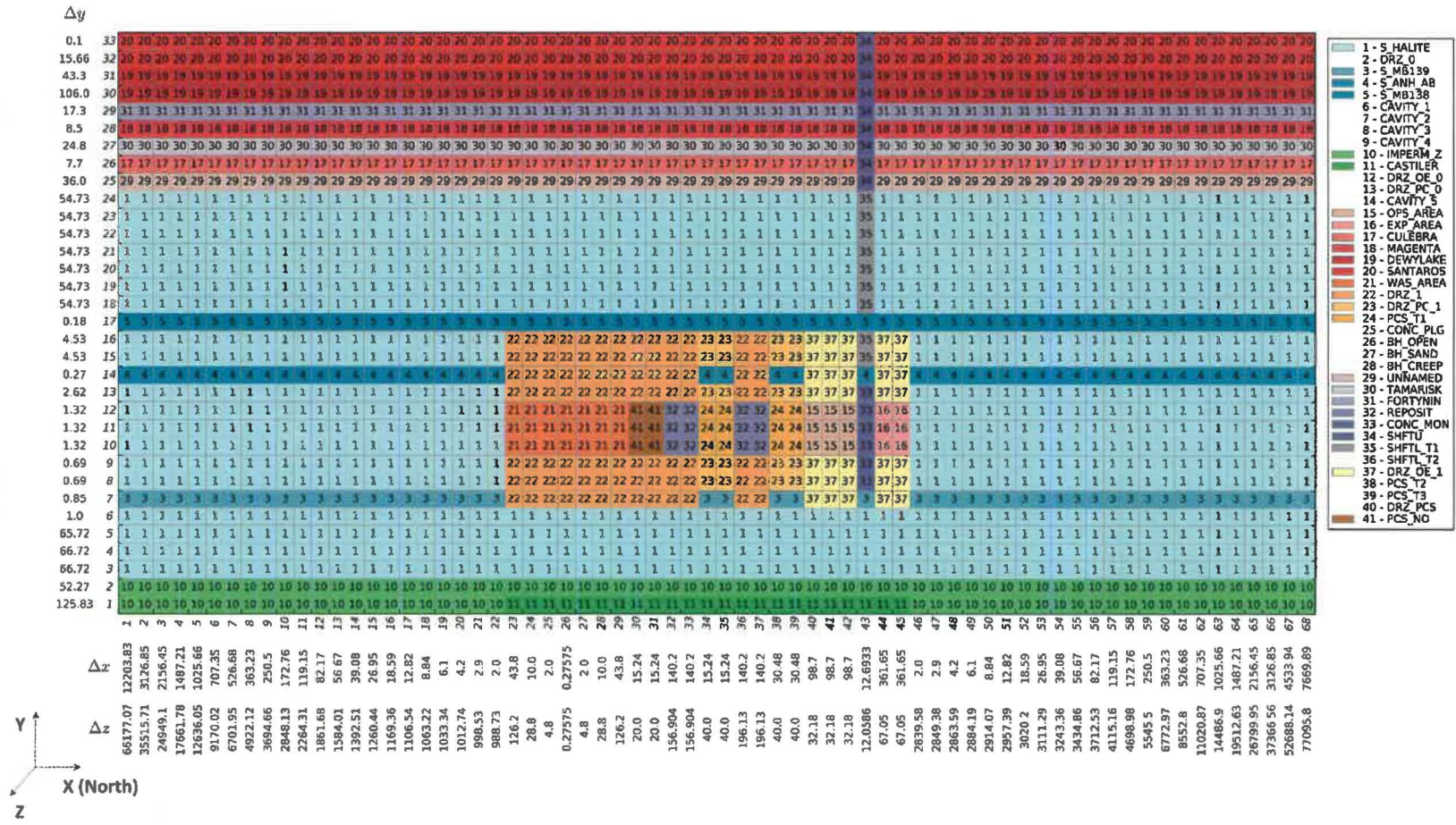


Figure 4 – CRA-2019 PA BRAGFLO Grid and Material Map; Years 0 to 100 [Scenarios S1-BF through S6-BF]

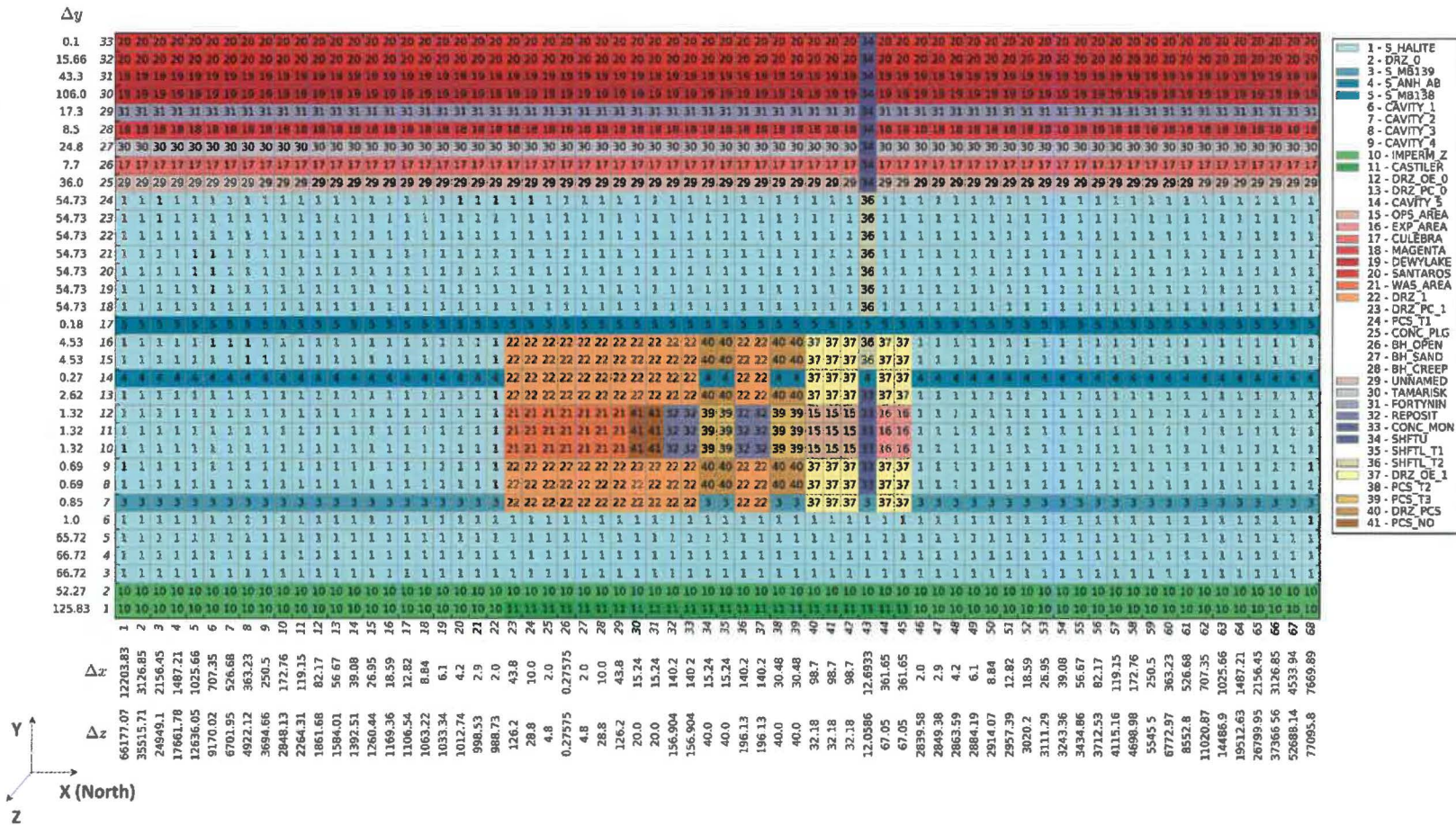


Figure 6 – CRA-2019 PA BRAGFLO Grid and Material Map; Years 200 to 10000 [Scenario S1-BF], Years 200 to Time of E1 or E2 Intrusion [Scenarios S2-BF through S6-BF]

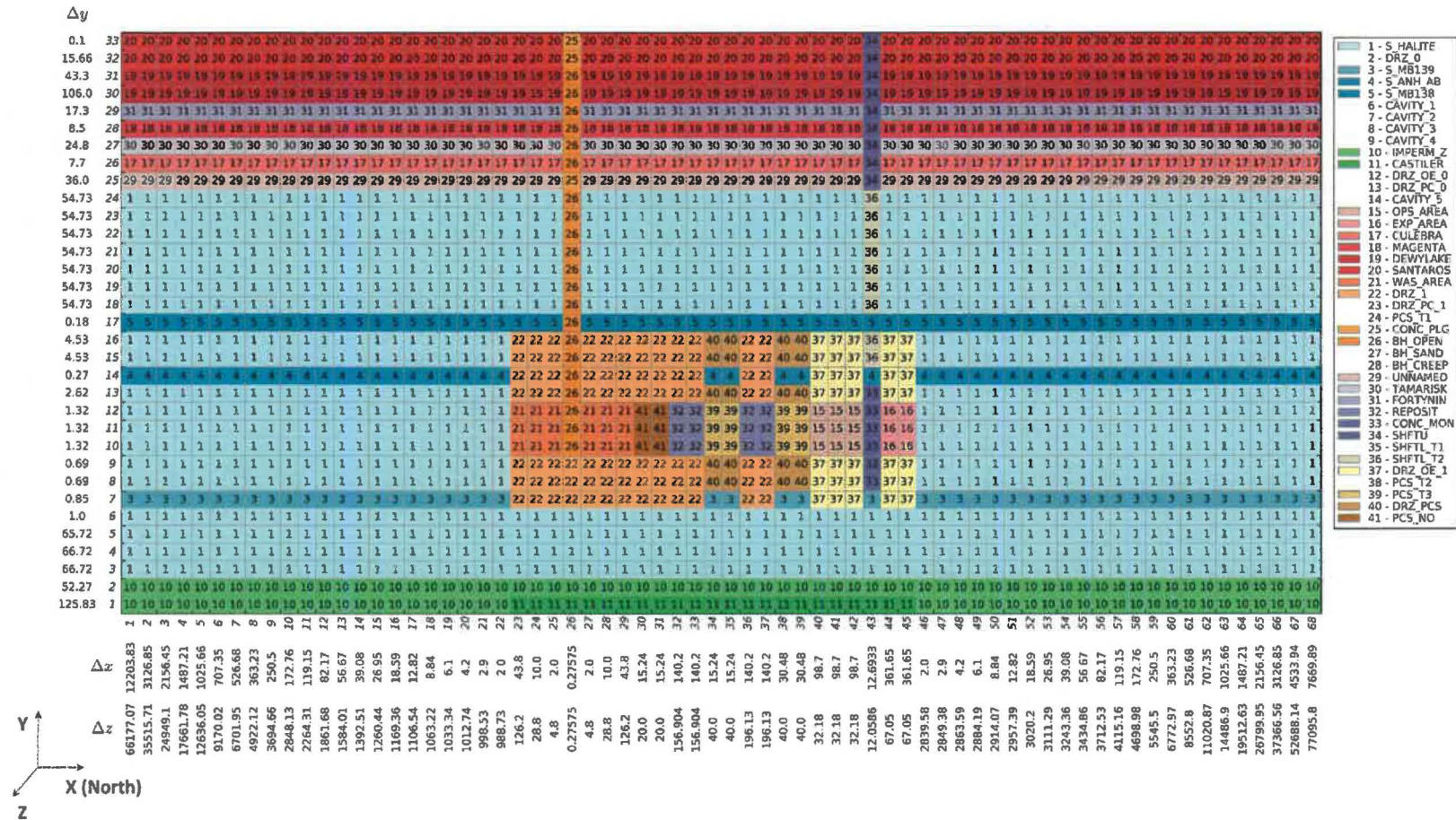


Figure 7 – CRA-2019 PA BRAGFLO Grid and Material Map; Time of E2 Intrusion to Time of E2 Intrusion Plus 200 Years [Scenarios S4-BF through S6-BF]

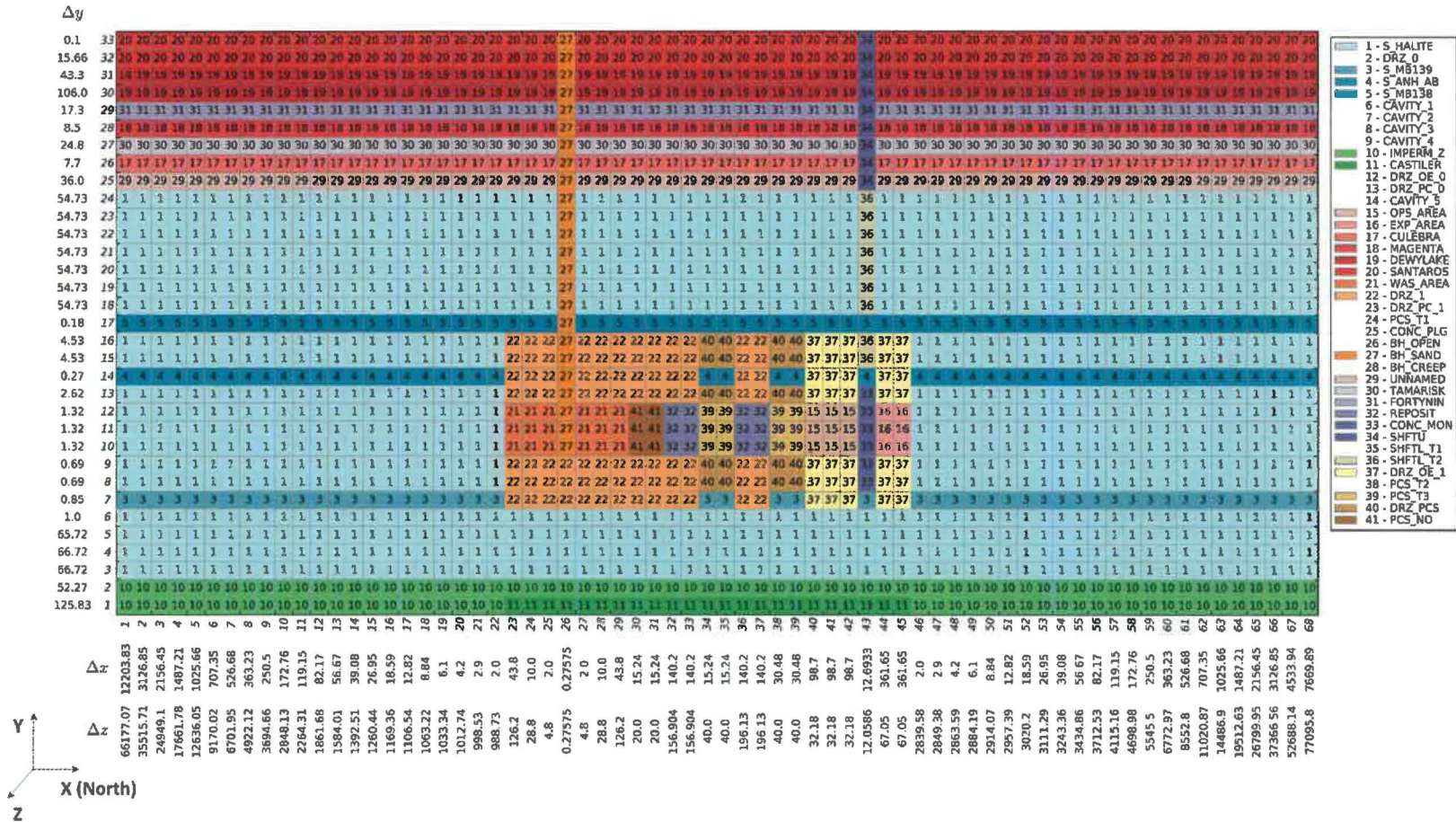


Figure 8 – CRA-2019 PA BRAGFLO Grid and Material Map; Time of E2 Intrusion Plus 200 Years to 10000 Years [Scenarios S4-BF and S5-BF], Time of E2 Intrusion Plus 200 Years to Time of E1 Intrusion [Scenario S6-BF]

Analysis Package for Salado Flow in the 2019 Compliance Recertification Application Performance Assessment (CRA-2019 PA)
 Rev. 0, ERMS 571368

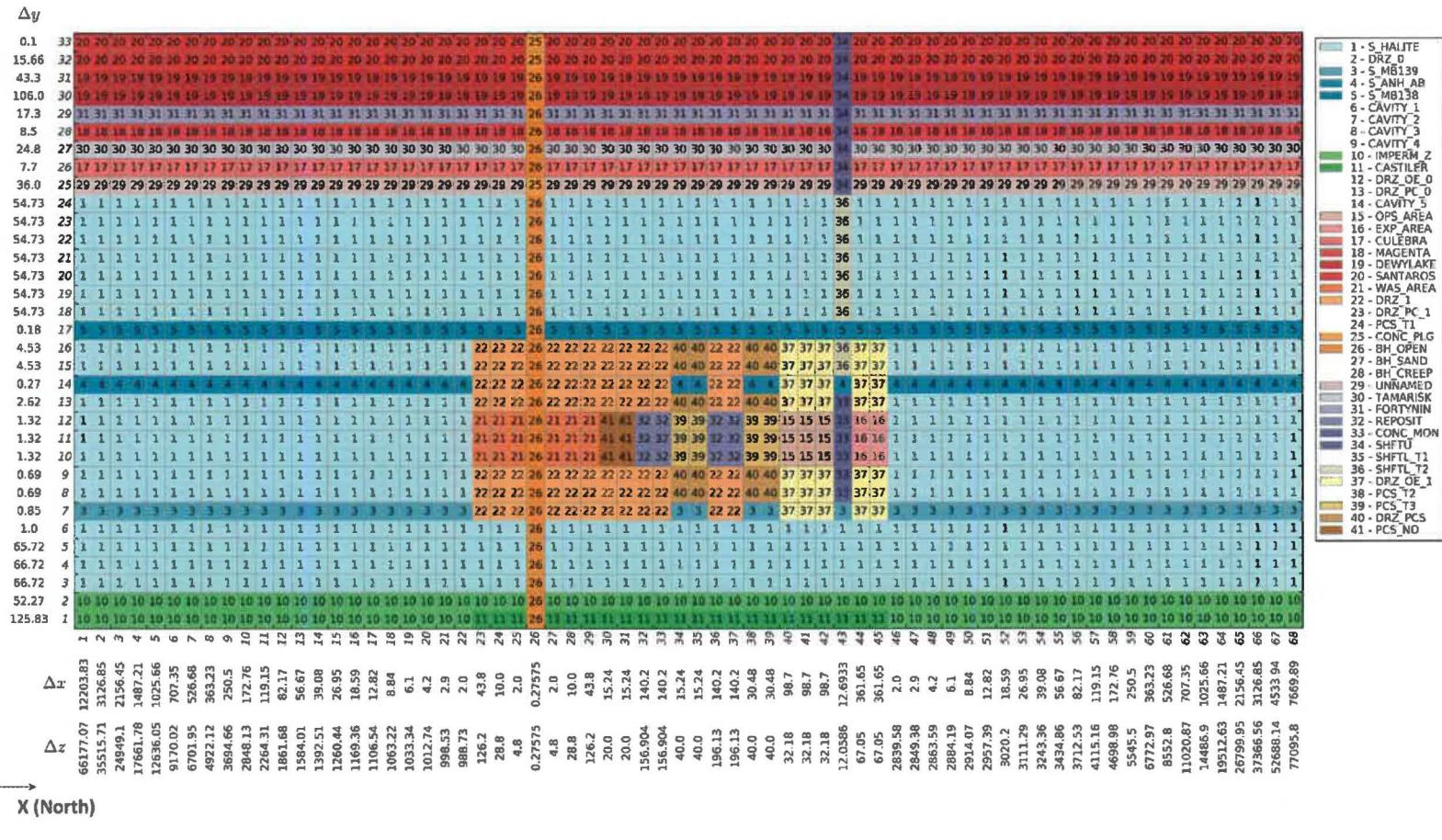


Figure 9 – CRA-2019 PA BRAGFLO Grid and Material Map; Time of E1 Intrusion to Time of E1 Intrusion Plus 200 Years [Scenarios S2-BF and S3-BF]

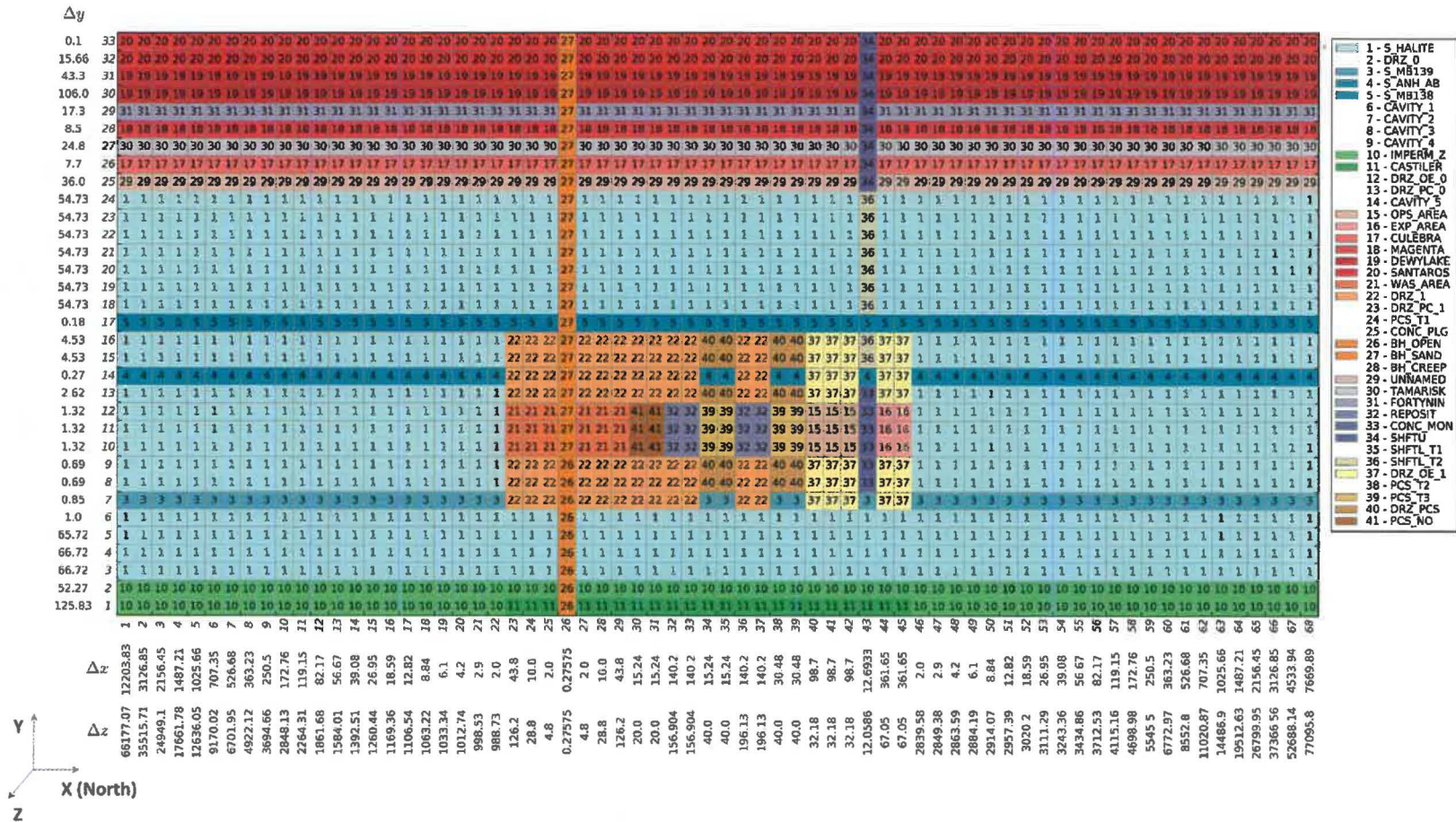


Figure 10 – CRA-2019 PA BRAGFLO Grid and Material Map; Time of E1 Intrusion to Time of E1 Intrusion Plus 200 Years [Scenario S6-BF]

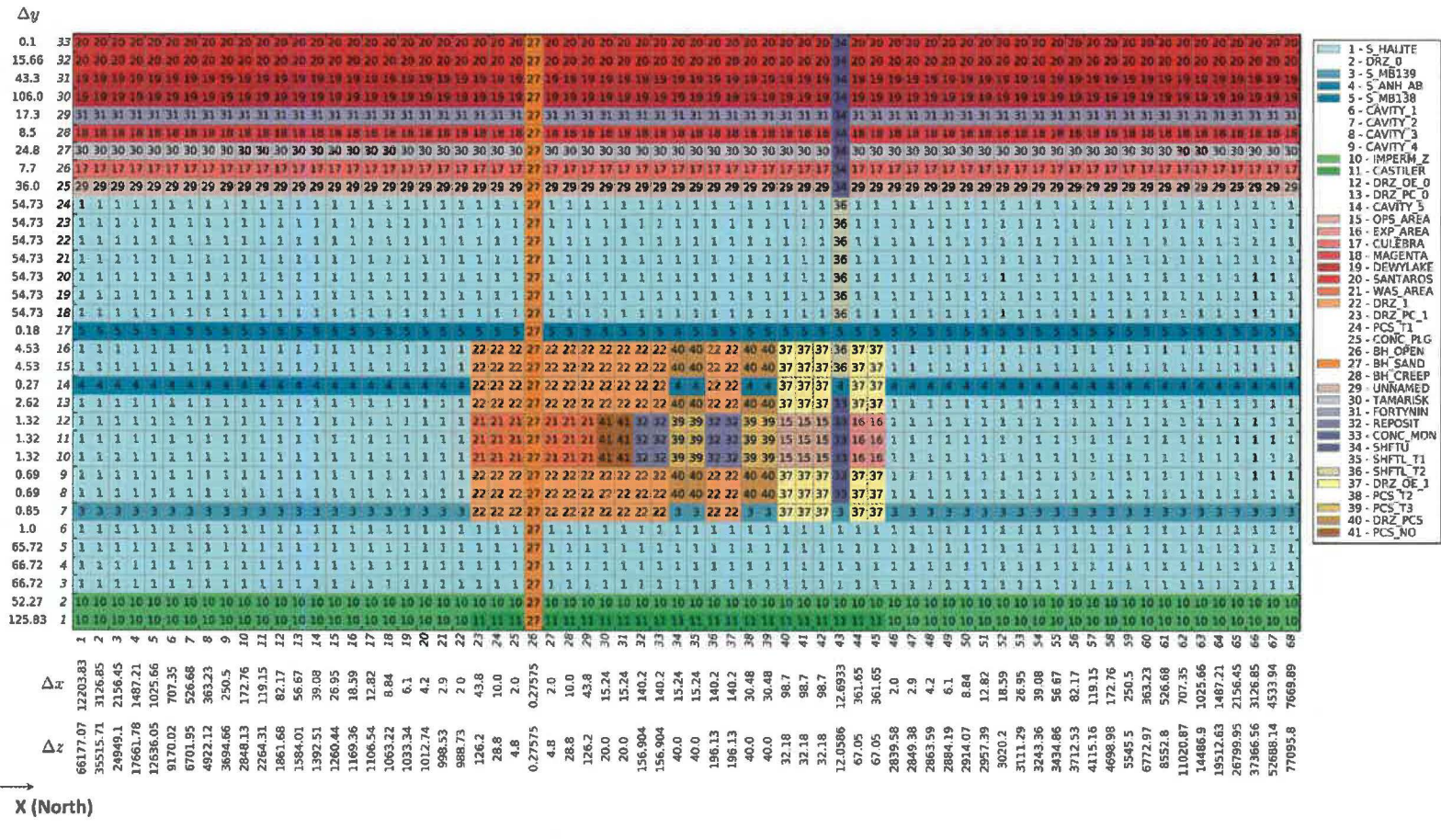


Figure 11 – CRA-2019 PA BRAGFLO Grid and Material Map; Time of E1 Intrusion Plus 200 Years to Time of E1 Intrusion Plus 1200 Years [Scenarios S2-BF, S3-BF, and S6-BF]

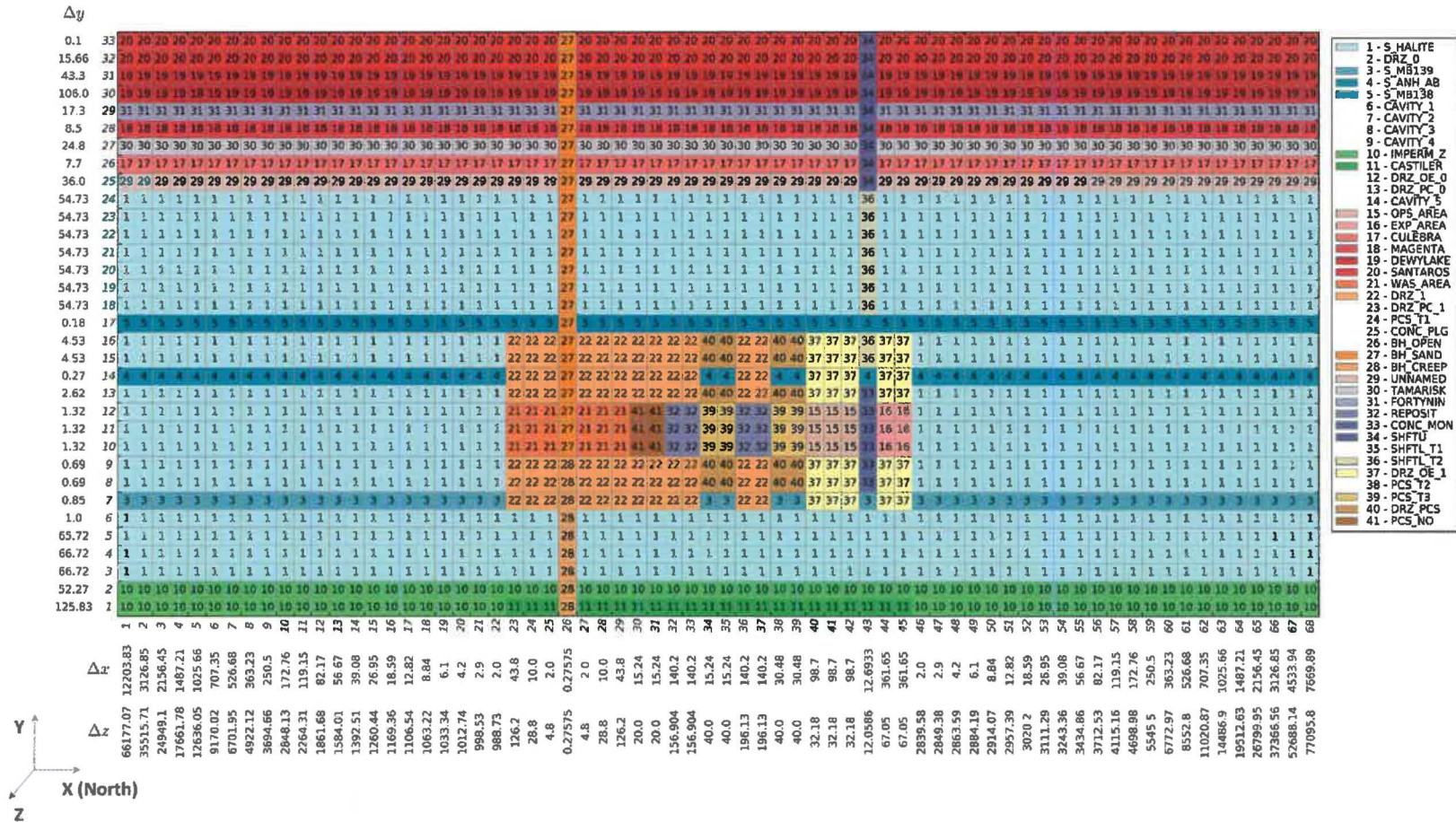


Figure 12 – CRA-2019 PA BRAGFLO Grid and Material Map; Time of E1 Intrusion Plus 1200 Years to 10000 Years [Scenarios S2-BF, S3-BF, and S6-BF]

This page intentionally left blank.

3.3 Code Execution and Run Control

Execution of the 1800 separate (3 replicates, 6 scenarios, 100 vectors) Salado flow simulations requires a series of steps which are automated by the WIPP PA Run Control system. A flow diagram that illustrates the execution order for the Salado flow solution is provided in Figure 13. A full description of the run control for the CRA19 analysis, including names and locations of input and output files, can be found in Long (2019). As outlined in AP-181 (Zeitler 2019a), in cases where comparisons are made to the CRA-2014 PA results, the CRA14 (Rev. 2) results from the Solaris migration integration tests are used (Kirchner et al. 2014, Kirchner et al. 2015) – for BRAGFLO results, these CRA14 (Rev. 2) results are the same as the CRA14 (Rev. 0) values (Kirchner 2013, Long 2013).

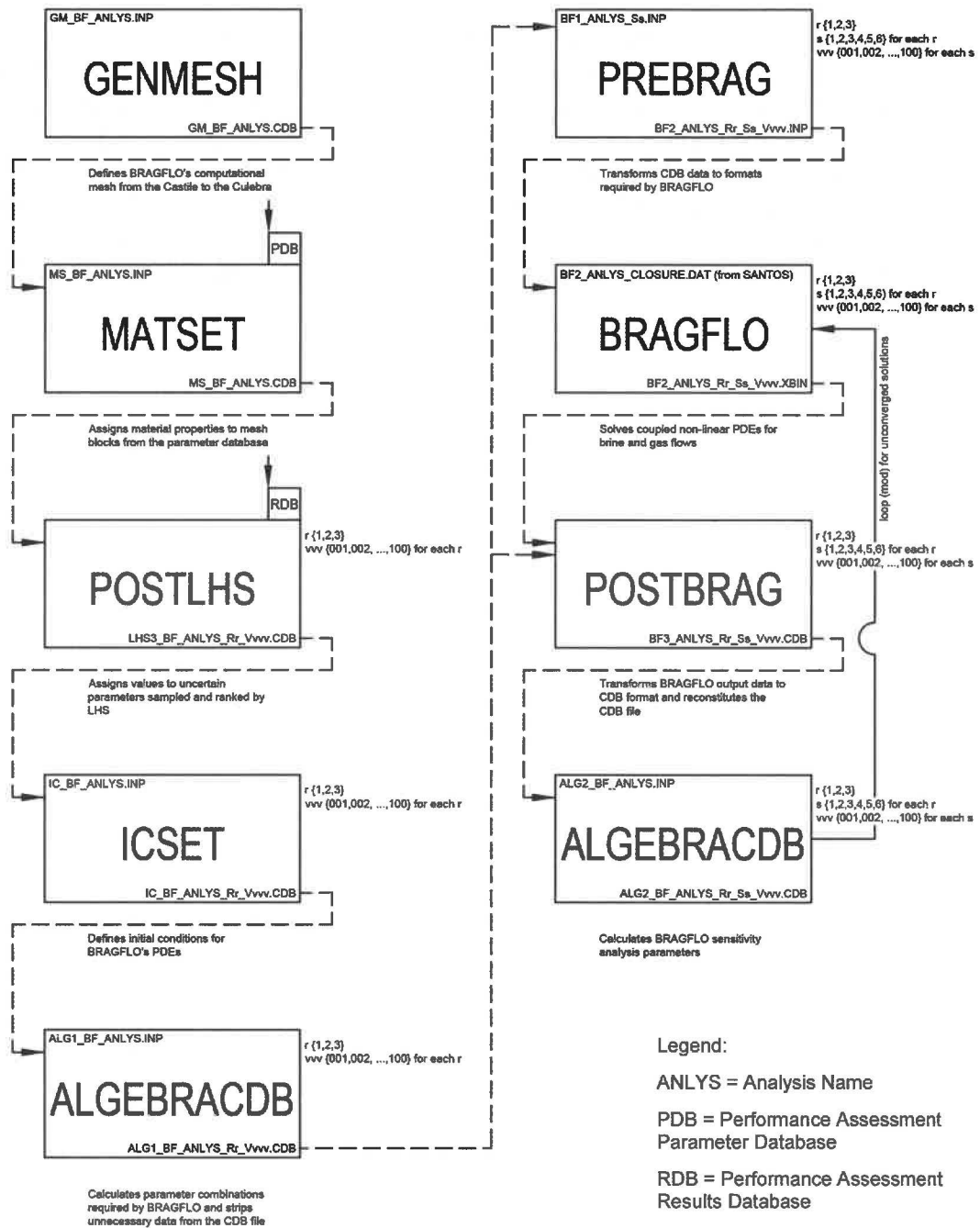


Figure 13 – Salado Flow Run Control Diagram

4.0 RESULTS

Salado flow results obtained after incorporating the changes summarized in Section 1.1 for the CRA-2019 PA are now compared with those obtained in the CRA-2014 PA. Results are discussed in terms of overall means. Overall means are obtained by forming the average of all realizations obtained for a given quantity and scenario. In WIPP PA, a replicate consists of 100 calculated realizations (vectors). Three replicates were used to generate results for CRA19 and CRA14. Means and statistics presented for the analyses are also calculated over all three replicates.

Results are presented in terms of volume-averaged quantities. For example, volume-averaged pressure is obtained by forming the product of grid block pressure and grid block volume for each grid block in the region of concern, summing this product up over all grid blocks in the region, and dividing by the bulk volume of the region. All other volume-averaged quantities are computed in the same manner. Cumulative flow volumes are also presented. Cumulative flow into a region is defined as the flow into a region integrated over time.

Results are presented for the undisturbed scenario S1-BF. Results associated with intrusions are presented for scenarios S2-BF and S4-BF, as these are representative of the intrusions considered in scenarios S3-BF and S5-BF, respectively, with the only differences being the timing of drilling intrusions. Results from BRAGFLO scenario S6-BF are also discussed. In the results that follow, summary statistics and plots were generated with Python, an open-source software package.

4.1 Pressure

The physical changes to the modeled repository associated with abandonment of the southernmost panel closure area, increased length of the northernmost panel closure area, increased volume of the experimental area along with gas generation and brine consumption changes resulting from an increased iron corrosion rate, addition of radiolytic gas generation, removal of iron sulfidation reactions, and increase in inventory quantities for iron and cellulose that are available for corrosion and biodegradation all impact repository pressures. Plots of mean brine pressure for the experimental area, operations area, north rest-of-repository, south rest-of-repository, and the waste panel are shown in Figure 14 to Figure 33.

For both undisturbed (S1-BF) and E2 intruded (S4-BF) scenarios, pressure within the operations and experimental areas for CRA19 are suppressed in comparison to CRA14 due to the modest change in pressures within the waste areas in concert with increased experimental area void space and enhanced isolation due to the increased length of the northernmost panel closure (Figure 14, Figure 16, Figure 18, and Figure 20). For E1 (S2-BF) and E2E1 (S6-BF) intruded scenarios that intersect the hypothetical Castile brine reservoir, pressure within the operations and experimental areas for CRA19 are increased in comparison to CRA14 due to the increase in pressures within the waste areas that results in additional gas flow to the north from the waste areas (Figure 15, Figure 17, Figure 19, and Figure 21).

Pressures within the north rest-of-repository are generally increased over all scenarios for CRA19 in comparison to CRA14 due to increased gas generation at early times for S1-BF and S4-BF and over all time for S2-BF and S6-BF (Figure 22 - Figure 25). Pressures within the

north rest-of-repository are increased by gas flow from the south to north and the slightly enhanced isolation from the void space within the operations and experimental areas due to the lengthened northernmost panel closure (see Section 4.5). It is noted that gas generation rates are suppressed at later times for CRA19 in non-Castile intruded scenarios (S4-BF) due to higher early-time gas generation and brine consumption (see Section 4.2 and 4.4).

The influences on pressures discussed above are also participating in the resultant pressures within the south rest-of-repository and the waste panel. However, a primary influence on pressure is the lack of ROMPCS in the southernmost panel closure to separate these two waste areas. For undisturbed (S1-BF) and E2 intruded (S4-BF) scenarios, the lack of emplaced ROMPCS allows for pressure equilibration between the south rest-of-repository and the waste panel. With waste panel pressures historically being higher than pressures in the south rest-of-repository, the pressures in the south rest-of-repository are increased over all time for CRA19 in comparison to CRA14 for S1-BF and S4-BF while the pressures in the waste panel area are slightly higher early (due to increased early-time gas generation) and less at later times (due to equilibration) (Figure 26, Figure 28, Figure 30, and Figure 32). For scenarios that intersect the hypothetical Castile brine reservoir (S2-BF and S6-BF), the lack of ROMPCS and pressure equilibration is exacerbated by flooding of both the waste panel and the south rest-of-repository with brine. This flooding substantially increases brine saturations (see Section 4.2) within the south rest-of-repository which causes a much higher quantity of gas generation (see Section 4.4) and substantially increases pressures within these areas for CRA19 in comparison to CRA14 (Figure 27, Figure 29, Figure 31, and Figure 33).

Pressure statistics for CRA19 and CRA14 are summarized in Table 17 and Table 18. Table 17 provides the 3-replicate mean (integrated over time) and 3-replicate maximum (over all time) pressure values. Table 18 provides the maximum pressure (over all time) for all individual vectors. The 3-replicate mean and maximum pressures for CRA19 as compared to CRA14 report mixed trends for pressures as both a function of scenario and location due to the interacting modifications described previously. The individual vector maximum pressure values for CRA19 are increased over CRA14 for all reported areas and scenarios with one exception – the slight reduction in maximum individual vector pressure within the waste panel for S4-BF.

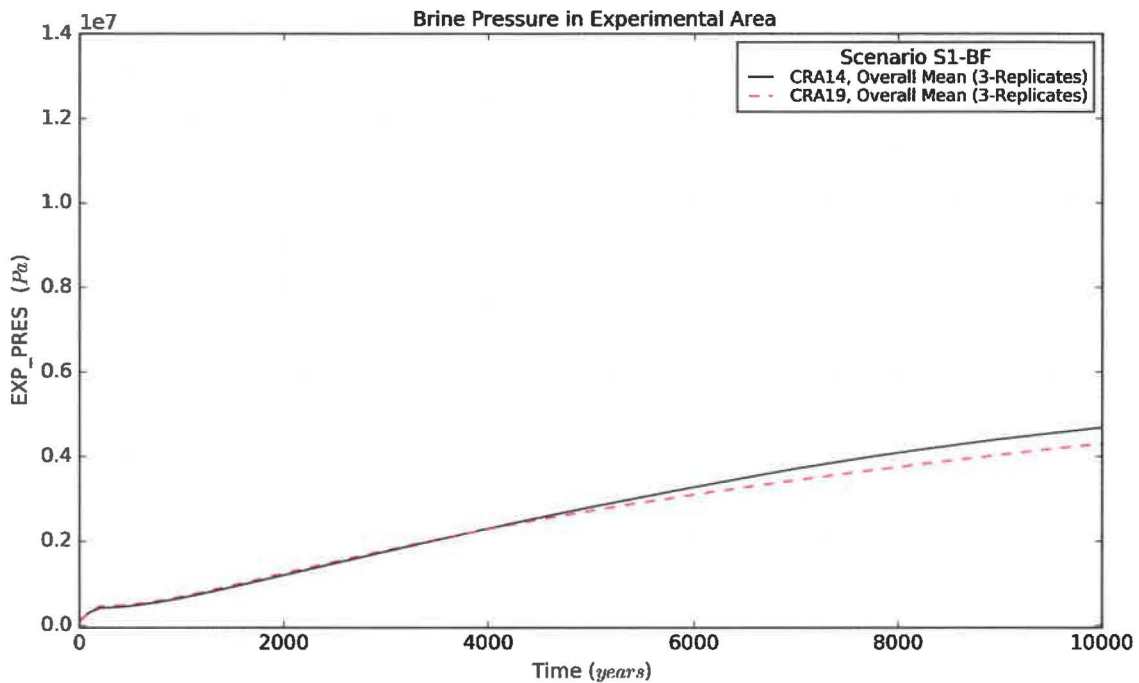


Figure 14 – Pressure Means for the Experimental Area, Scenario S1-BF

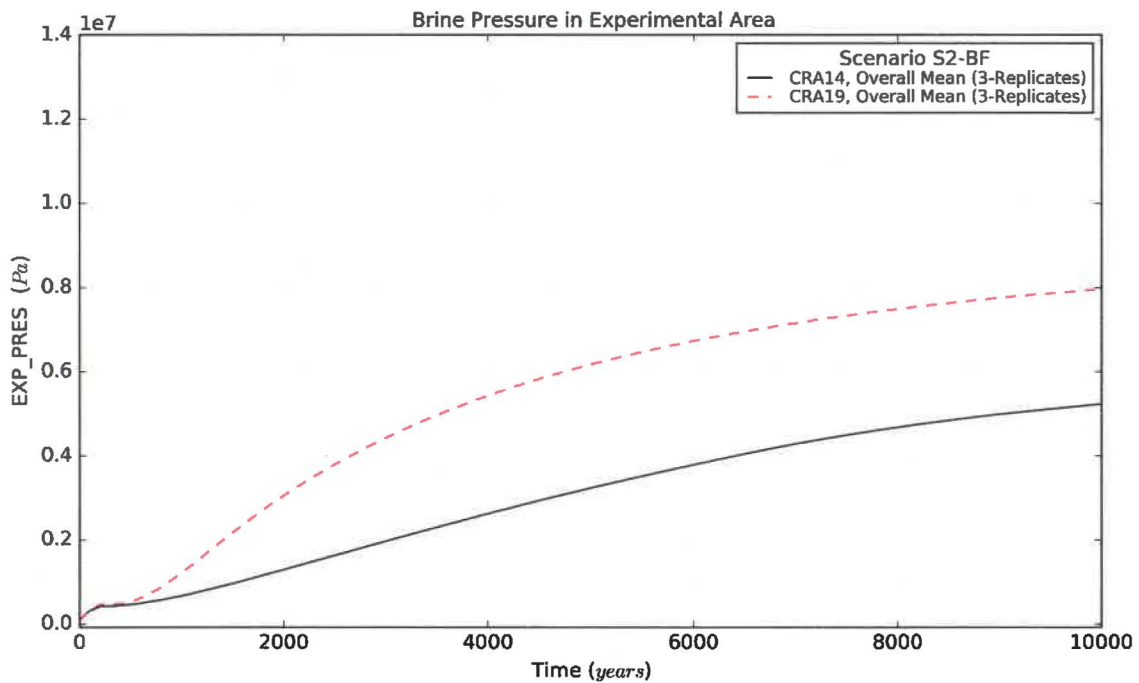


Figure 15 – Pressure Means for the Experimental Area, Scenario S2-BF

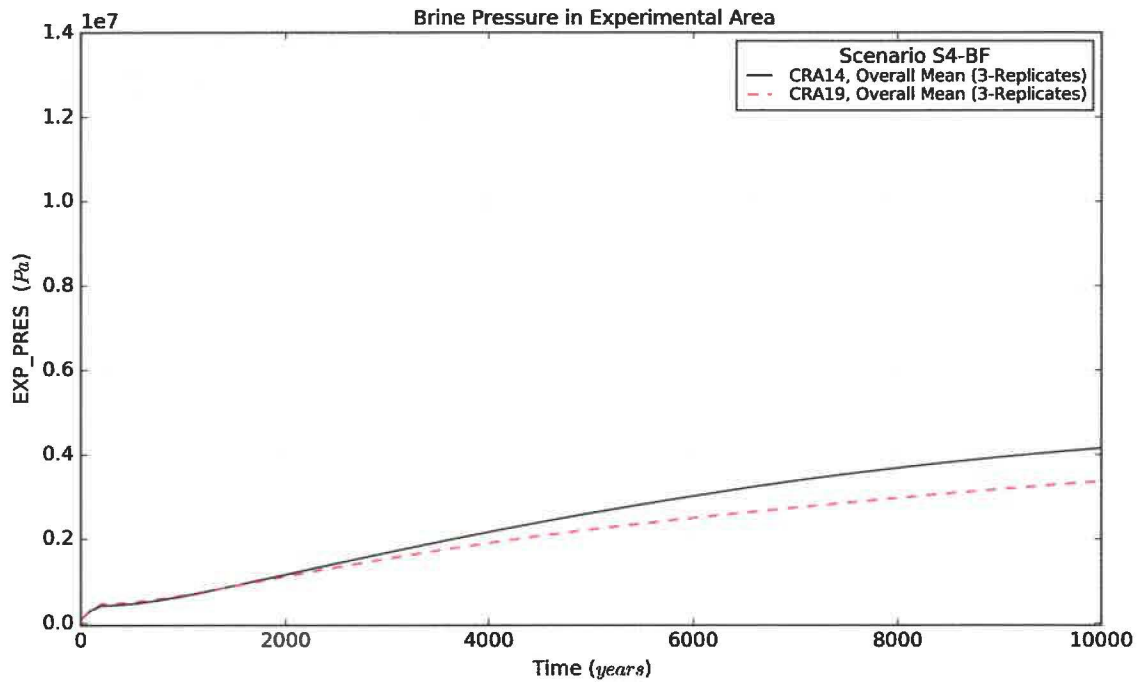


Figure 16 – Pressure Means for the Experimental Area, Scenario S4-BF

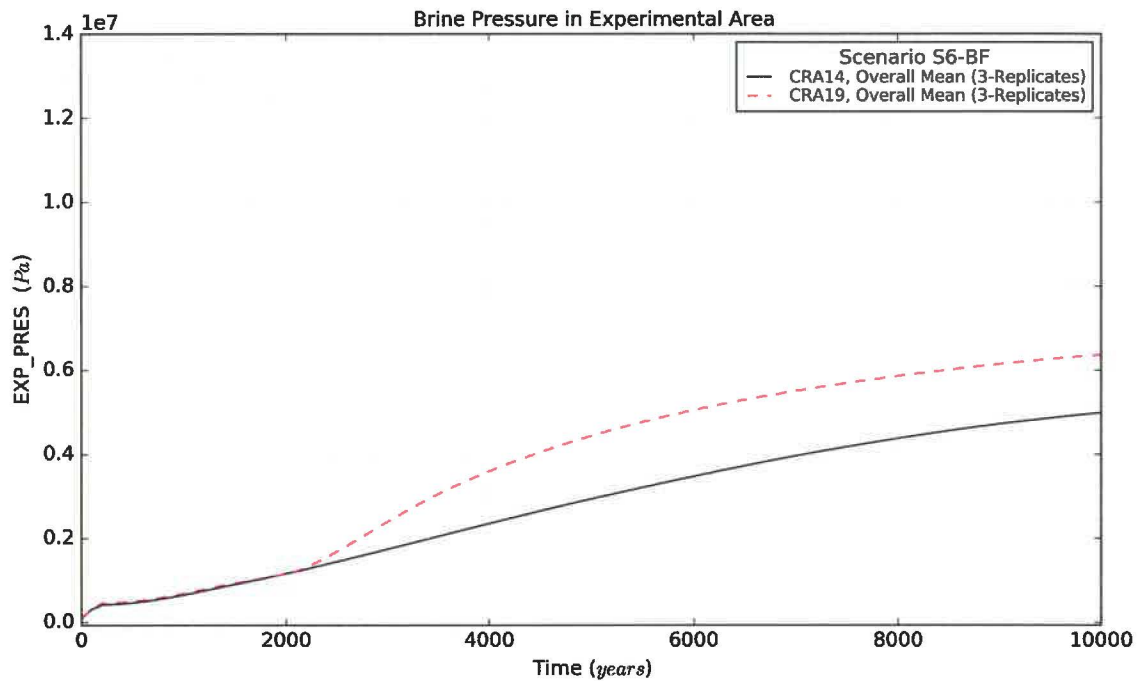


Figure 17 – Pressure Means for the Experimental Area, Scenario S6-BF

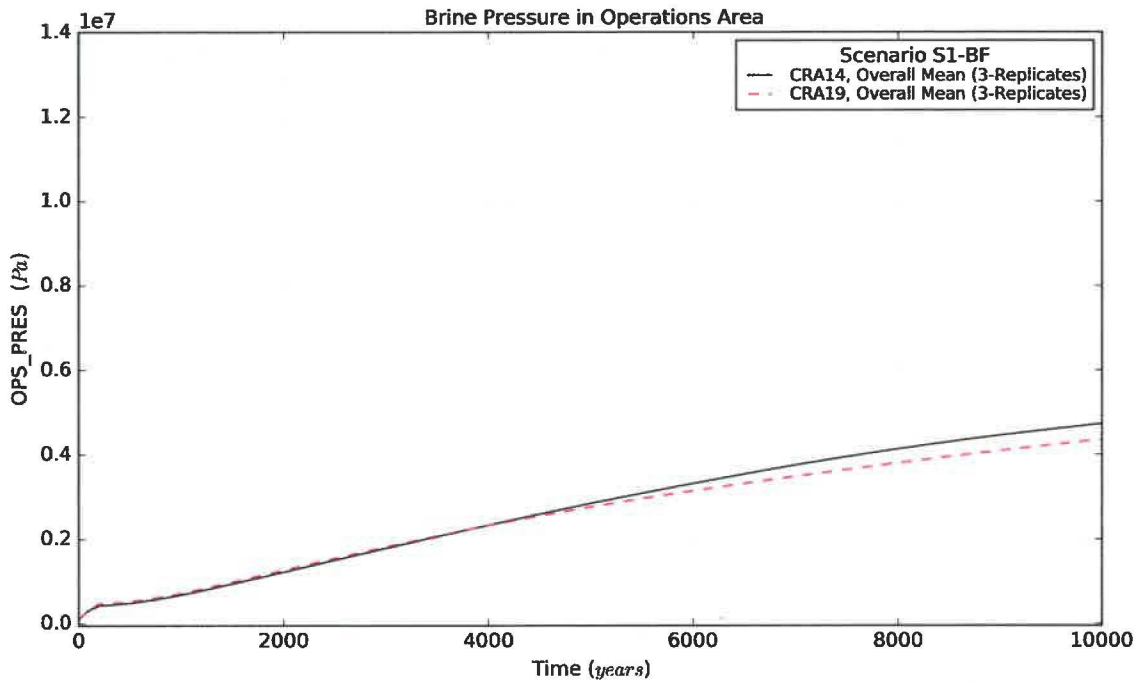


Figure 18 – Pressure Means for the Operations Area, Scenario S1-BF

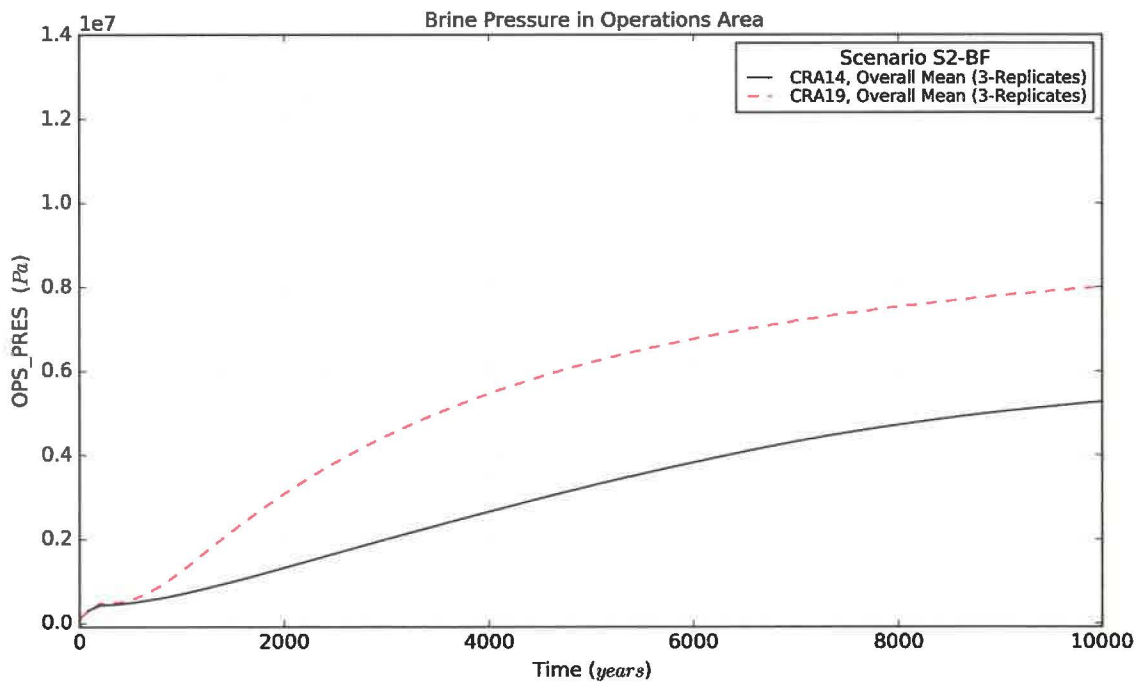


Figure 19 – Pressure Means for the Operations Area, Scenario S2-BF

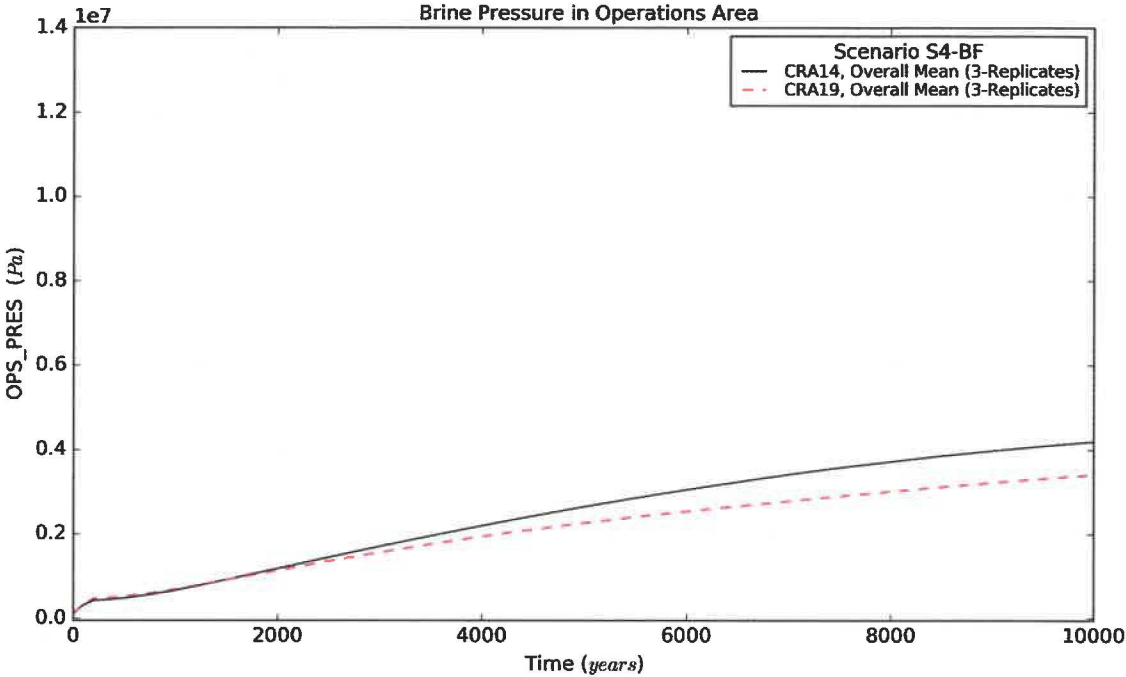


Figure 20 – Pressure Means for the Operations Area, Scenario S4-BF

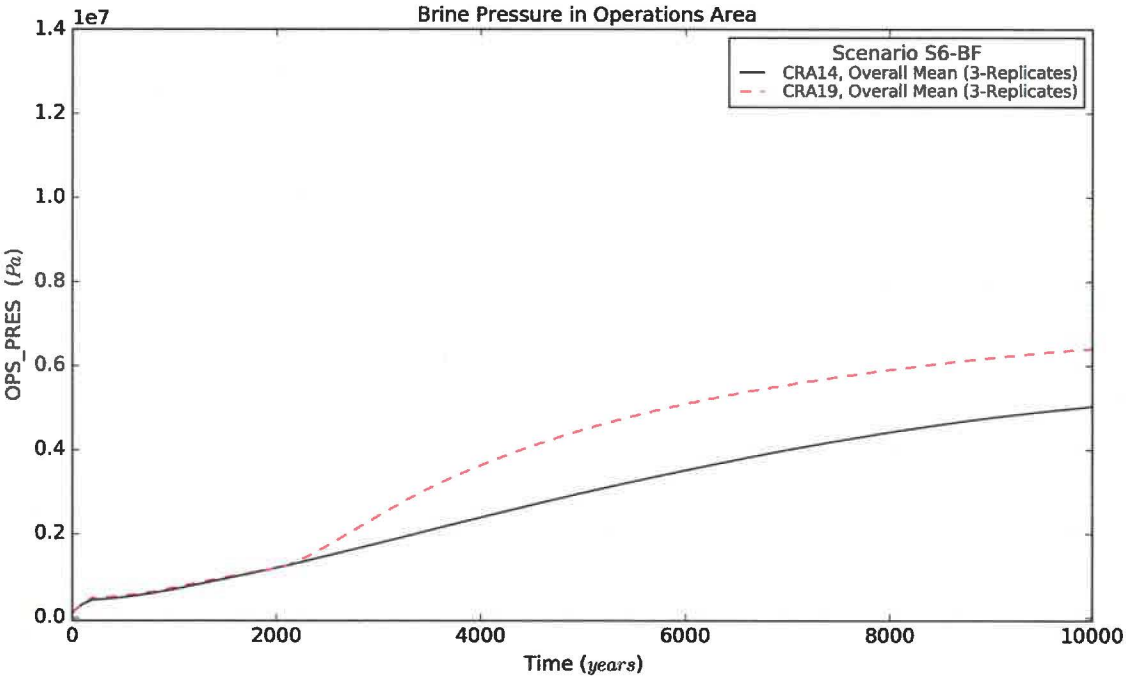


Figure 21 – Pressure Means for the Operations Area, Scenario S6-BF

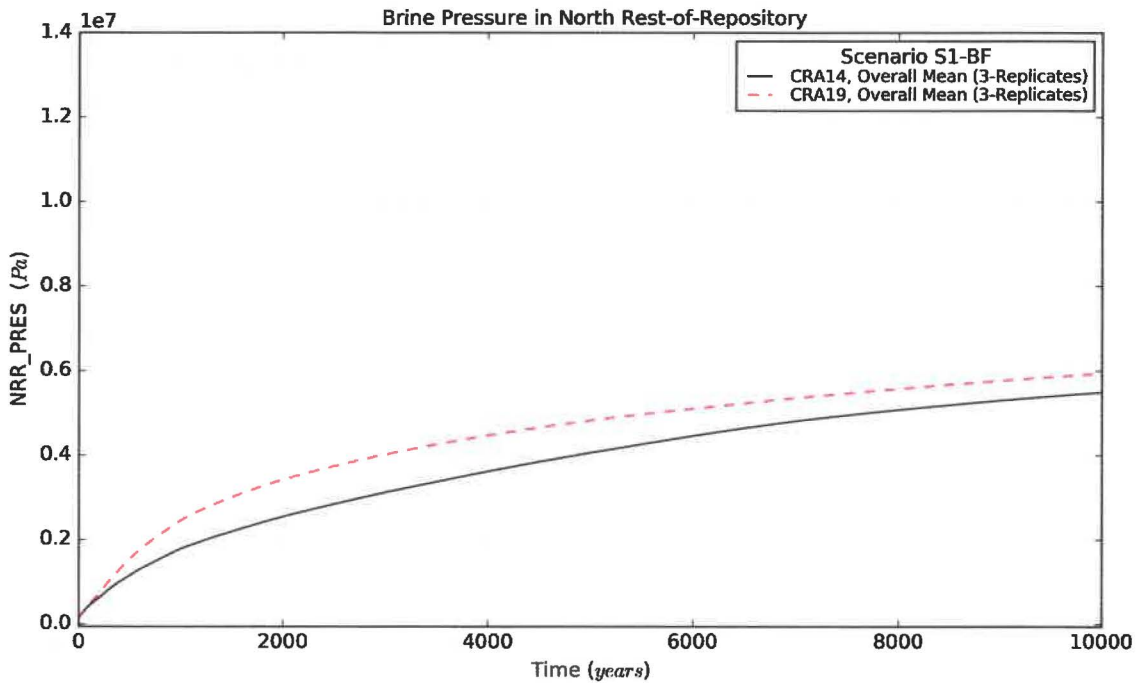


Figure 22 – Pressure Means for the North Rest-of-Repository, Scenario S1-BF

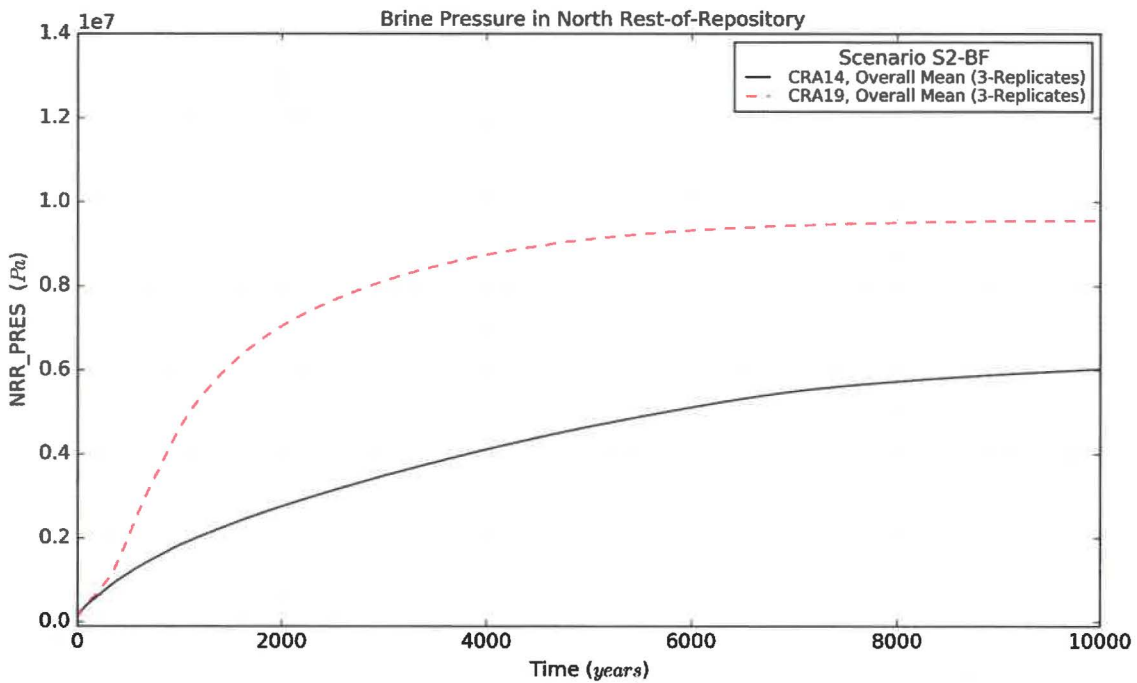


Figure 23 – Pressure Means for the North Rest-of-Repository, Scenario S2-BF

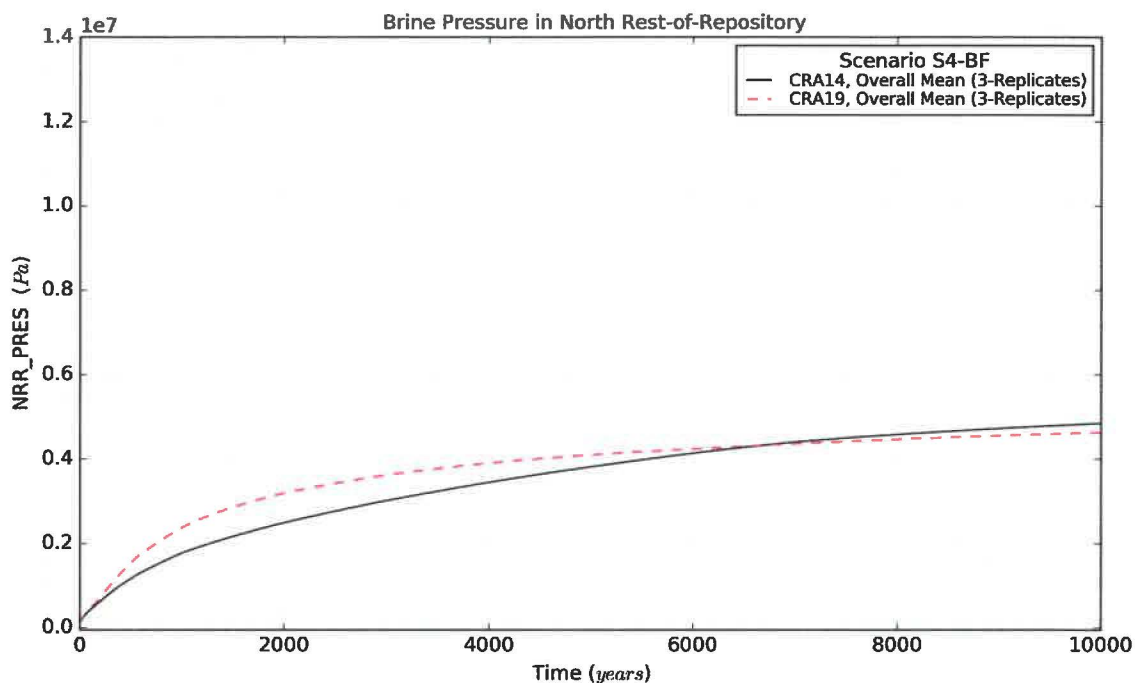


Figure 24 – Pressure Means for the North Rest-of-Repository, Scenario S4-BF

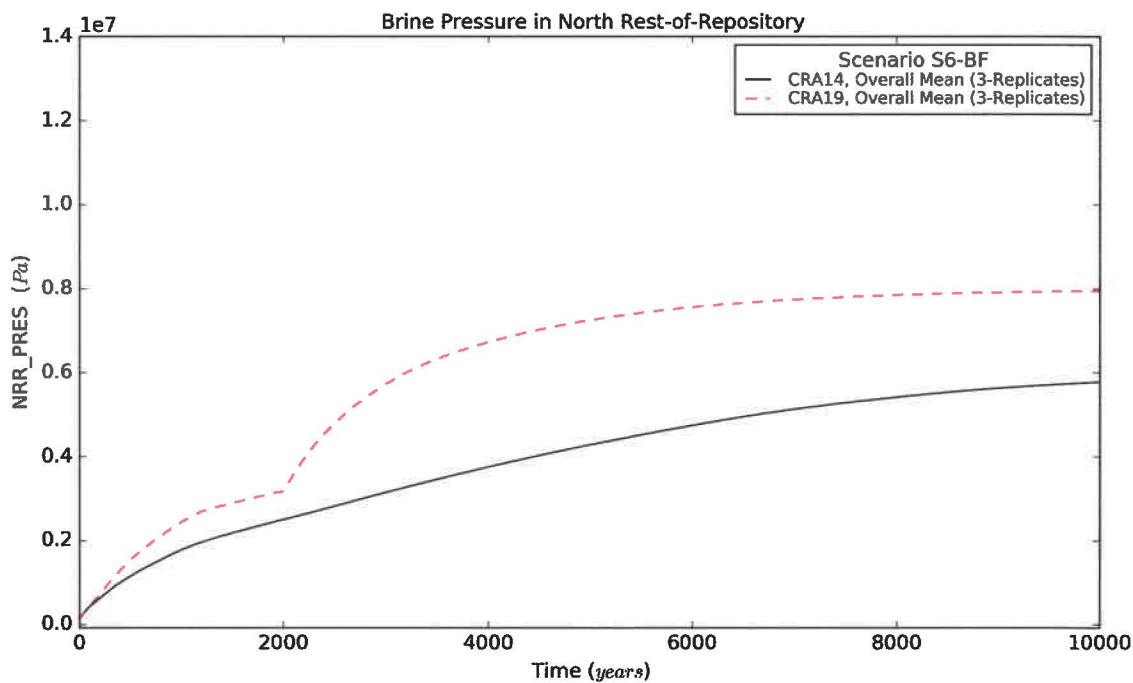


Figure 25 – Pressure Means for the North Rest-of-Repository, Scenario S6-BF

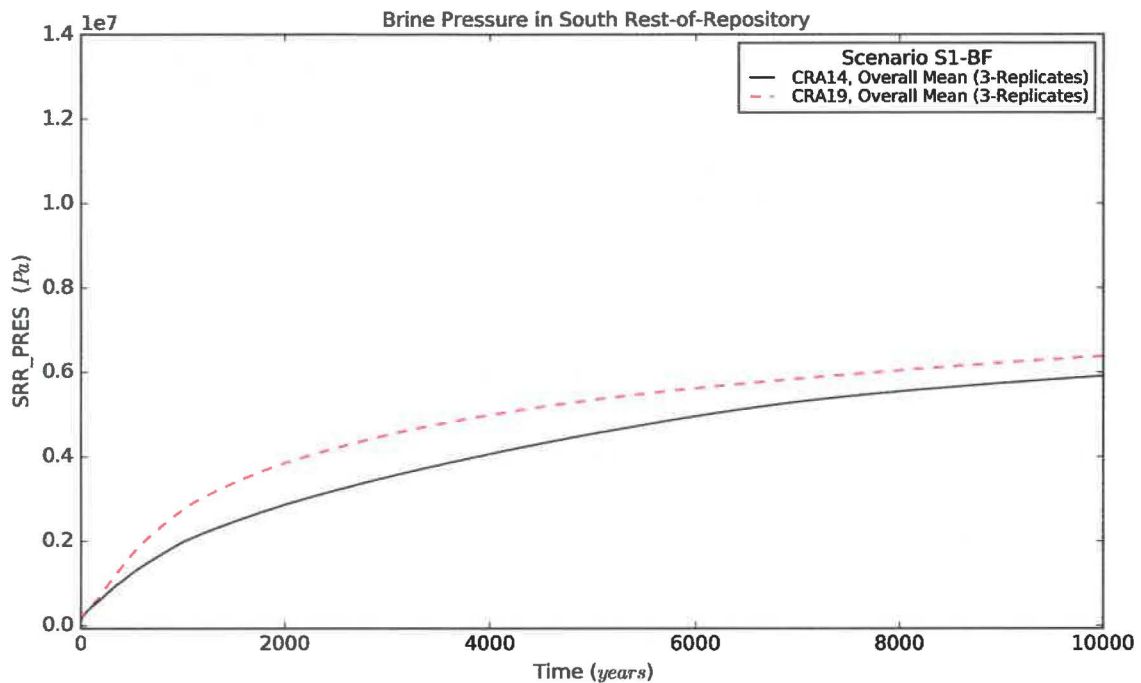


Figure 26 – Pressure Means for the South Rest-of-Repository, Scenario S1-BF

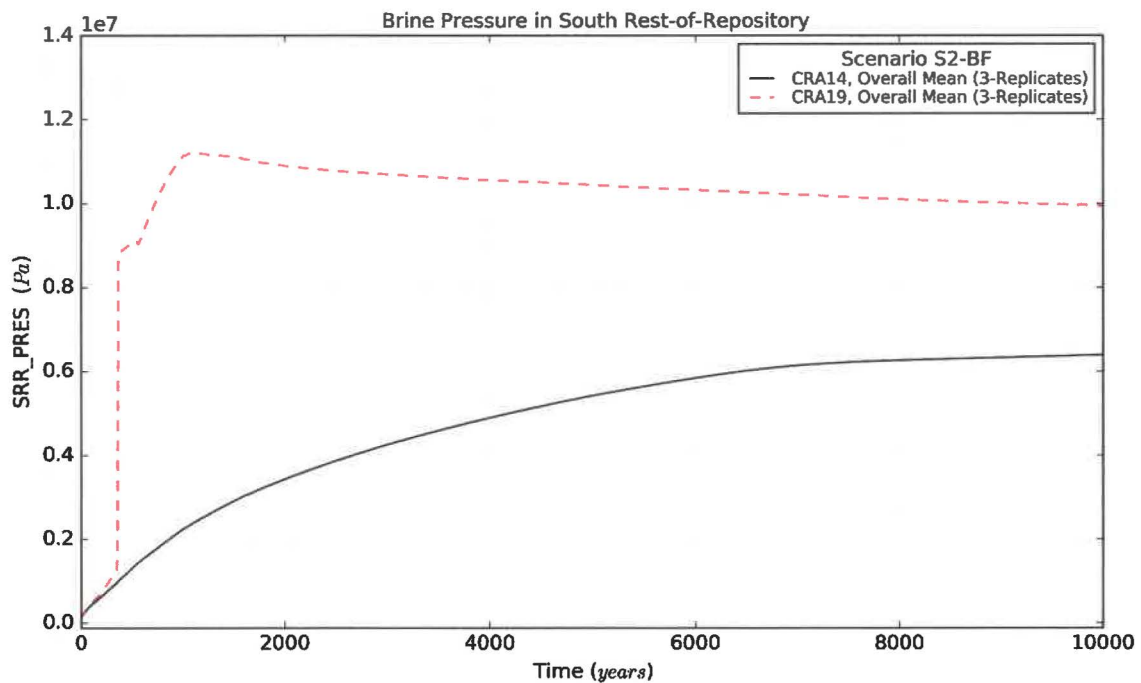


Figure 27 – Pressure Means for the South Rest-of-Repository, Scenario S2-BF

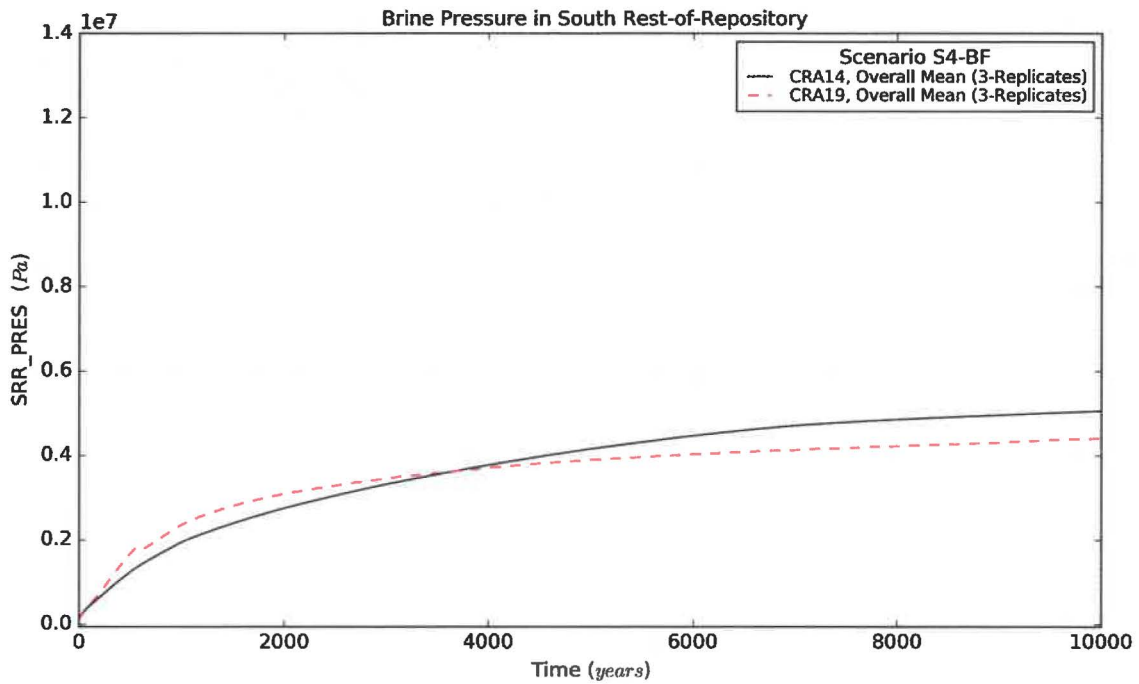


Figure 28 – Pressure Means for the South Rest-of-Repository, Scenario S4-BF

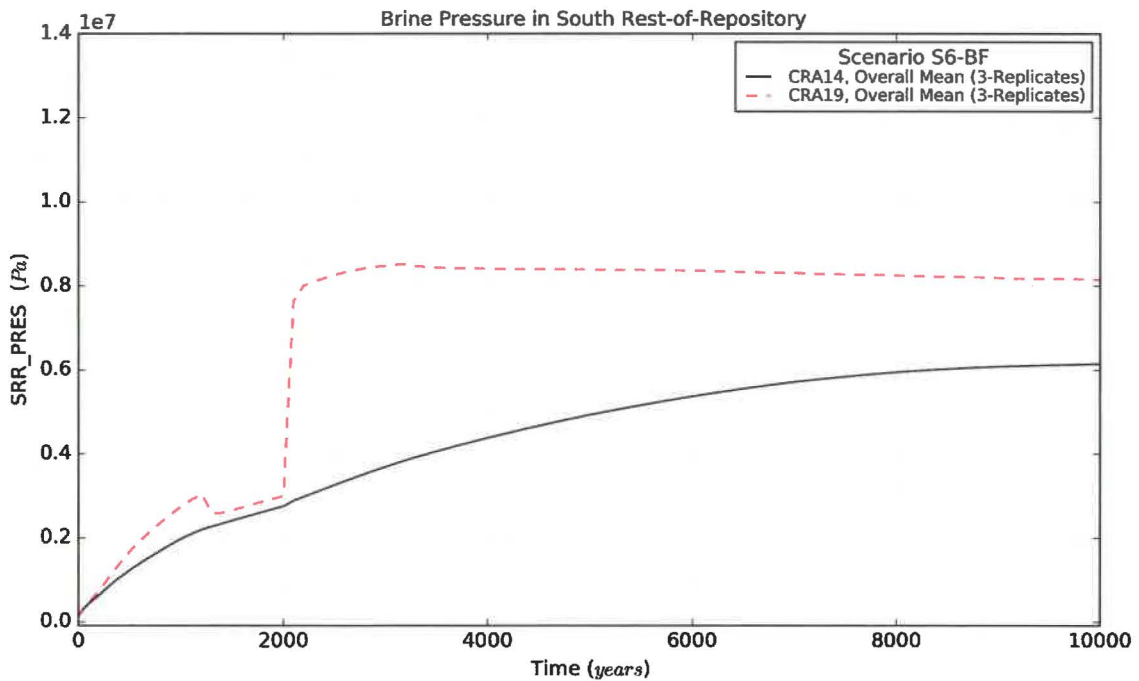


Figure 29 – Pressure Means for the South Rest-of-Repository, Scenario S6-BF

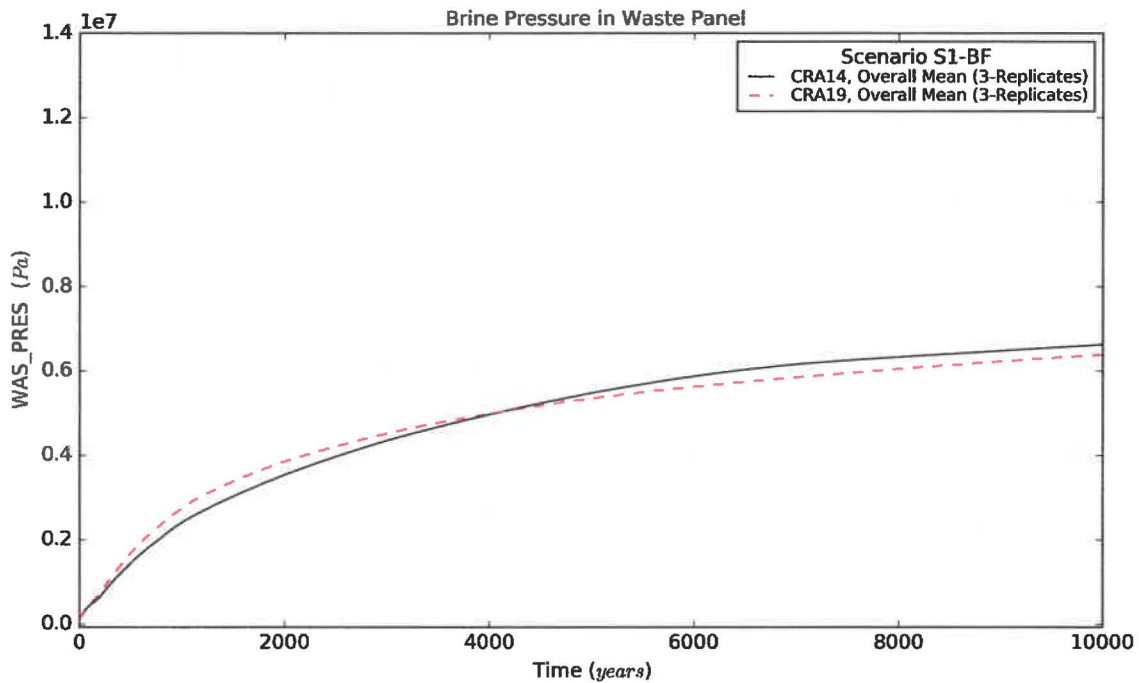


Figure 30 – Pressure Means for the Waste Panel, Scenario S1-BF

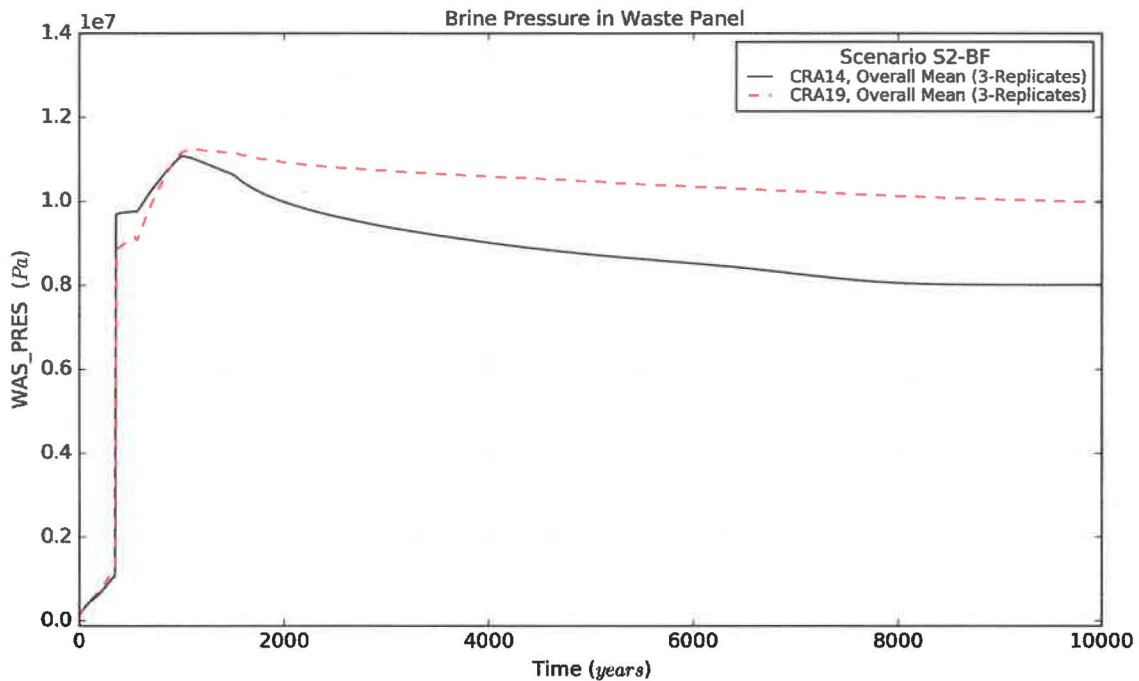


Figure 31 – Pressure Means for the Waste Panel, Scenario S2-BF

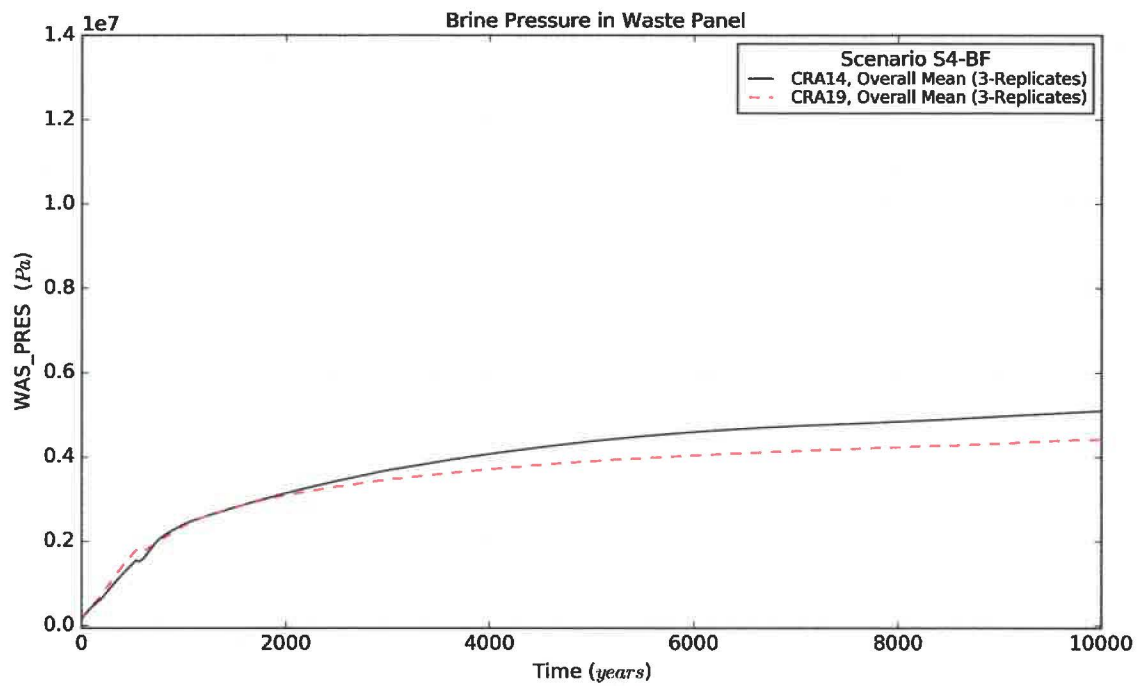


Figure 32 – Pressure Means for the Waste Panel, Scenario S4-BF

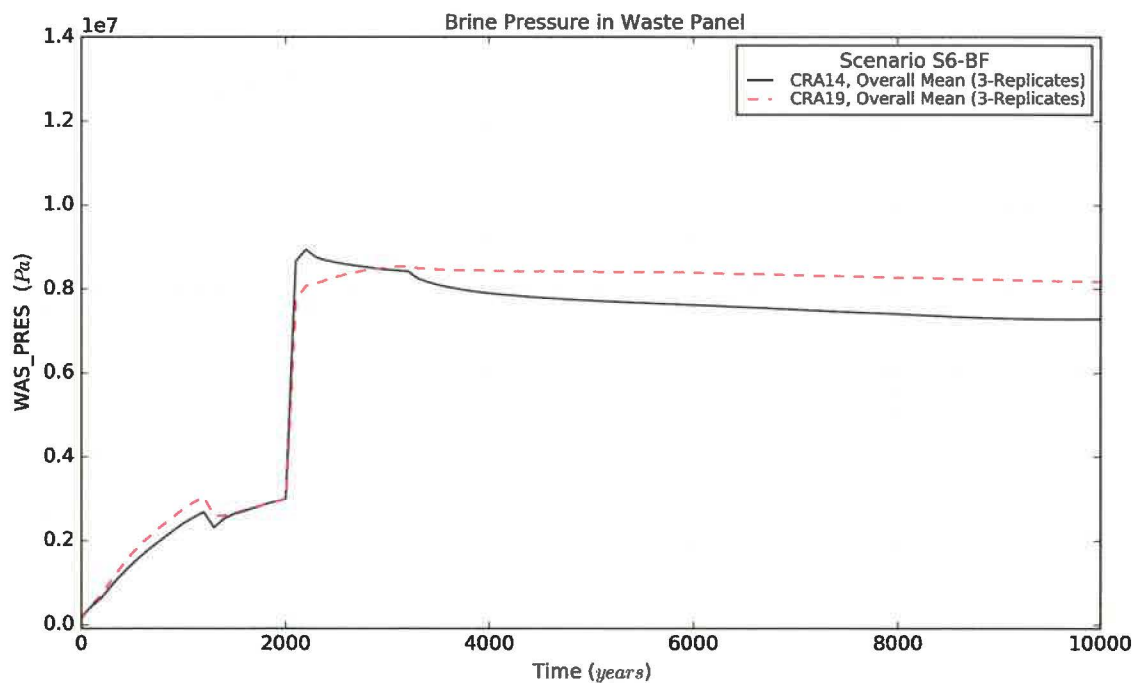


Figure 33 – Pressure Means for the Waste Panel, Scenario S6-BF

Table 17 – Pressure Statistics on Overall Means for CRA14 and CRA19

Quantity (units)	Description	Scenario	Mean Value ¹		Maximum Value ²	
			CRA14	CRA19	CRA14	CRA19
EXP_PRES (Pa)	Brine Pressure in Experimental Area	S1-BF	2.67E+06	2.54E+06	4.69E+06	4.31E+06
		S2-BF	3.03E+06	5.36E+06	5.23E+06	7.97E+06
		S4-BF	2.45E+06	2.07E+06	4.16E+06	3.37E+06
		S6-BF	2.81E+06	3.83E+06	4.99E+06	6.37E+06
OPS_PRES (Pa)	Brine Pressure in Operations Area	S1-BF	2.70E+06	2.58E+06	4.73E+06	4.36E+06
		S2-BF	3.07E+06	5.40E+06	5.28E+06	8.01E+06
		S4-BF	2.49E+06	2.11E+06	4.20E+06	3.42E+06
		S6-BF	2.84E+06	3.87E+06	5.04E+06	6.42E+06
NRR_PRES (Pa)	Brine Pressure in North Rest-of-Repository	S1-BF	3.78E+06	4.43E+06	5.49E+06	5.94E+06
		S2-BF	4.24E+06	8.05E+06	6.03E+06	9.56E+06
		S4-BF	3.51E+06	3.75E+06	4.85E+06	4.64E+06
		S6-BF	3.96E+06	6.11E+06	5.78E+06	7.96E+06
SRR_PRES (Pa)	Brine Pressure in South Rest-of-Repository	S1-BF	4.17E+06	4.87E+06	5.91E+06	6.39E+06
		S2-BF	4.83E+06	1.00E+07	6.39E+06	1.12E+07
		S4-BF	3.77E+06	3.58E+06	5.06E+06	4.41E+06
		S6-BF	4.42E+06	7.06E+06	6.15E+06	8.53E+06
WAS_PRES (Pa)	Brine Pressure in Waste Panel	S1-BF	4.92E+06	4.88E+06	6.63E+06	6.39E+06
		S2-BF	8.64E+06	1.01E+07	1.11E+07	1.13E+07
		S4-BF	3.96E+06	3.59E+06	5.10E+06	4.42E+06
		S6-BF	6.57E+06	7.08E+06	8.94E+06	8.55E+06

Notes:

- 1 Calculated as the function average (integrated) over the time interval (0-10,000 years) for the overall means (3 replicates)
- 2 Calculated as the function maximum over the time interval (0-10,000 years) for the overall means (3 replicates)

Table 18 – Pressure Statistics on Individual Vectors for CRA14 and CRA19

Quantity (units)	Description	Scenario	Maximum Value ³	
			CRA14	CRA19
EXP_PRES (Pa)	Brine Pressure in Experimental Area	S1-BF	1.43E+07	1.49E+07
		S2-BF	1.42E+07	1.61E+07
		S4-BF	1.38E+07	1.40E+07
		S6-BF	1.39E+07	1.46E+07
OPS_PRES (Pa)	Brine Pressure in Operations Area	S1-BF	1.43E+07	1.49E+07
		S2-BF	1.43E+07	1.61E+07
		S4-BF	1.39E+07	1.41E+07
		S6-BF	1.40E+07	1.47E+07
NRR_PRES (Pa)	Brine Pressure in North Rest-of-Repository	S1-BF	1.57E+07	1.74E+07
		S2-BF	1.57E+07	1.74E+07
		S4-BF	1.56E+07	1.73E+07
		S6-BF	1.56E+07	1.74E+07
SRR_PRES (Pa)	Brine Pressure in South Rest-of-Repository	S1-BF	1.58E+07	1.74E+07
		S2-BF	1.58E+07	1.81E+07
		S4-BF	1.58E+07	1.48E+07
		S6-BF	1.58E+07	1.63E+07
WAS_PRES (Pa)	Brine Pressure in Waste Panel	S1-BF	1.57E+07	1.74E+07
		S2-BF	1.62E+07	1.81E+07
		S4-BF	1.49E+07	1.48E+07
		S6-BF	1.50E+07	1.63E+07

Notes:

- 3 Calculated as the function maximum over the time interval (0-10,000 years) for all replicates (300 vectors)

4.2 Brine Saturation

Brine pressure and saturation changes in the operations and experimental areas, north rest-of-repository, south rest-of-repository, and waste panel are typically inversely related to one another as increased repository pressures tend to reduce brine infiltration into the repository (from the DRZ/Salado) and induce flow within the repository (and possibly to the nearby strata). In addition, the iron corrosion and magnesium oxide reactions (also radiolysis in CRA19), when active, consume brine faster than the other reactions generate brine, causing brine saturations to decrease over time. Brine saturations also generally increase toward the south in the repository due to the 1-degree Salado dip and the associated gravity-driven flow of brine.

This general trend of inversely related pressures and saturations is maintained for CRA19 in the experimental area, operations area, and north rest-of-repository for all scenarios (Figure 34 - Figure 45), with the saturations in the north rest-of-repository being reduced for CRA19 in comparison to CRA14. Furthermore, the trend is maintained for the south rest-of-repository in the undisturbed (S1-BF) and E2 intruded (S4-BF) scenarios (Figure 46 and Figure 48). In contrast, the south rest-of-repository experiences substantial increases in brine saturation under scenarios that intersect the hypothetical Castile brine reservoir (S2-BF and S6-BF) due to the inflow of brine from the waste panel across the southernmost panel closure area that lacks an ROMPCS (Figure 47 and Figure 49). Although brine pressure in the waste panel is initially increased for CRA19 in comparison to CRA14 at early times and then decreased thereafter for the unintruded (S1-BF) and E2 intruded (S4-BF) scenarios, brine saturation within the waste panel is reduced for CRA19 over all time (Figure 50 and Figure 52). The saturation reductions in the waste panel under S1-BF and S4-BF are attributed to the substantially increased brine consumption in the waste panel as a result of inventory increases in cellulose and iron, increased inundated iron corrosion rates, and the application of radiolytic gas generation for CRA19 in comparison to CRA14 (see Section 4.4). For E1 (S2-BF) and E2E1 (S6-BF) intruded scenarios that intersect the hypothetical Castile brine reservoir, saturations within the waste area for CRA19 are decreased in comparison to CRA14 due to the increase in pressures within the waste areas that result in increased south to north brine flow out of the waste area into the south rest-of-repository across the “open” southernmost panel closure area (Figure 51 and Figure 53).

Brine saturation statistics for CRA19 and CRA14 are summarized in Table 19 and Table 20. Table 19 provides the 3-replicate mean (integrated over time) and 3-replicate maximum (over all time) brine saturation values. Table 20 provides the maximum brine saturation (over all time) for all individual vectors. The 3-replicate mean and maximum brine saturations for CRA19 as compared to CRA14 report mixed trends for saturation as both a function of scenario and location due to the interacting modifications described previously. The individual vector maximum brine saturation values for CRA19 are the same or decreased under CRA14 for all reported areas and scenarios with three exceptions – the slight increase in maximum individual vector brine saturation within the south rest-of-repository for S2-BF, S4-BF, and S6-BF.

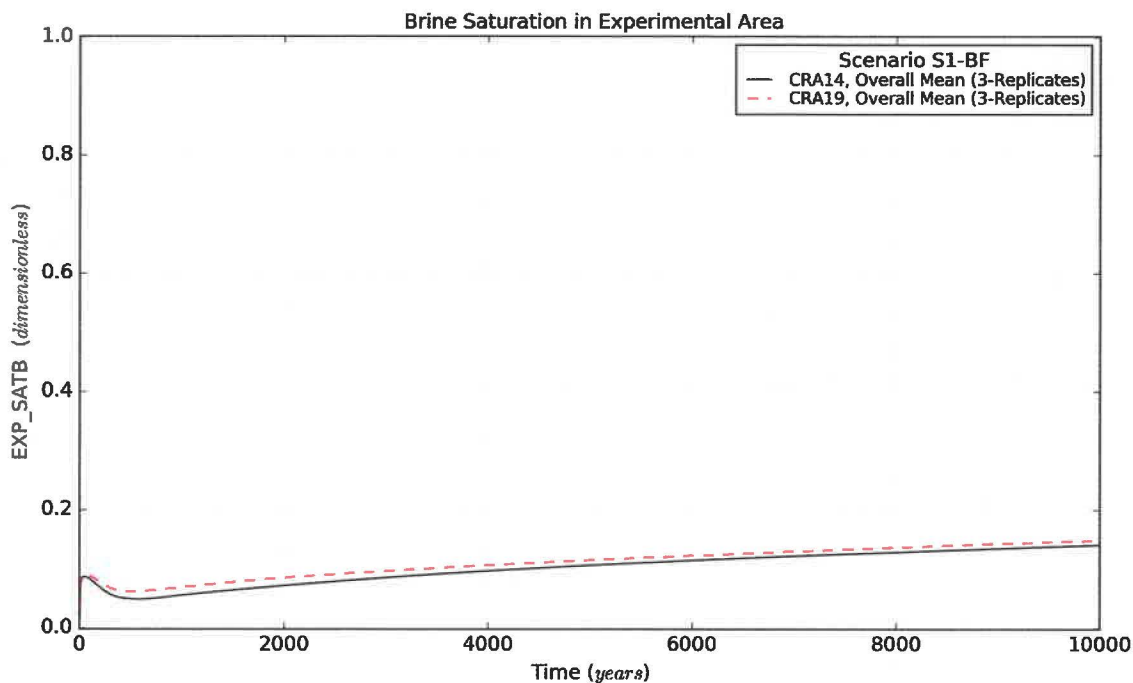


Figure 34 – Brine Saturation Means for the Experimental Area, Scenario S1-BF

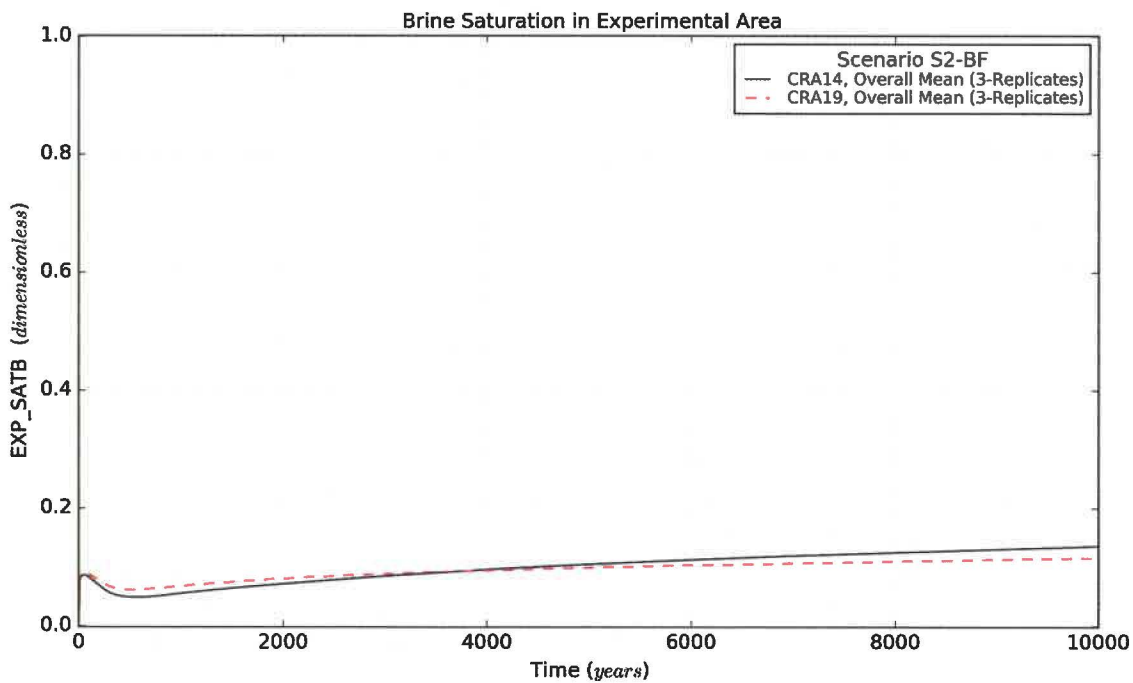


Figure 35 – Brine Saturation Means for the Experimental Area, Scenario S2-BF

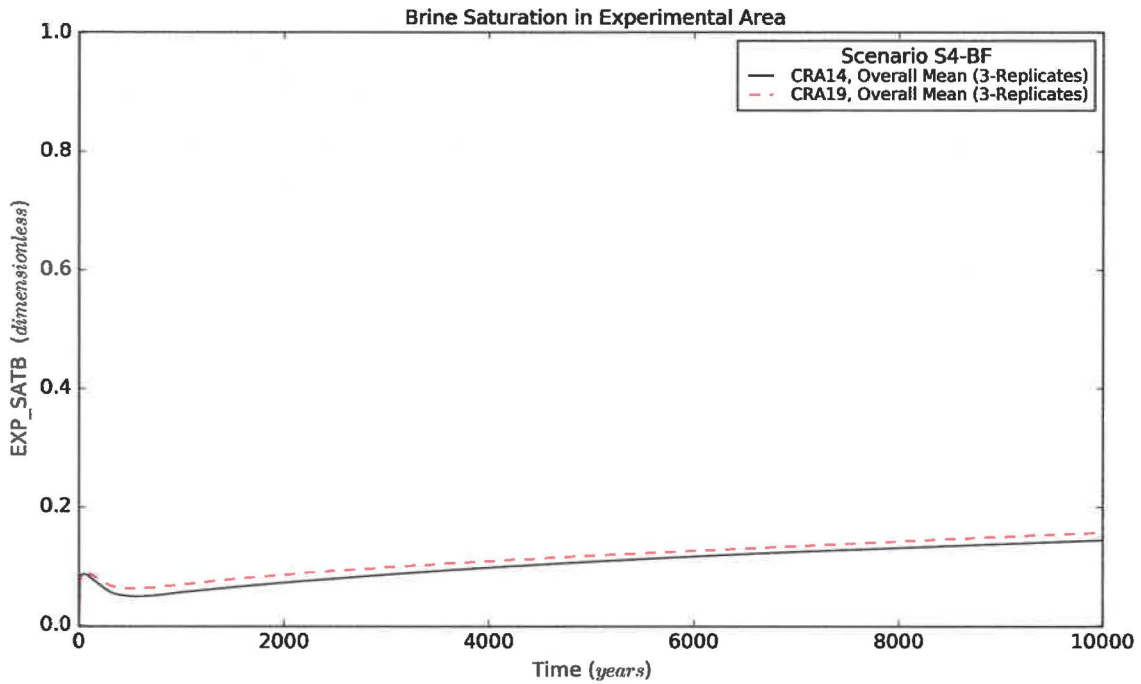


Figure 36 – Brine Saturation Means for the Experimental Area, Scenario S4-BF

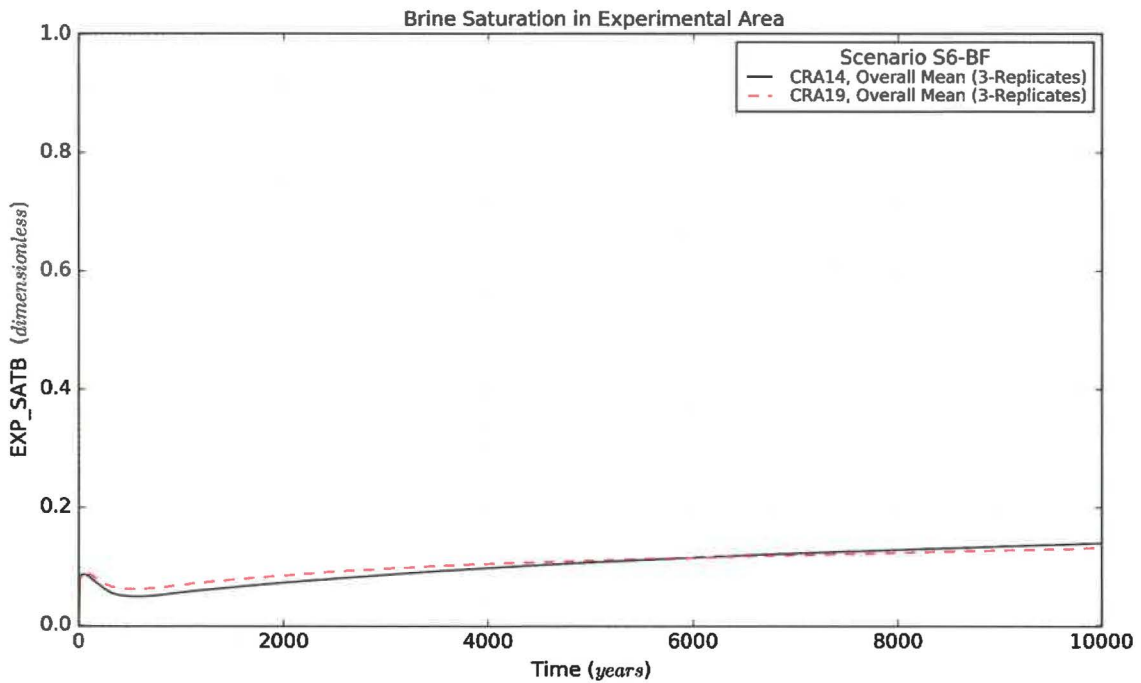


Figure 37 – Brine Saturation Means for the Experimental Area, Scenario S6-BF

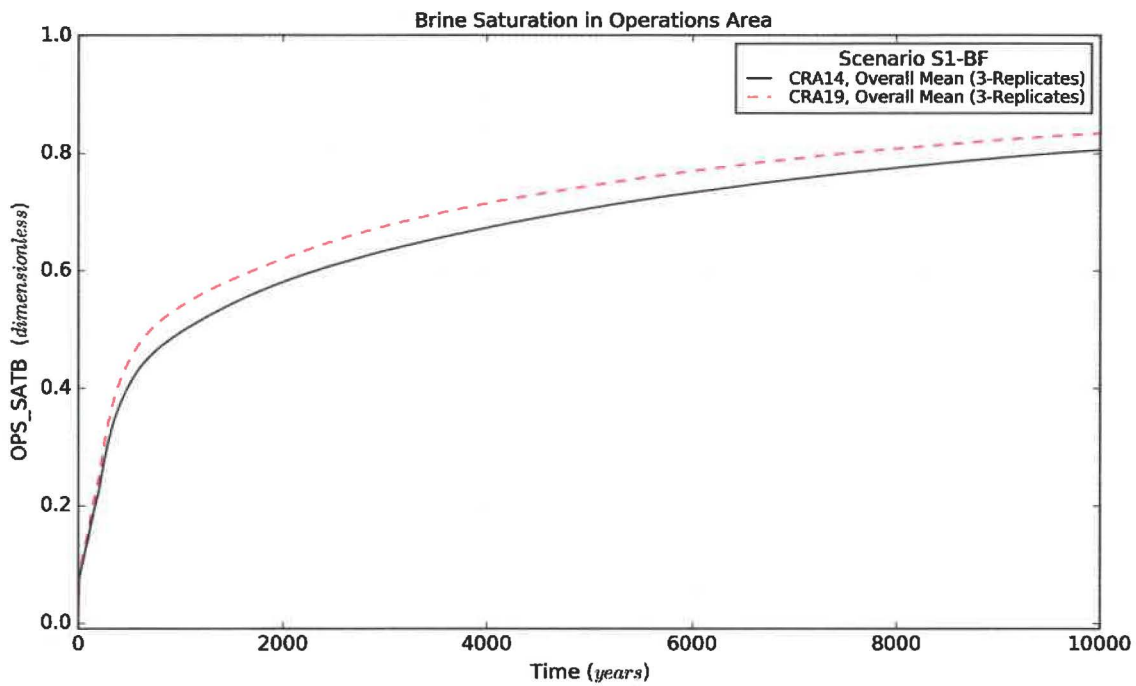


Figure 38 – Brine Saturation Means for the Operations Area, Scenario S1-BF

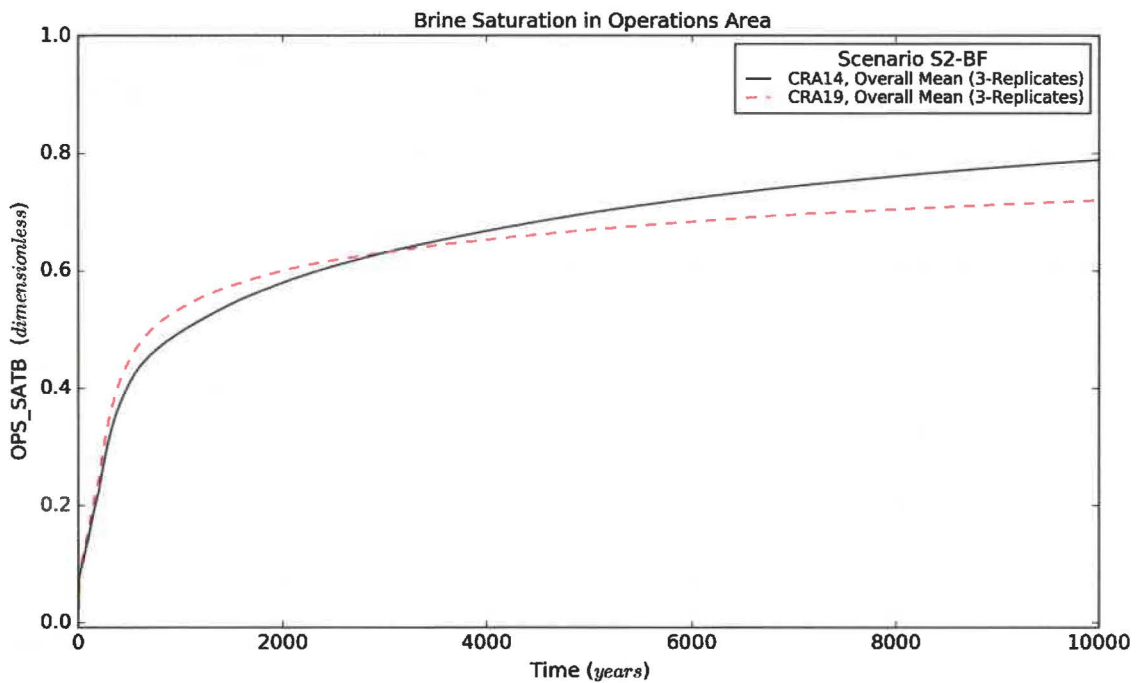


Figure 39 – Brine Saturation Means for the Operations Area, Scenario S2-BF

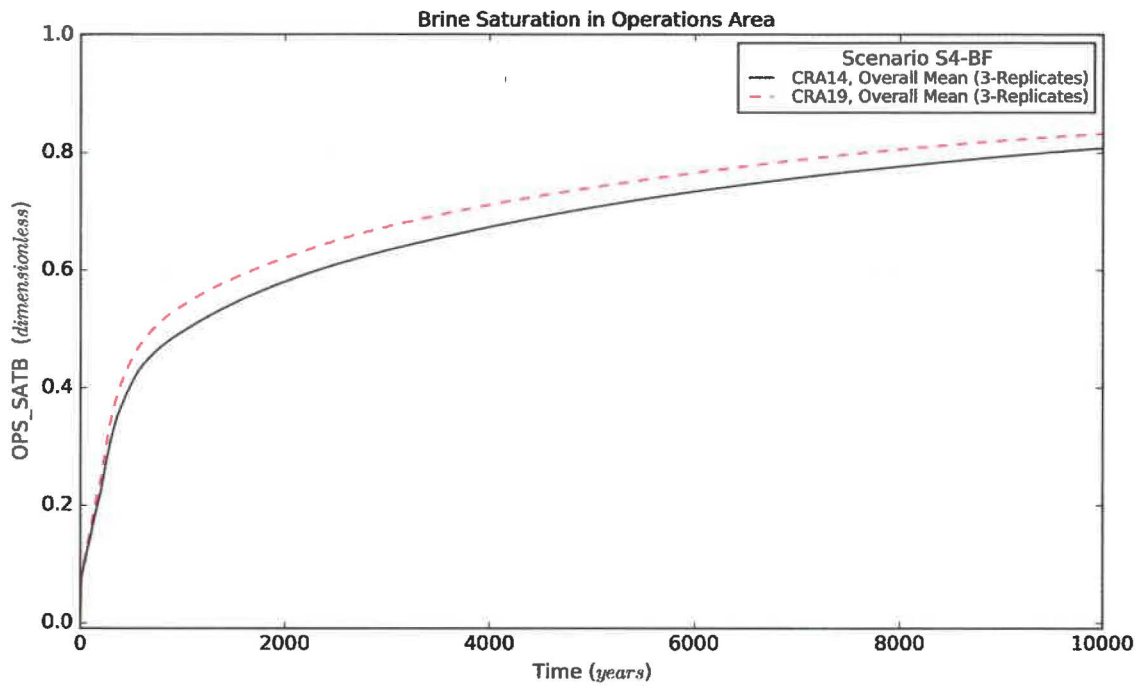


Figure 40 – Brine Saturation Means for the Operations Area, Scenario S4-BF

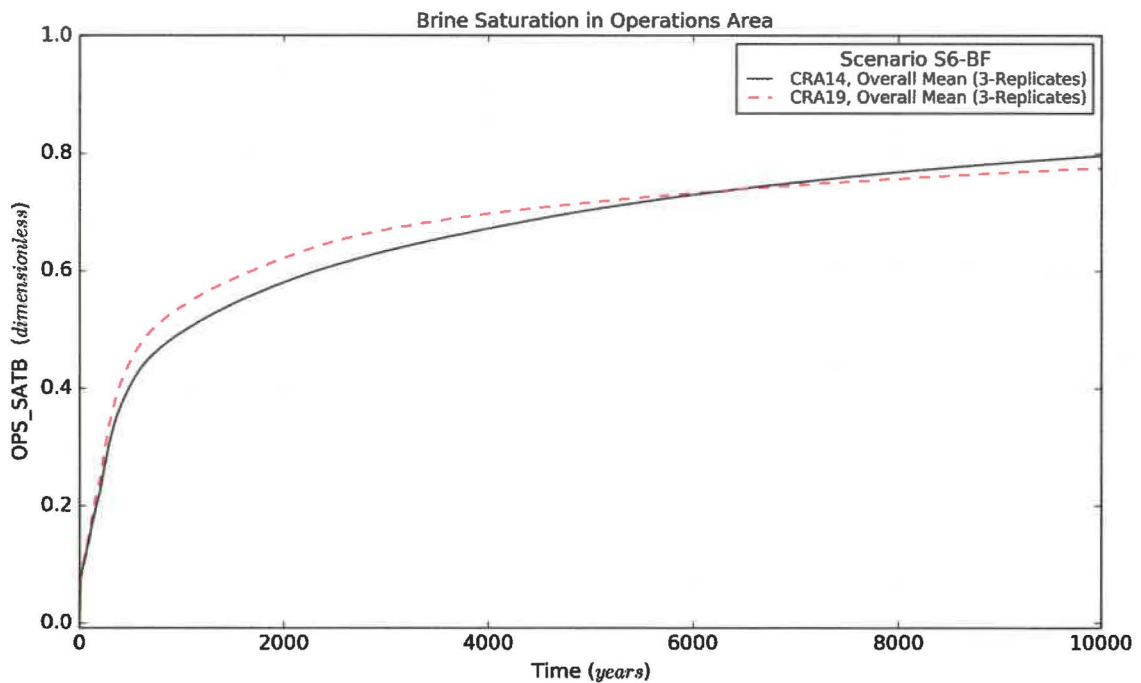


Figure 41 – Brine Saturation Means for the Operations Area, Scenario S6-BF

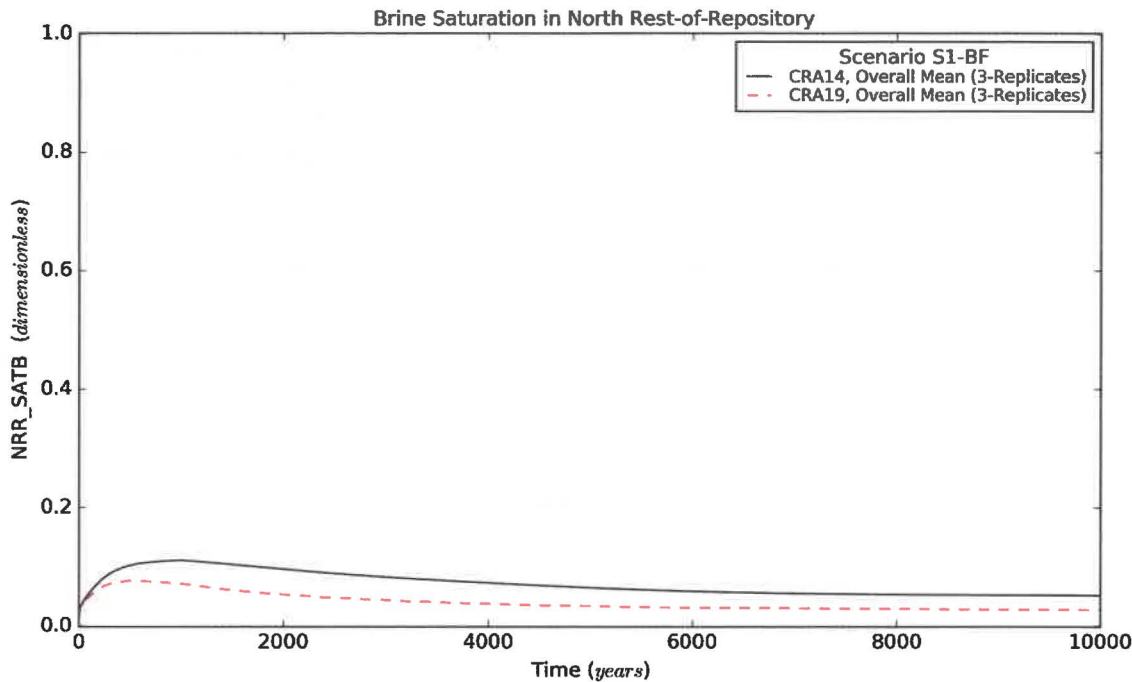


Figure 42 – Brine Saturation Means for the North Rest-of-Repository, Scenario S1-BF

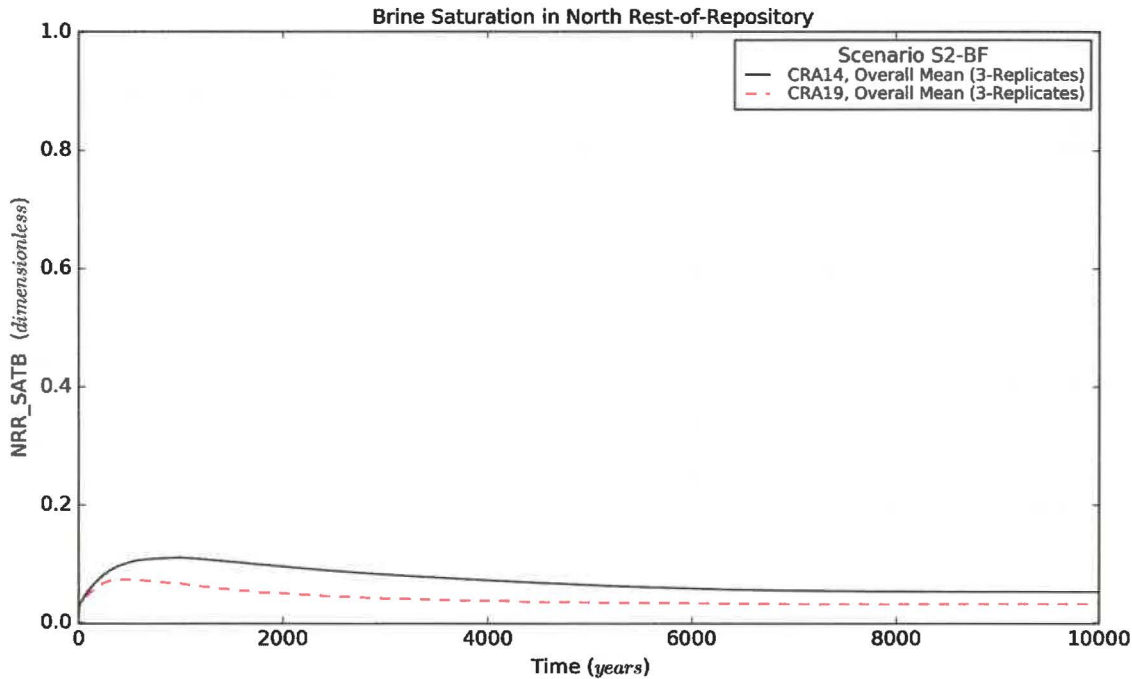


Figure 43 – Brine Saturation Means for the North Rest-of-Repository, Scenario S2-BF

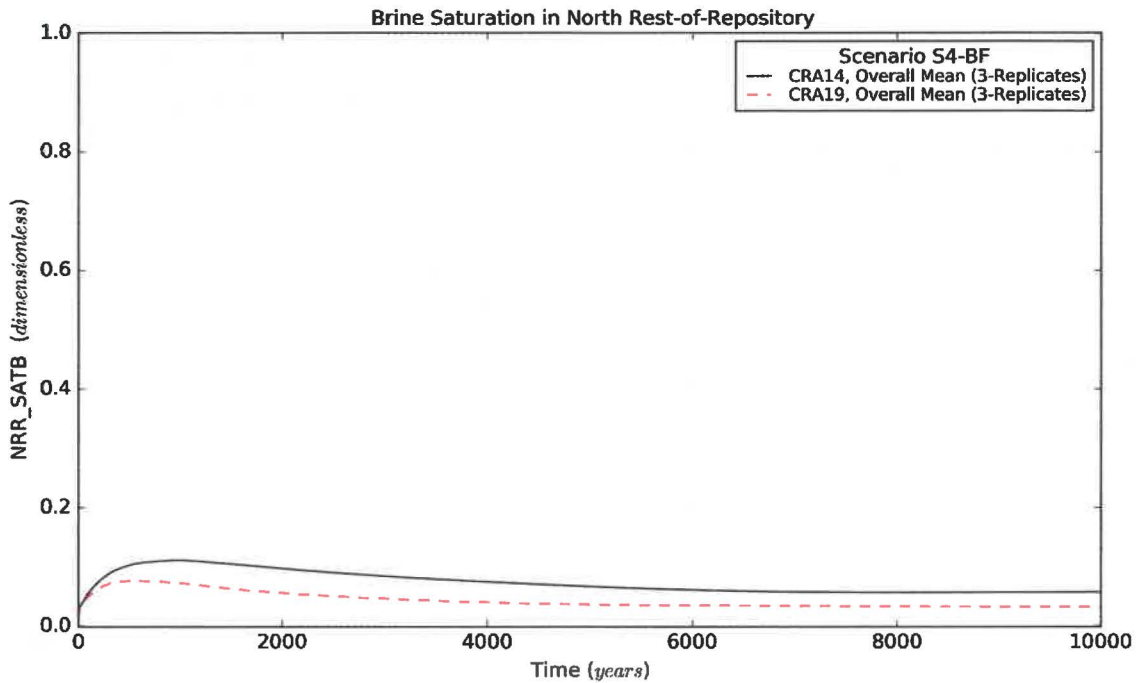


Figure 44 – Brine Saturation Means for the North Rest-of-Repository, Scenario S4-BF

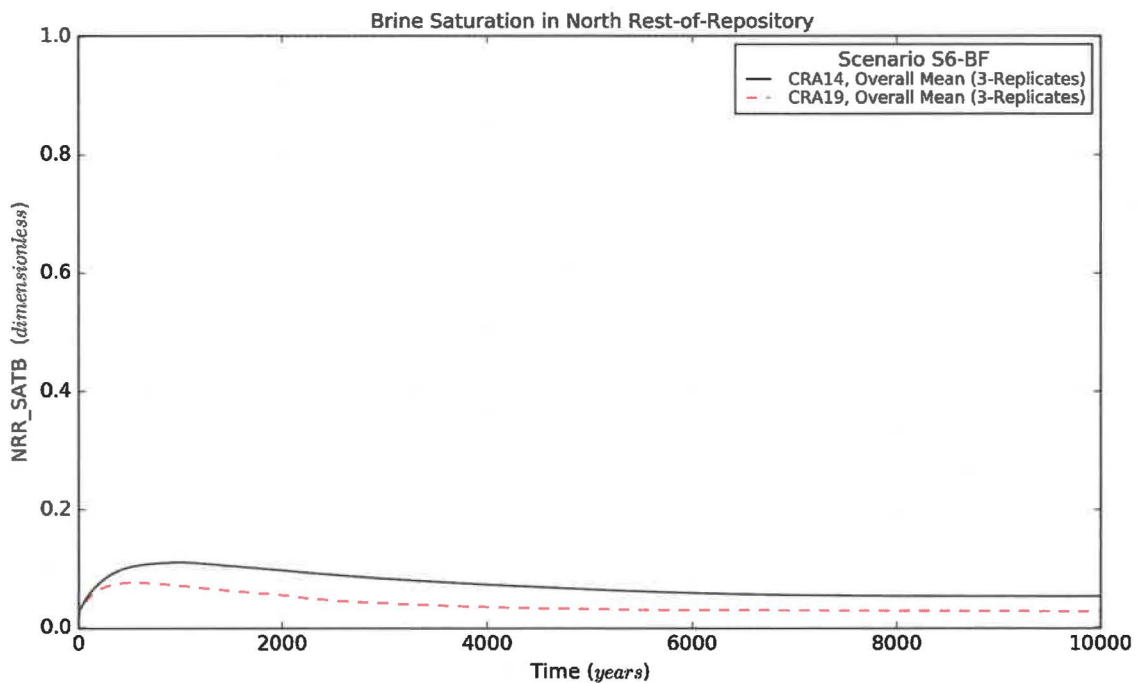


Figure 45 – Brine Saturation Means for the North Rest-of-Repository, Scenario S6-BF

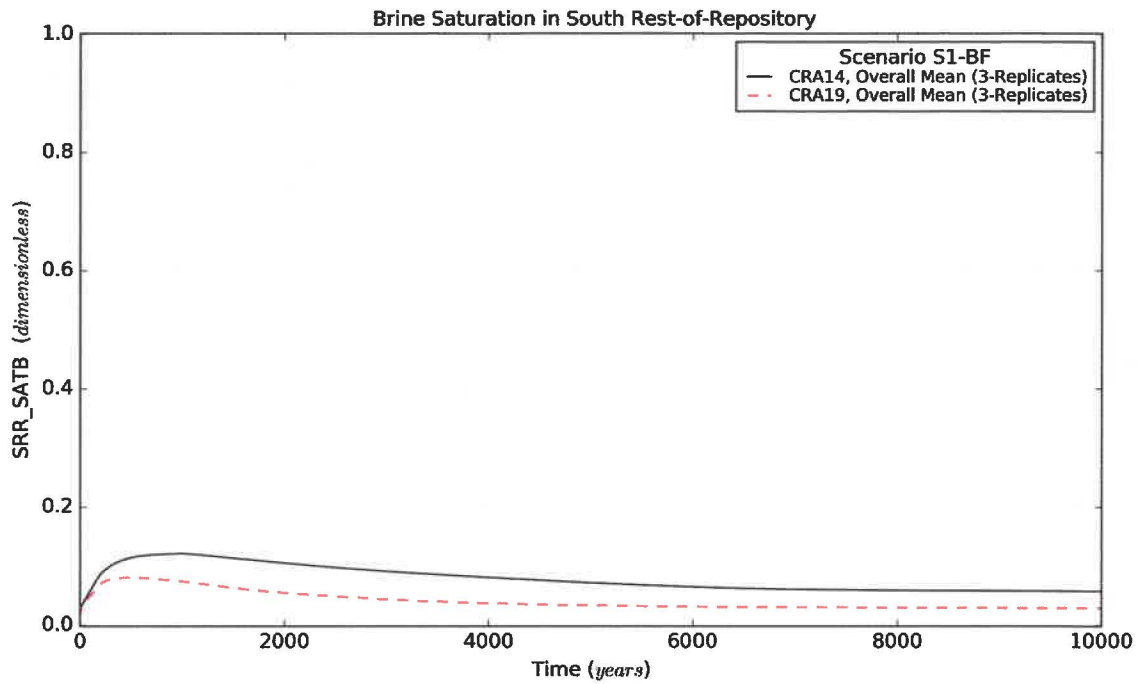


Figure 46 – Brine Saturation Means for the South Rest-of-Repository, Scenario S1-BF

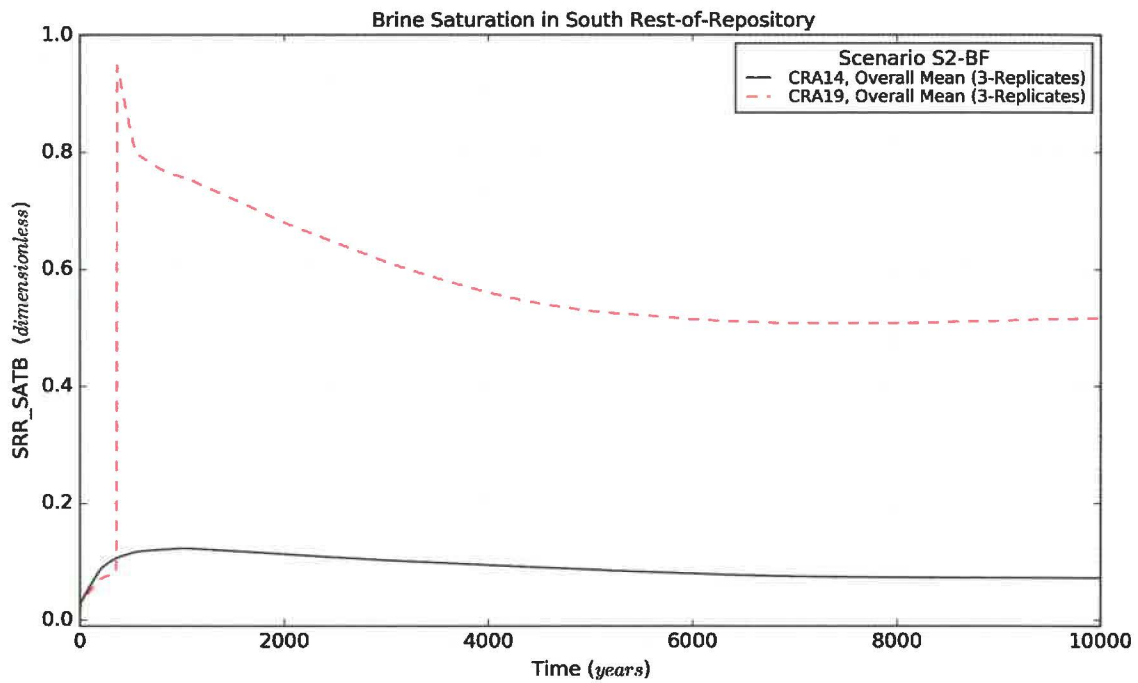


Figure 47 – Brine Saturation Means for the South Rest-of-Repository, Scenario S2-BF

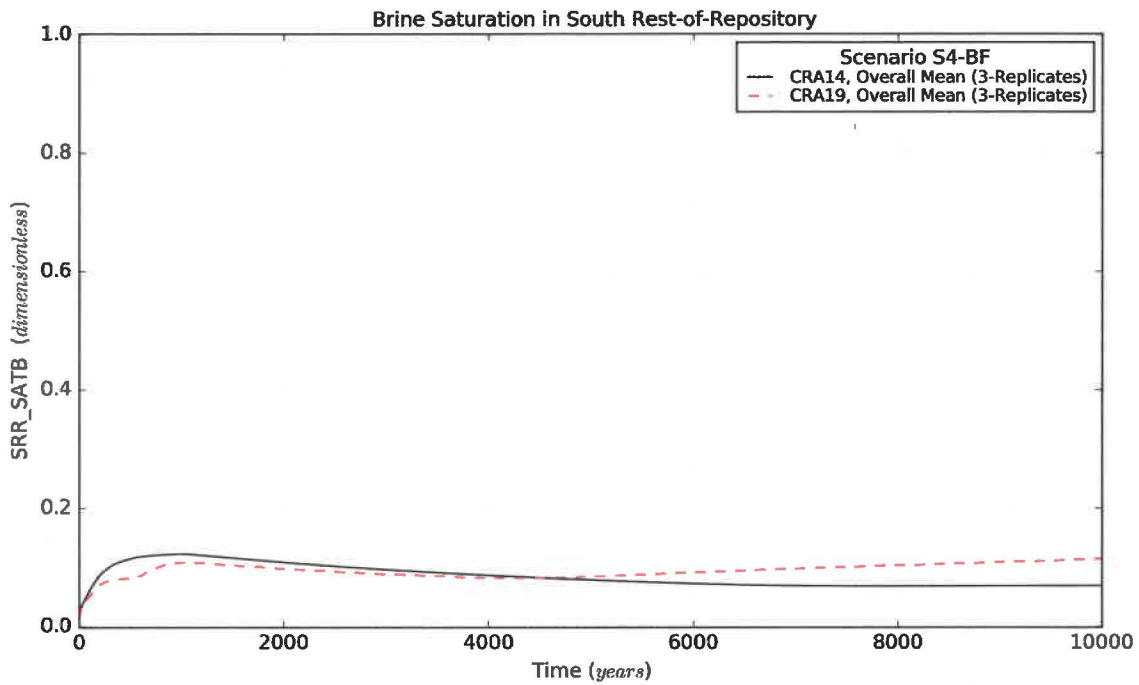


Figure 48 – Brine Saturation Means for the South Rest-of-Repository, Scenario S4-BF

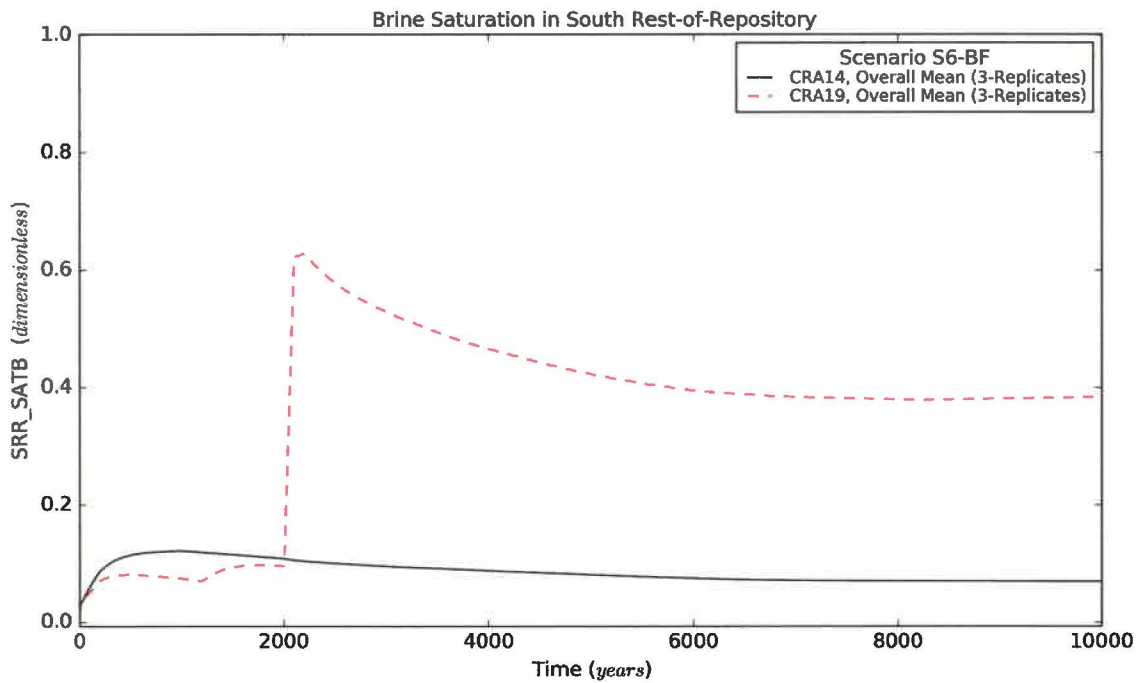


Figure 49 – Brine Saturation Means for the South Rest-of-Repository, Scenario S6-BF

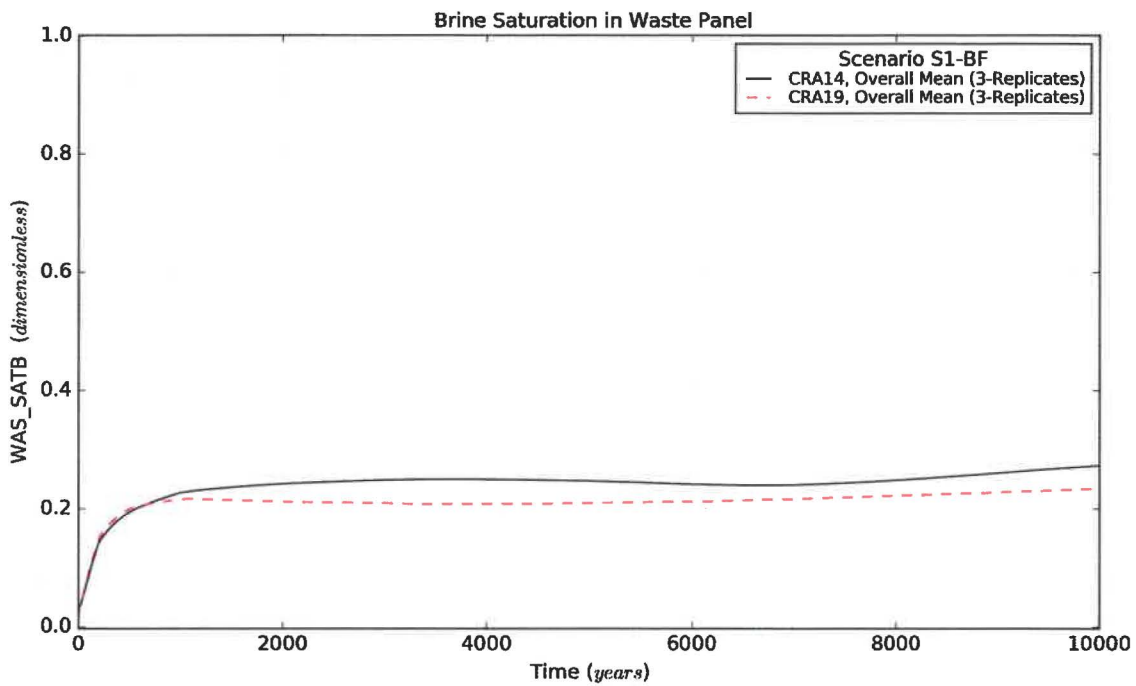


Figure 50 – Brine Saturation Means for the Waste Panel, Scenario S1-BF

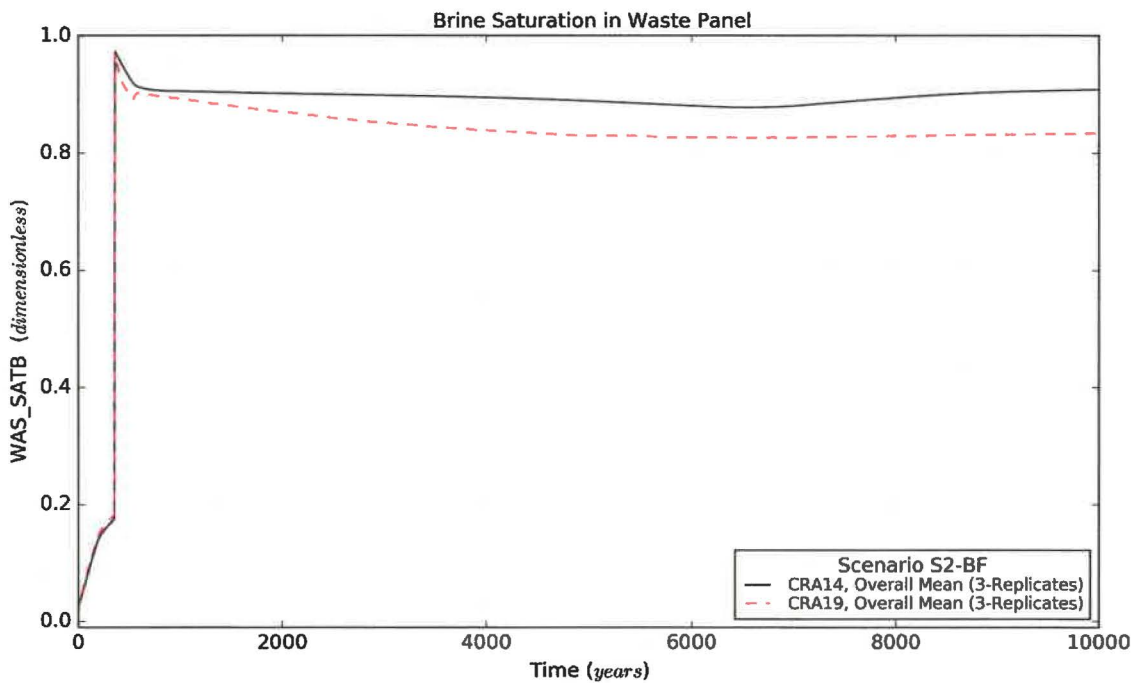


Figure 51 – Brine Saturation Means for the Waste Panel, Scenario S2-BF

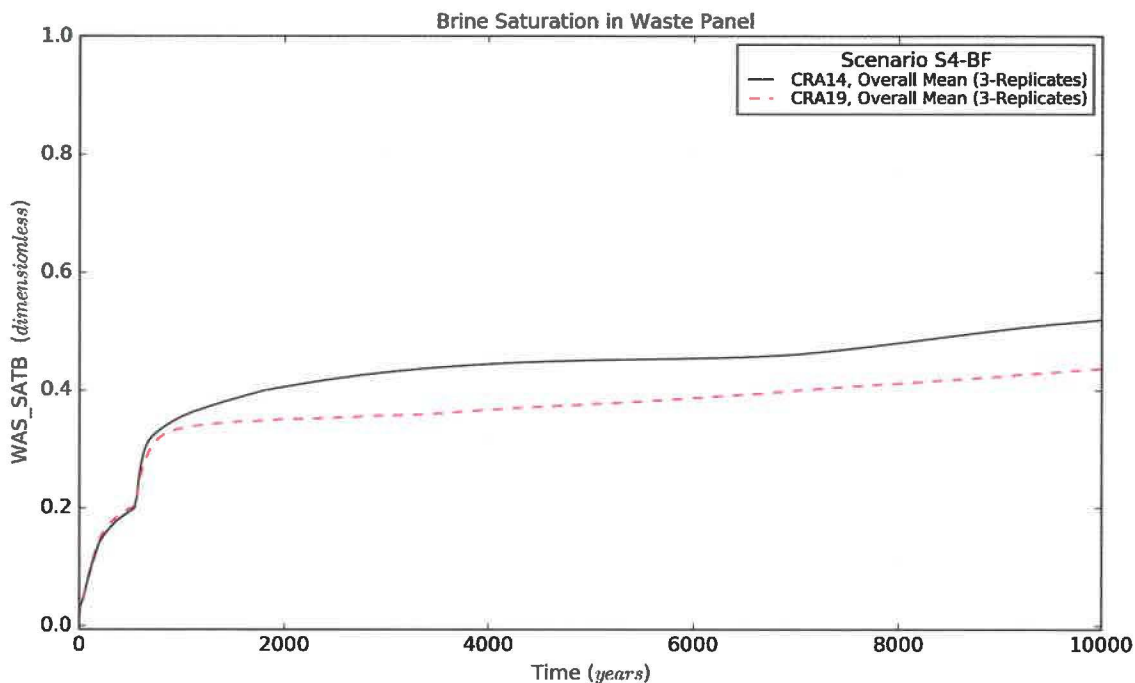


Figure 52 – Brine Saturation Means for the Waste Panel, Scenario S4-BF

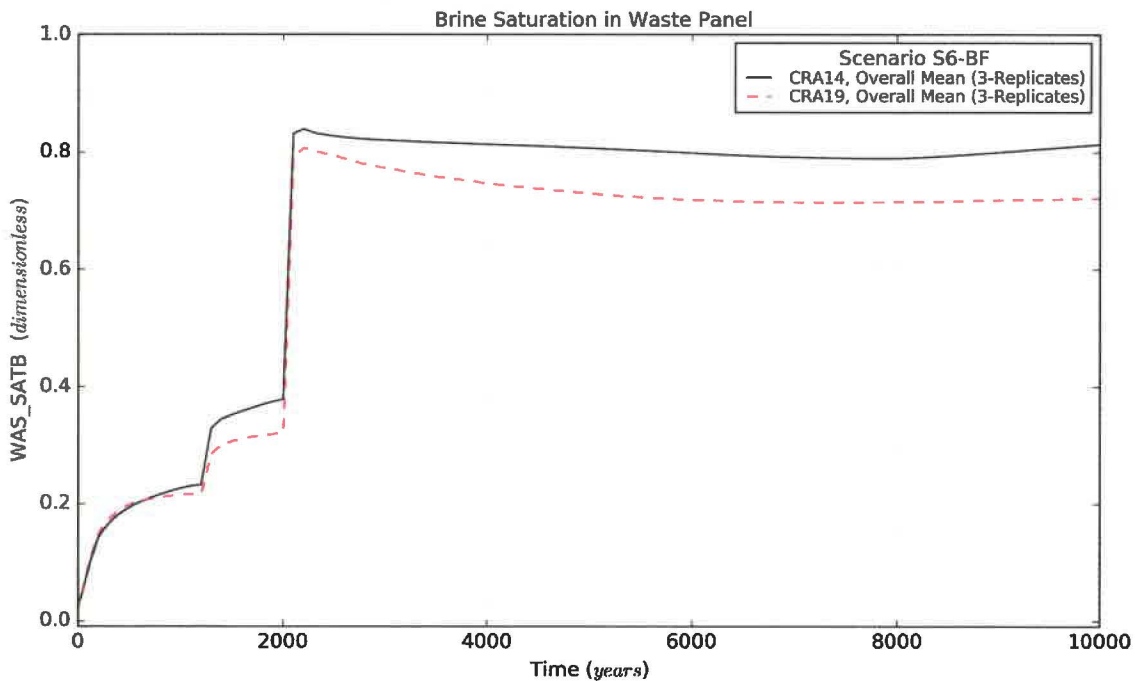


Figure 53 – Brine Saturation Means for the Waste Panel, Scenario S6-BF

This page intentionally left blank.

Table 19 – Brine Saturation Statistics on Overall Means for CRA14 and CRA19

Quantity (units)	Description	Scenario	Mean Value ¹		Maximum Value ²	
			CRA14	CRA19	CRA14	CRA19
EXP_SATB (dimensionless)	Brine Saturation in Experimental Area	S1-BF	1.02E-01	1.12E-01	1.41E-01	1.49E-01
		S2-BF	1.00E-01	9.64E-02	1.36E-01	1.17E-01
		S4-BF	1.03E-01	1.15E-01	1.44E-01	1.57E-01
		S6-BF	1.02E-01	1.05E-01	1.40E-01	1.31E-01
OPS_SATB (dimensionless)	Brine Saturation in Operations Area	S1-BF	6.67E-01	7.04E-01	8.06E-01	8.34E-01
		S2-BF	6.59E-01	6.39E-01	7.89E-01	7.21E-01
		S4-BF	6.68E-01	7.02E-01	8.08E-01	8.33E-01
		S6-BF	6.64E-01	6.78E-01	7.97E-01	7.76E-01
NRR_SATB (dimensionless)	Brine Saturation in North Rest-of-Repository	S1-BF	7.10E-02	4.04E-02	1.11E-01	7.69E-02
		S2-BF	7.07E-02	4.09E-02	1.11E-01	7.38E-02
		S4-BF	7.32E-02	4.34E-02	1.11E-01	7.69E-02
		S6-BF	7.13E-02	3.97E-02	1.11E-01	7.69E-02
SRR_SATB (dimensionless)	Brine Saturation in South Rest-of-Repository	S1-BF	7.86E-02	4.16E-02	1.22E-01	8.15E-02
		S2-BF	8.99E-02	5.61E-01	1.23E-01	9.49E-01
		S4-BF	8.48E-02	9.49E-02	1.23E-01	1.15E-01
		S6-BF	8.57E-02	3.60E-01	1.22E-01	6.28E-01
WAS_SATB (dimensionless)	Brine Saturation in Waste Panel	S1-BF	2.40E-01	2.12E-01	2.73E-01	2.35E-01
		S2-BF	8.69E-01	8.20E-01	9.74E-01	9.72E-01
		S4-BF	4.30E-01	3.68E-01	5.20E-01	4.37E-01
		S6-BF	6.93E-01	6.32E-01	8.40E-01	8.08E-01

Notes:

- 1 Calculated as the function average (integrated) over the time interval (0-10,000 years) for the overall means (3 replicates)
- 2 Calculated as the function maximum over the time interval (0-10,000 years) for the overall means (3 replicates)

Table 20 – Brine Saturation Statistics on Individual Vectors for CRA14 and CRA19

Quantity (units)	Description	Scenario	Maximum Value ³	
			CRA14	CRA19
EXP_SATB (dimensionless)	Brine Saturation in Experimental Area	S1-BF	8.67E-01	7.41E-01
		S2-BF	9.05E-01	7.24E-01
		S4-BF	9.08E-01	8.19E-01
		S6-BF	9.06E-01	7.47E-01
OPS_SATB (dimensionless)	Brine Saturation in Operations Area	S1-BF	1.00E+00	1.00E+00
		S2-BF	1.00E+00	1.00E+00
		S4-BF	1.00E+00	1.00E+00
		S6-BF	1.00E+00	1.00E+00
NRR_SATB (dimensionless)	Brine Saturation in North Rest-of-Repository	S1-BF	7.21E-01	5.51E-01
		S2-BF	7.20E-01	5.47E-01
		S4-BF	7.22E-01	5.51E-01
		S6-BF	7.21E-01	5.50E-01
SRR_SATB (dimensionless)	Brine Saturation in South Rest-of-Repository	S1-BF	9.36E-01	9.33E-01
		S2-BF	9.36E-01	9.95E-01
		S4-BF	9.36E-01	9.80E-01
		S6-BF	9.36E-01	9.95E-01
WAS_SATB (dimensionless)	Brine Saturation in Waste Panel	S1-BF	9.91E-01	9.69E-01
		S2-BF	9.99E-01	9.98E-01
		S4-BF	9.96E-01	9.94E-01
		S6-BF	9.99E-01	9.98E-01

Notes:

3 Calculated as the function maximum over the time interval (0-10,000 years) for all replicates (300 vectors)

4.3 Gas Saturation

Gas saturation results are not explicitly provided herein, but are inferred from the brine saturation results presented in Section 4.2, with gas saturation equal to one minus the brine saturation.

4.4 Gas Generation

Gas generation due to the sum of cellulose biodegradation and iron corrosion in all waste areas is marginally increased for undisturbed (S1-BF) and E2 intruded (S4-BF) scenarios and substantially increased (more than doubled on average at 10,000 years) for E1 (S2-BF) and E2E1 intruded (S6-BF) scenarios for CRA19 in comparison to CRA14 as shown in Figure 54 to Figure 57. Cumulative gas generation is generally higher over all scenarios for CRA19 due to the substantial increase in inundated iron corrosion rates, increased iron and cellulose mass in the waste inventory, and the addition of brine radiolysis. Cellulose biodegradation rates for CRA19 are below CRA14 for scenarios without an E1 intrusion (S1-BF, S4-BF) and higher for scenarios with an E1 intrusion (S2-BF, S6-BF) due to the respectively lower and higher overall brine saturations. Even with the variable saturation changes across scenarios, the increased inundated iron corrosion rate for CRA19 results in increased iron corrosion gas generation over all scenarios in comparison to CRA14. The total moles of gas generated from all sources under CRA19 is substantially larger than for CRA14 with iron corrosion consistently being the largest contributor and radiolytic/microbial gas generation being comparable lesser contributors under all reported scenarios (Figure 58 to Figure 61).

Cellulose biodegradation and iron corrosion gas generation statistics for CRA19 and CRA14 are summarized in Table 21 and Table 22 along with total gas generation statistics for CRA19 that includes radiolysis. Table 21 provides the 3-replicate mean (integrated over time) and 3-replicate maximum (over all time) values. Table 22 provides the maximum values (over all time) over all individual vectors.

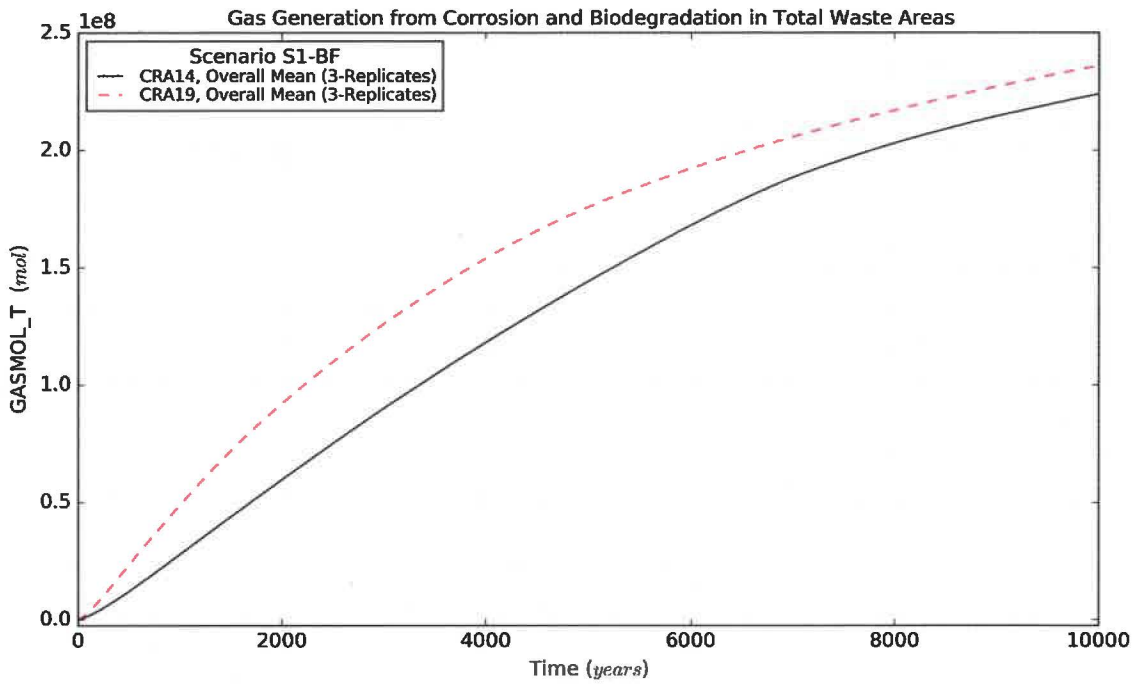


Figure 54 – Gas Generation from Corrosion and Biodegradation, Scenario S1-BF

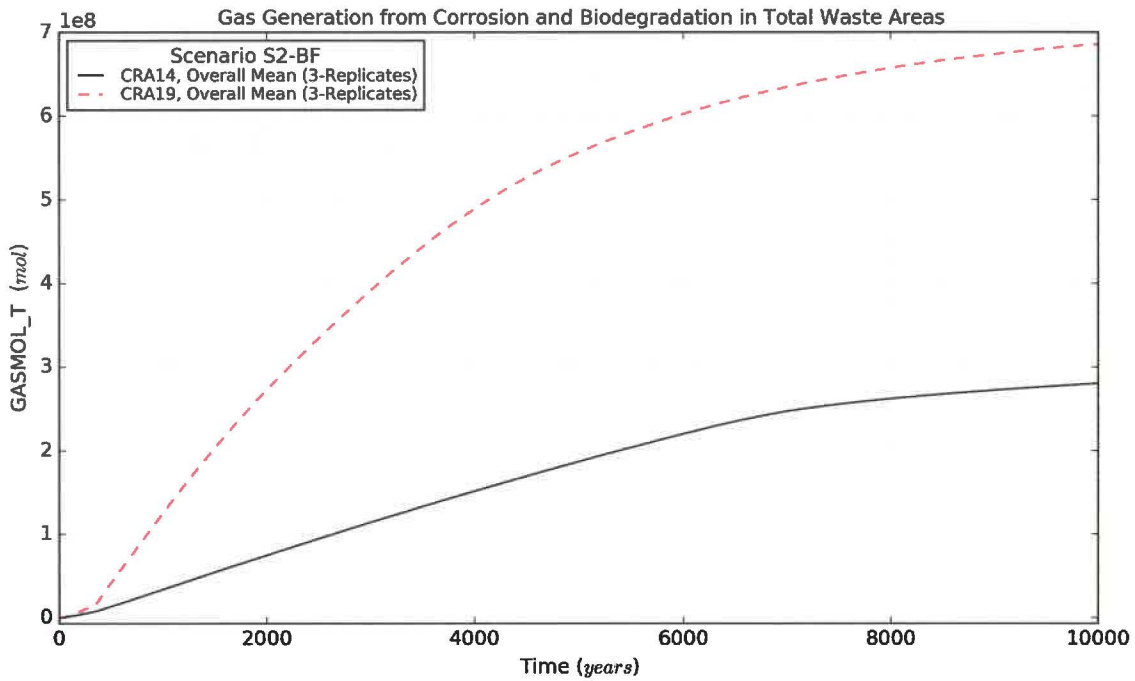


Figure 55 – Gas Generation from Corrosion and Biodegradation, Scenario S2-BF

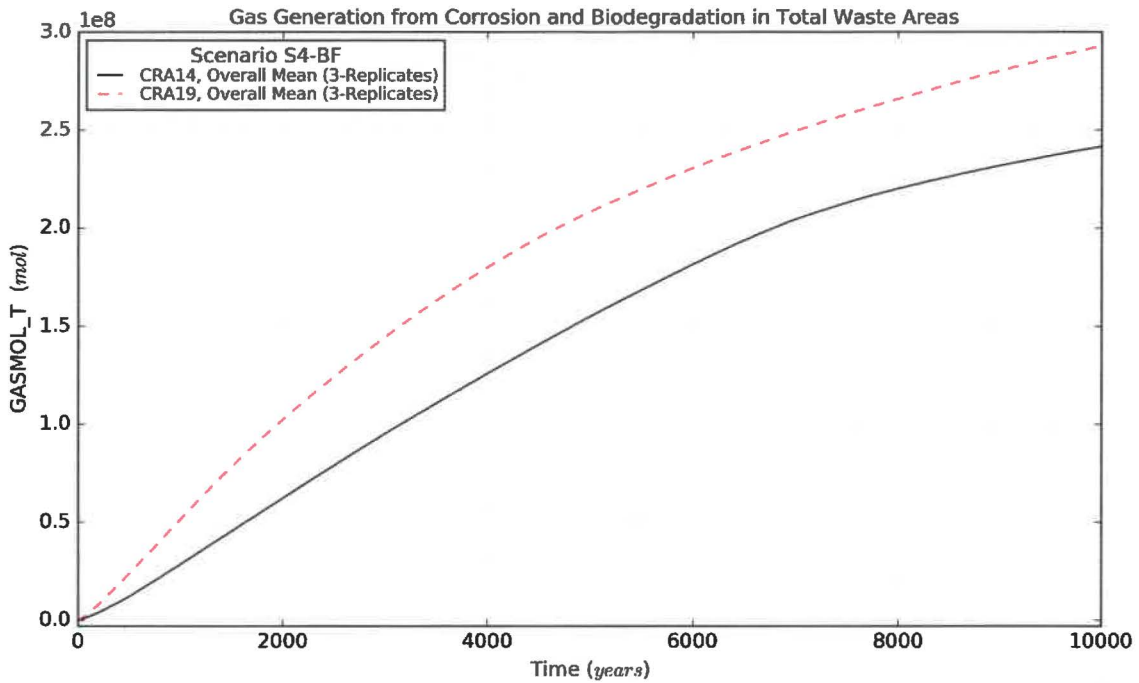


Figure 56 – Gas Generation from Corrosion and Biodegradation, Scenario S4-BF

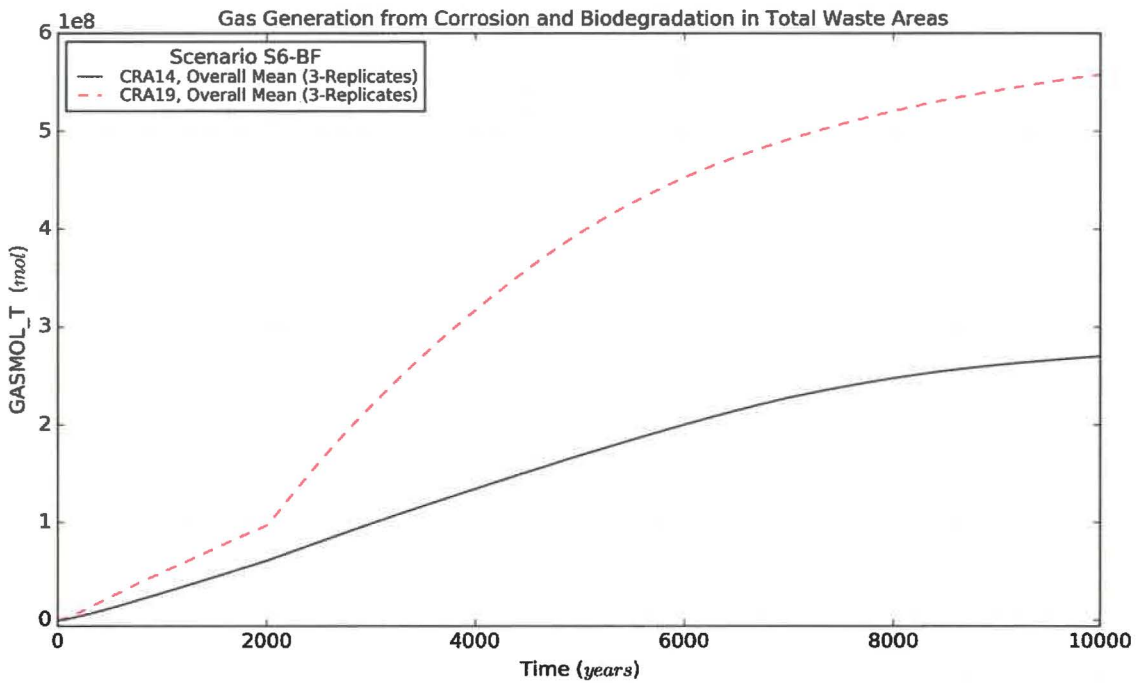


Figure 57 – Gas Generation from Corrosion and Biodegradation, Scenario S6-BF

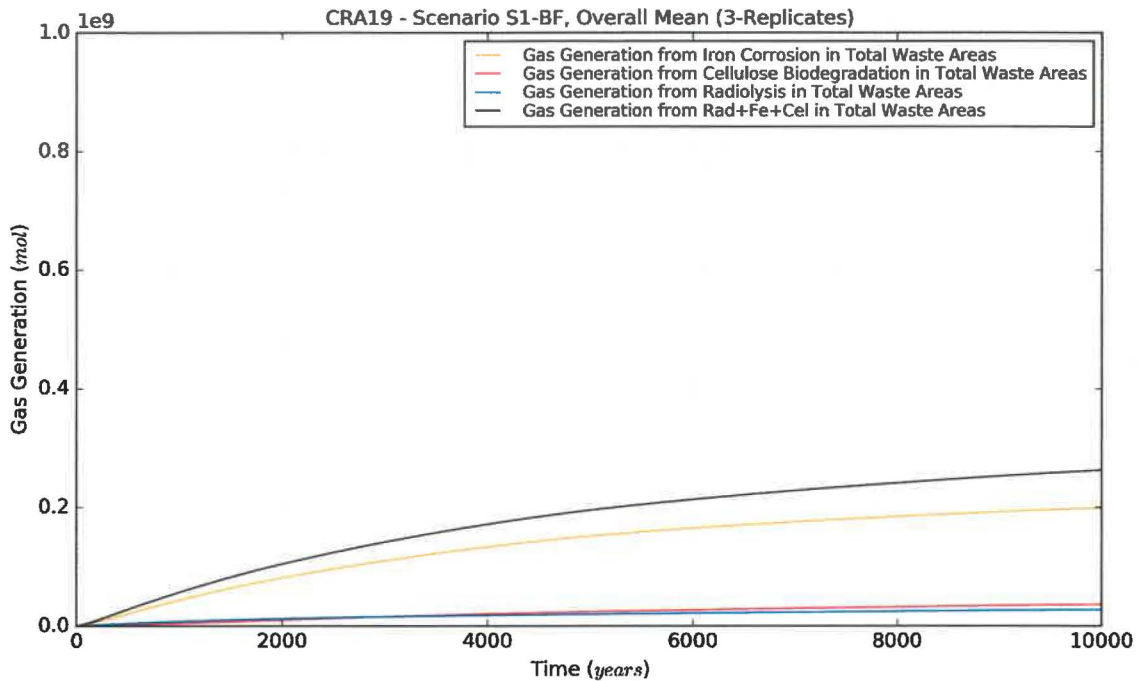


Figure 58 – CRA19 Moles of Gas Generated by All Sources, Scenario S1-BF

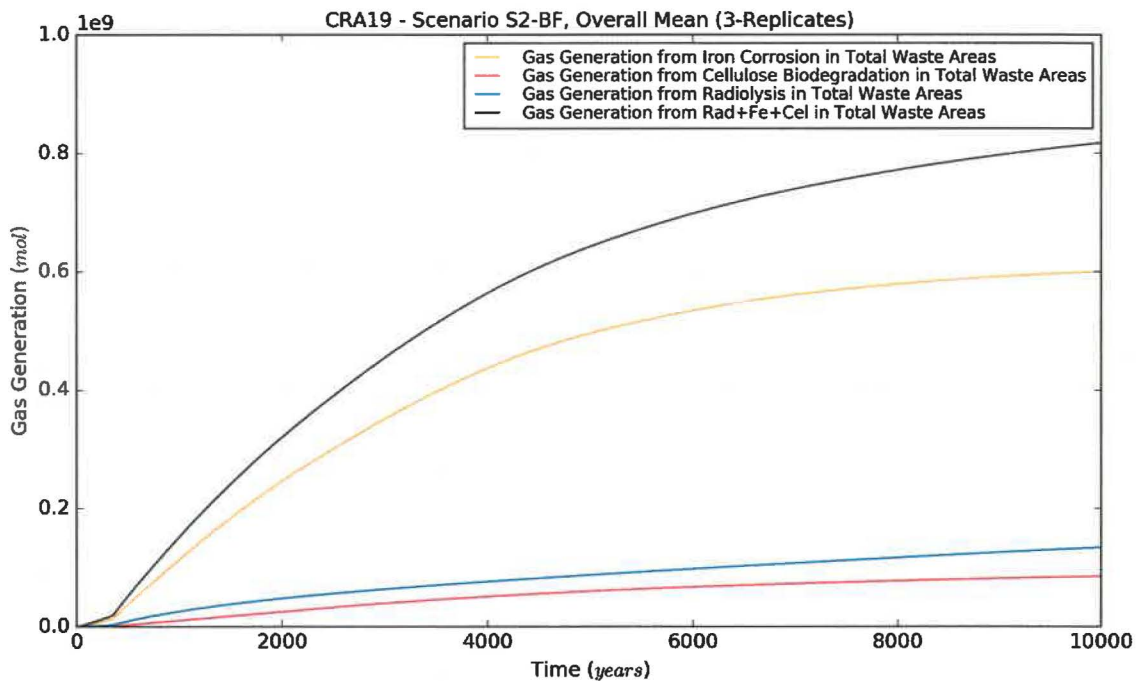


Figure 59 – CRA19 Moles of Gas Generated by All Sources, Scenario S2-BF

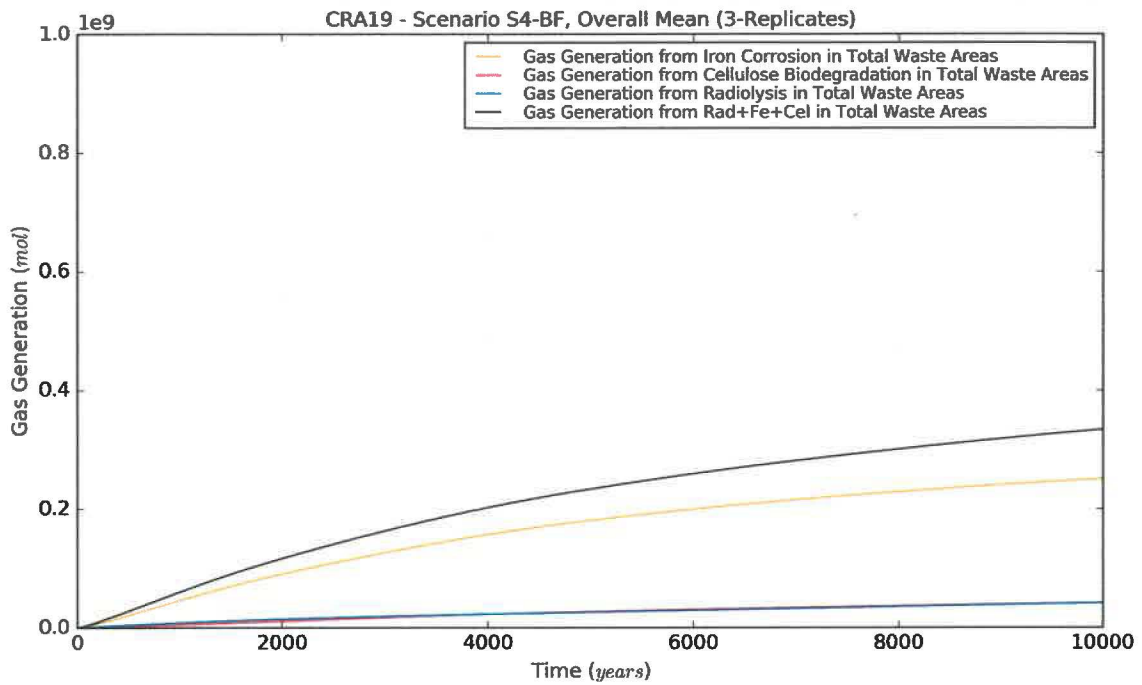


Figure 60 – CRA19 Moles of Gas Generated by All Sources, Scenario S4-BF

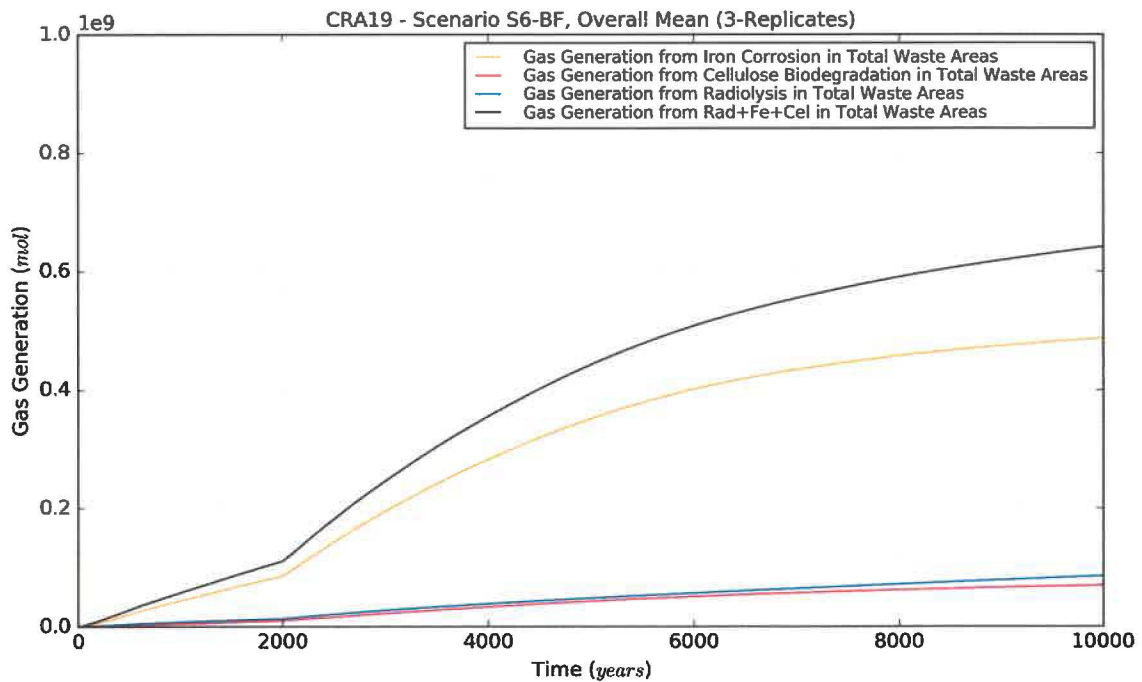


Figure 61 – CRA19 Moles of Gas Generated by All Sources, Scenario S6-BF

This page intentionally left blank

Table 21 – Gas Generation Statistics on Overall Means for CRA14 and CRA19

Quantity (units)	Description	Scenario	Mean Value ¹		Maximum Value ²	
			CRA14	CRA19	CRA14	CRA19
GASMOL_T (mol)	Gas Generation from Corrosion and Biodegradation in Total Waste Areas	S1-BF	1.33E+08	1.56E+08	2.24E+08	2.36E+08
		S2-BF	1.70E+08	4.75E+08	2.80E+08	6.86E+08
		S4-BF	1.43E+08	1.86E+08	2.42E+08	2.93E+08
		S6-BF	1.56E+08	3.37E+08	2.70E+08	5.58E+08
FEMOL_T (mol)	Gas Generation from Iron Corrosion in Total Waste Areas	S1-BF	1.06E+08	1.34E+08	1.78E+08	2.00E+08
		S2-BF	1.39E+08	4.22E+08	2.28E+08	6.01E+08
		S4-BF	1.15E+08	1.62E+08	1.94E+08	2.51E+08
		S6-BF	1.27E+08	2.98E+08	2.19E+08	4.88E+08
CELMOL_T (mol)	Gas Generation from Cellulose Biodegradation in Total Waste Areas	S1-BF	2.65E+07	2.20E+07	4.60E+07	3.67E+07
		S2-BF	3.12E+07	5.32E+07	5.29E+07	8.56E+07
		S4-BF	2.76E+07	2.46E+07	4.80E+07	4.19E+07
		S6-BF	2.93E+07	3.90E+07	5.13E+07	7.04E+07
ALL_HRDC (mol)	Gas Generation from Radiolysis in Total Waste Areas	S1-BF	-	1.84E+07	-	2.74E+07
		S2-BF	-	8.17E+07	-	1.34E+08
		S4-BF	-	2.48E+07	-	4.17E+07
		S6-BF	-	4.54E+07	-	8.59E+07
ALL_H TTC (mol)	Gas Generation from Rad+Fe+Cel in Total Waste Areas	S1-BF	1.33E+08	1.74E+08	2.24E+08	2.63E+08
		S2-BF	1.70E+08	5.55E+08	2.80E+08	8.18E+08
		S4-BF	1.43E+08	2.11E+08	2.42E+08	3.34E+08
		S6-BF	1.56E+08	3.82E+08	2.70E+08	6.42E+08

Notes:

- 1 Calculated as the function average (integrated) over the time interval (0-10,000 years) for the overall means (3 replicates)
- 2 Calculated as the function maximum over the time interval (0-10,000 years) for the overall means (3 replicates)

Table 22 – Gas Generation Statistics on Individual Vectors for CRA14 and CRA19

Quantity (units)	Description	Scenario	Maximum Value ³	
			CRA14	CRA19
GASMOL_T (mol)	Gas Generation from Corrosion and Biodegradation in Total Waste Areas	S1-BF	8.79E+08	1.59E+09
		S2-BF	8.79E+08	1.59E+09
		S4-BF	8.79E+08	1.59E+09
		S6-BF	8.79E+08	1.59E+09
FEMOL_T (mol)	Gas Generation from Iron Corrosion in Total Waste Areas	S1-BF	7.96E+08	1.13E+09
		S2-BF	7.96E+08	1.13E+09
		S4-BF	7.96E+08	1.13E+09
		S6-BF	7.96E+08	1.13E+09
CELMOL_T (mol)	Gas Generation from Cellulose Biodegradation in Total Waste Areas	S1-BF	4.05E+08	4.62E+08
		S2-BF	4.05E+08	4.62E+08
		S4-BF	4.05E+08	4.62E+08
		S6-BF	4.05E+08	4.62E+08
ALL_HRDC (mol)	Gas Generation from Radiolysis in Total Waste Areas	S1-BF	-	2.93E+08
		S2-BF	-	4.42E+08
		S4-BF	-	3.50E+08
		S6-BF	-	4.10E+08
ALL_H TTC (mol)	Gas Generation from Rad+Fe+Cel in Total Waste Areas	S1-BF	8.79E+08	1.63E+09
		S2-BF	8.79E+08	1.76E+09
		S4-BF	8.79E+08	1.67E+09
		S6-BF	8.79E+08	1.73E+09

Notes:

3 Calculated as the function maximum over the time interval (0-10,000 years) for all replicates (300 vectors)

4.5 Brine and Gas Flows

The larger DRZ associated with an expanded experimental area to accommodate the 5th shaft access drifts and greater communication between the waste panel and south rest-of-repository facilitated by the lack of ROMPCS emplacement in the southernmost panel closure area results in a net increase in brine inflow to the repository across all scenarios. The inflow increases associated with undisturbed (S1-BF) and non-Castile intrusions (S4-BF) are rather modest when compared to the inflow increases for intrusions that are associated with the hypothetical Castile brine reservoir (S2-BF and S6-BF). For S2-BF and S6-BF, pressure-limited flows from the Castile brine reservoir across the unemplaced southernmost panel closure flood the waste panel and south rest-of-repository, resulting in total repository brine inflows that are essentially doubled for CRA19 in comparison to CRA14. Figure 62 to Figure 65 show the magnitude of brine influx to the repository for all reported scenarios. Figure 66 shows a representative case for brine influx to the experimental area under the undisturbed scenario (S1-BF).

Mean brine flows up the shaft under CRA19 remain relatively small but are increased over all scenarios in comparison to CRA14 due a combination of scenario-dependent factors such as brine pressures and saturations in the operations and experimental areas and the increased cross-sectional area of the composite shaft which includes the additional 5th shaft. The comparatively greater brine flows up the shaft observed in the S4-BF and S6-BF scenarios are associated with the higher brine pressures and saturations previously discussed (Figure 67 - Figure 70).

Mean brine flows up the intrusion borehole under CRA19 are slightly reduced for Castile intruded scenarios (S2-BF and S6-BF) in comparison to those predicted under CRA14 (Figure 71 and Figure 73). The slight reduction in brine flow up the intrusion borehole for these scenarios is attributed to the reduced average brine saturations observed in the waste panel. The observed (on average) reduced brine pressures and saturations in the waste panel under S4-BF do not predict the slightly delayed and increased mean flow of brine up the intrusion borehole (Figure 72). Further consideration of this unexpected observation is explained by the fact that the mean brine flow up the intrusion borehole under S4-BF is primarily influenced by a relatively few number of vectors (15 out of 300) that have higher than average waste panel brine pressures and saturations along with higher than average permeabilities resulting from the sampled BH_SAND borehole material (Figure 74).

Mean gas flows out of the south rest-of-repository and north rest-of-repository (across the panel closure plane, which includes the panel closure and associated upper and lower DRZ) are increased for CRA19 in comparison to CRA14. A representative comparison of gas flows out of the south rest-of-repository (into the north rest-of-repository) and out of the north rest-of-repository (into the operations area) for S2-BF are provided in Figure 75 and Figure 76 to illustrate the enhanced flow of generated gas to the north that is partially impeded by the increased length of the northernmost panel closure.

Brine flow statistics for CRA19 and CRA14 are summarized in Table 23 and Table 24. Table 23 provides the 3-replicate mean (integrated over time) and 3-replicate maximum (over all time) brine flow values. Table 24 provides the maximum brine flow (over all time) for all individual vectors. The 3-replicate mean and maximum brine flows for CRA19 as compared to CRA14

report increased brine flow into the repository and up the shaft for all scenarios along with decreased brine flow up the intrusion borehole for all applicable scenarios with the exception of S4-BF. The individual vector maximum brine flow values for CRA19 into the repository and up the shaft are increased above CRA14 for all scenarios. The individual vector maximum brine flow values for CRA19 up the intrusion borehole are decreased below CRA14 for all scenarios with one exception – the substantial increase in maximum individual vector brine flow up the intrusion borehole for S4-BF.

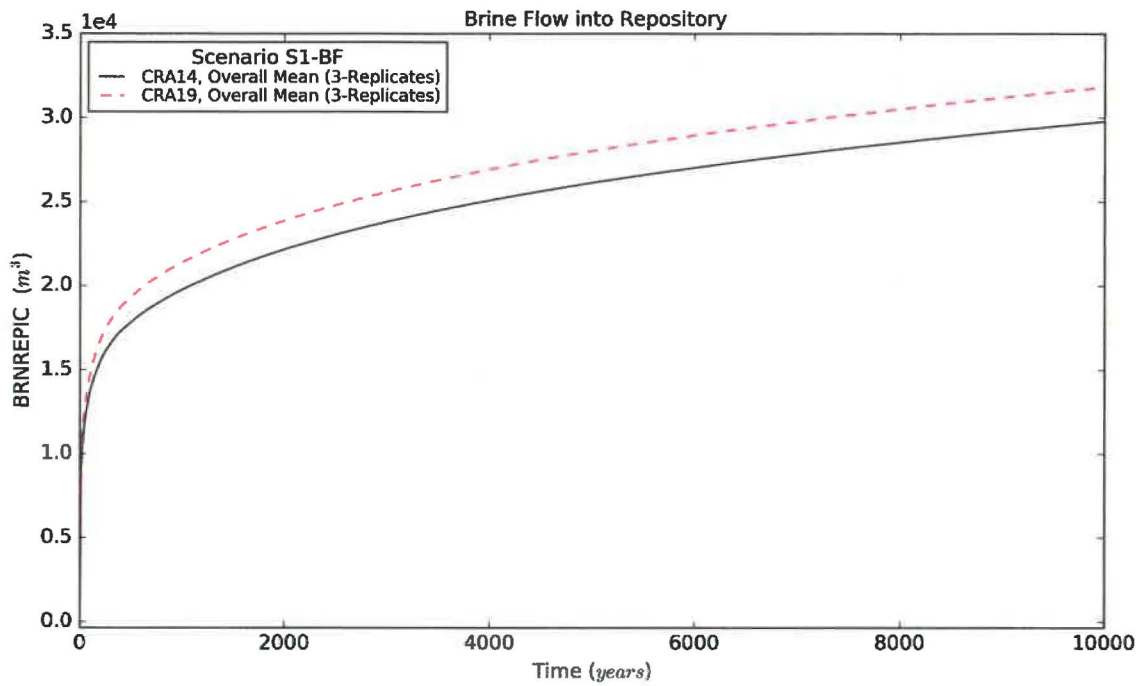


Figure 62 – Brine Flow Means into Repository, Scenario S1-BF

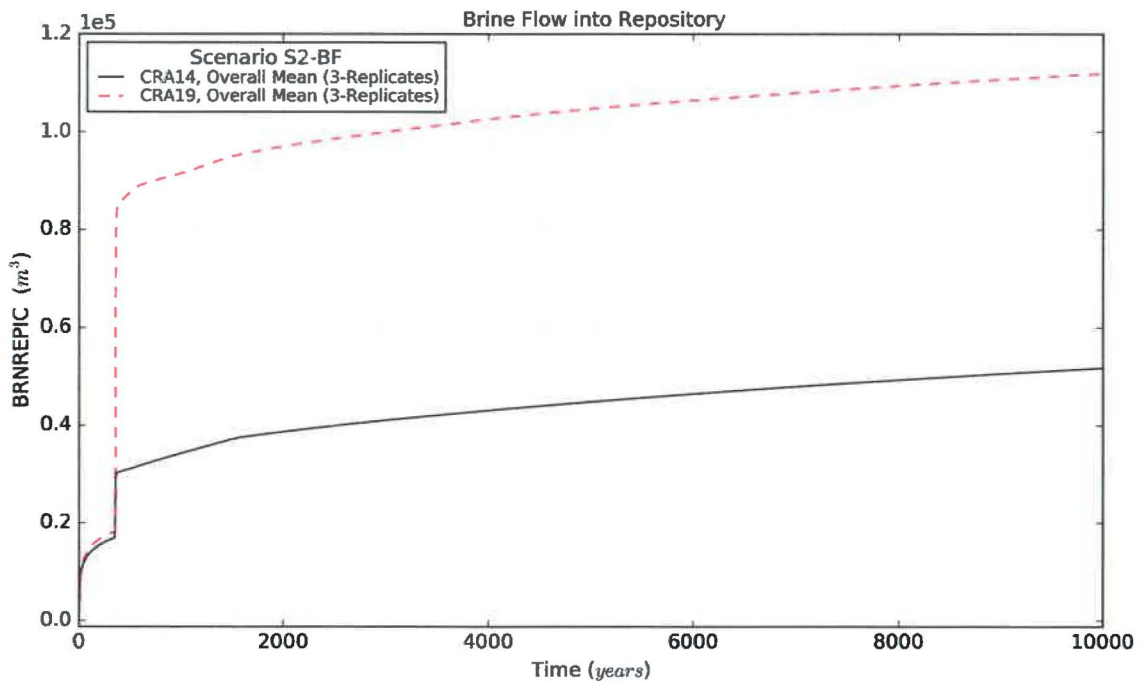


Figure 63 – Brine Flow Means into Repository, Scenario S2-BF

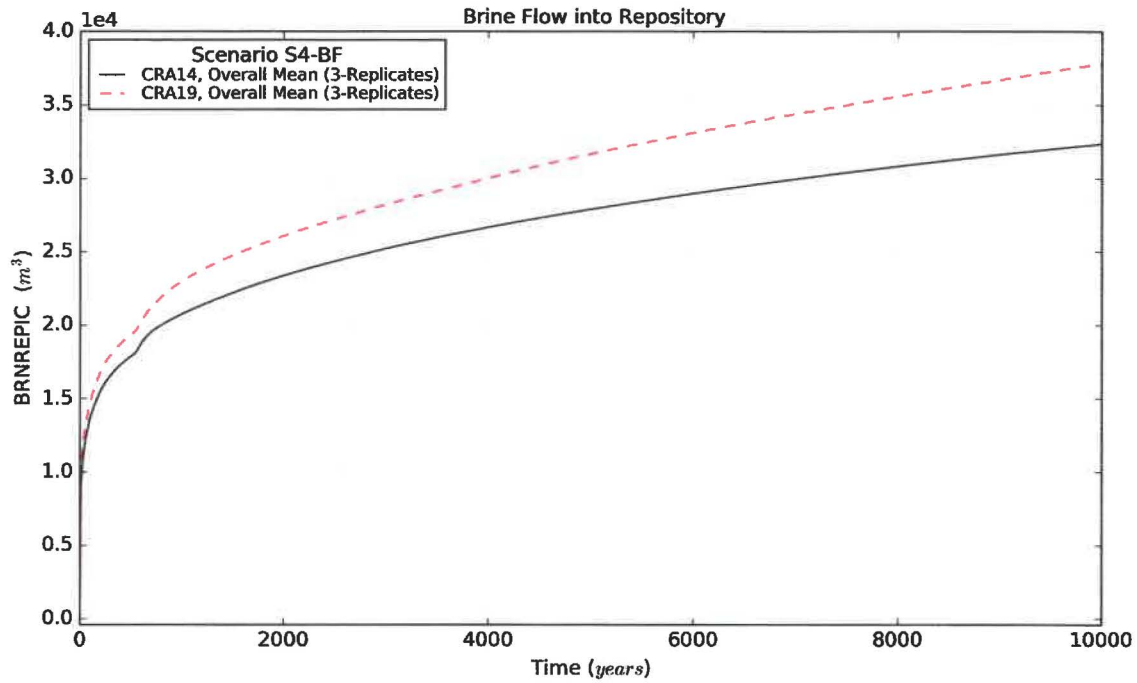


Figure 64 – Brine Flow Means into Repository, Scenario S4-BF

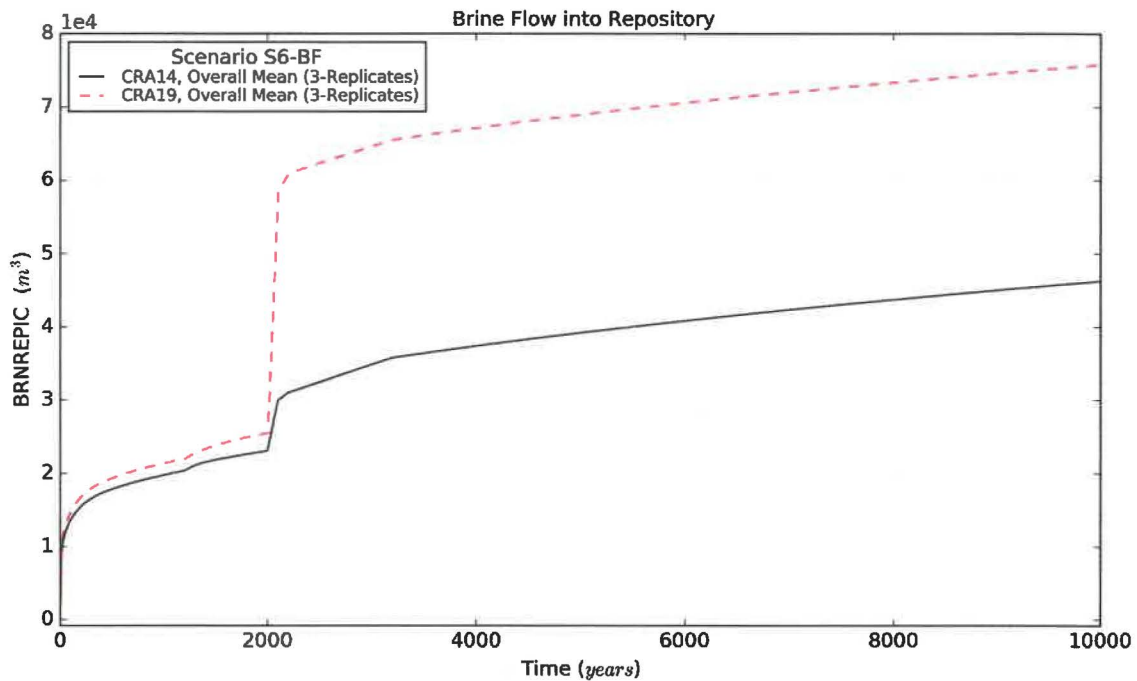


Figure 65 – Brine Flow Means into Repository, Scenario S6-BF

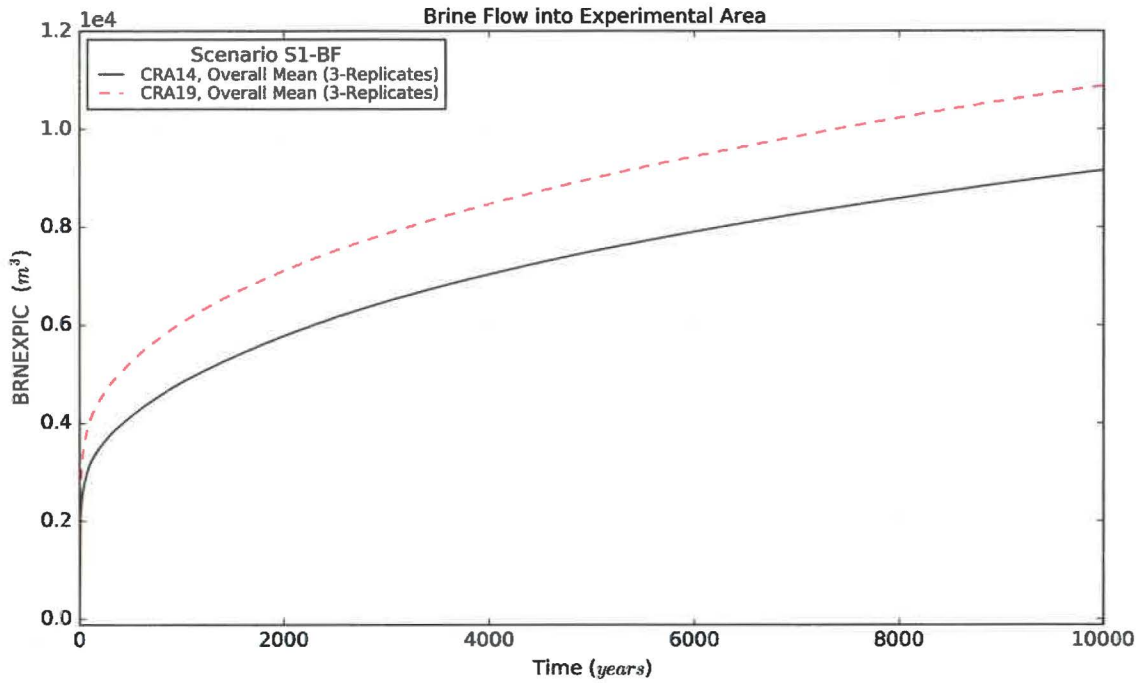


Figure 66 – Brine Flow Means into Experimental Area, Scenario S1-BF

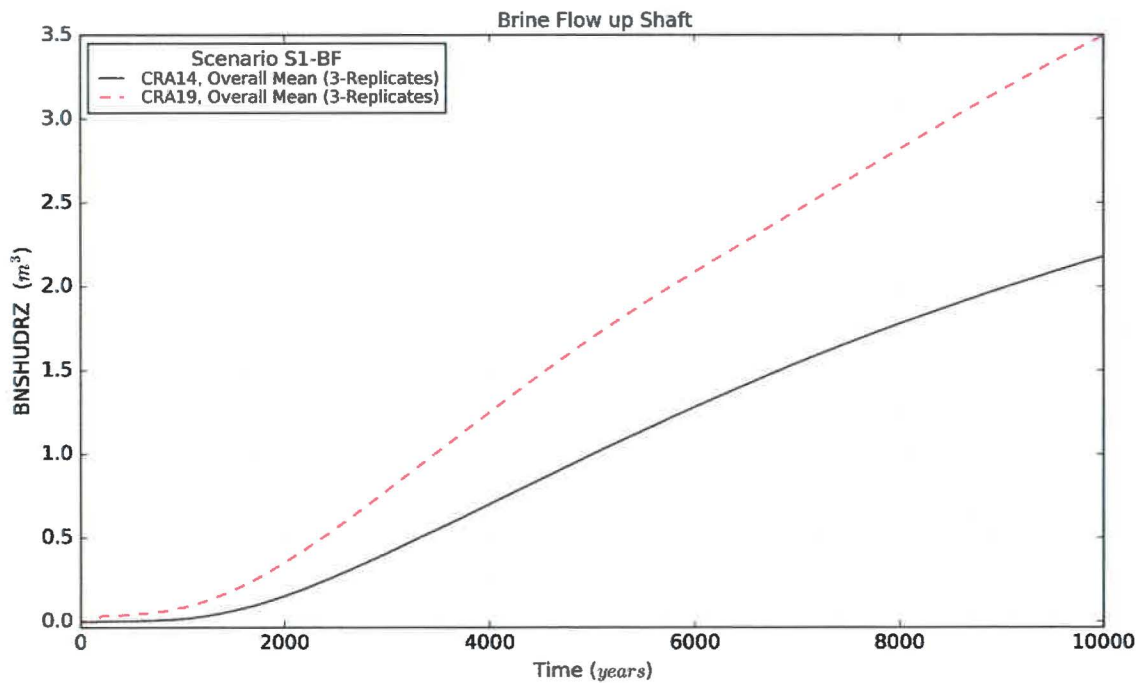


Figure 67 – Brine Flow Means up the Shaft, Scenario S1-BF

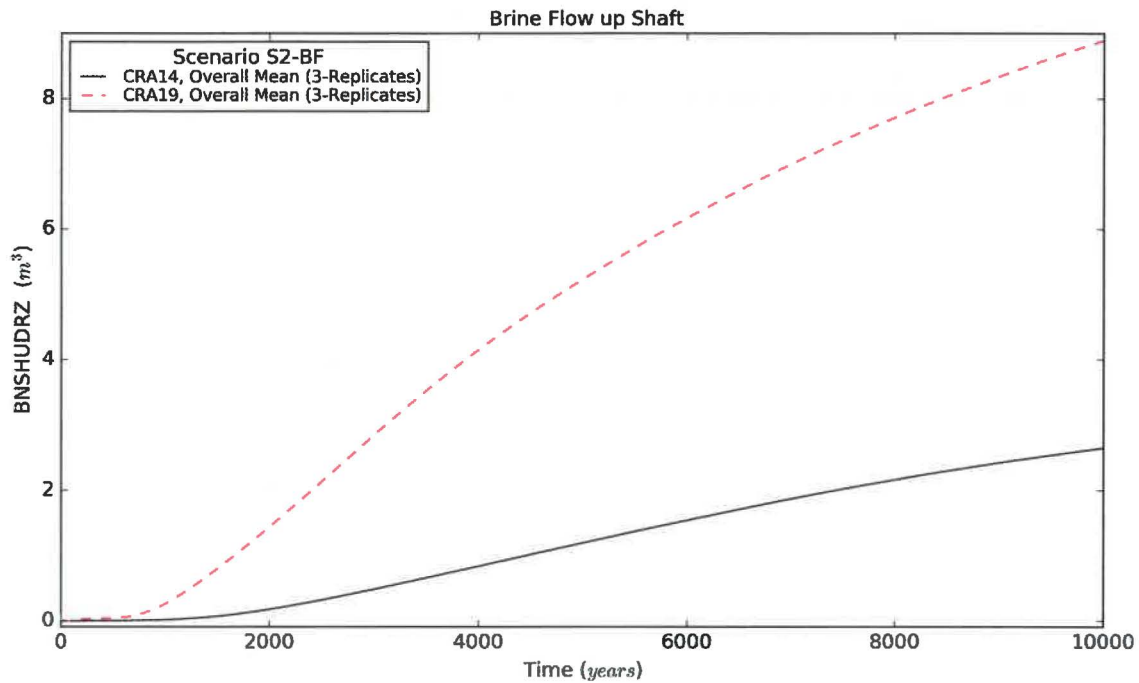


Figure 68 – Brine Flow Means up the Shaft, Scenario S2-BF

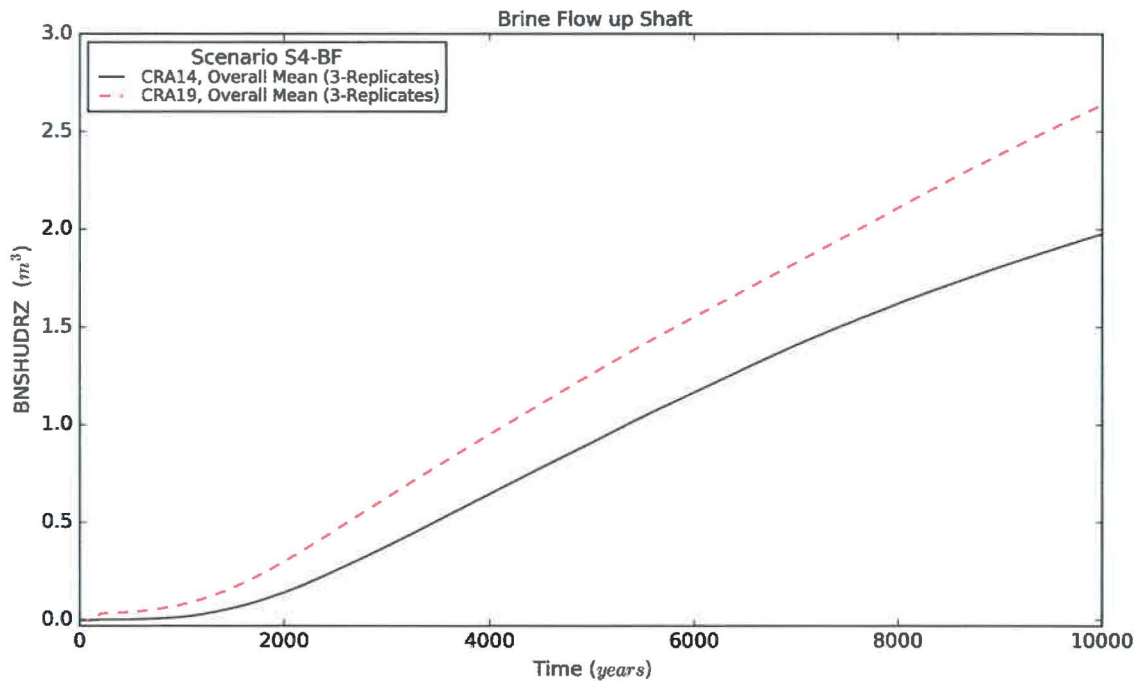


Figure 69 – Brine Flow Means up the Shaft, Scenario S4-BF

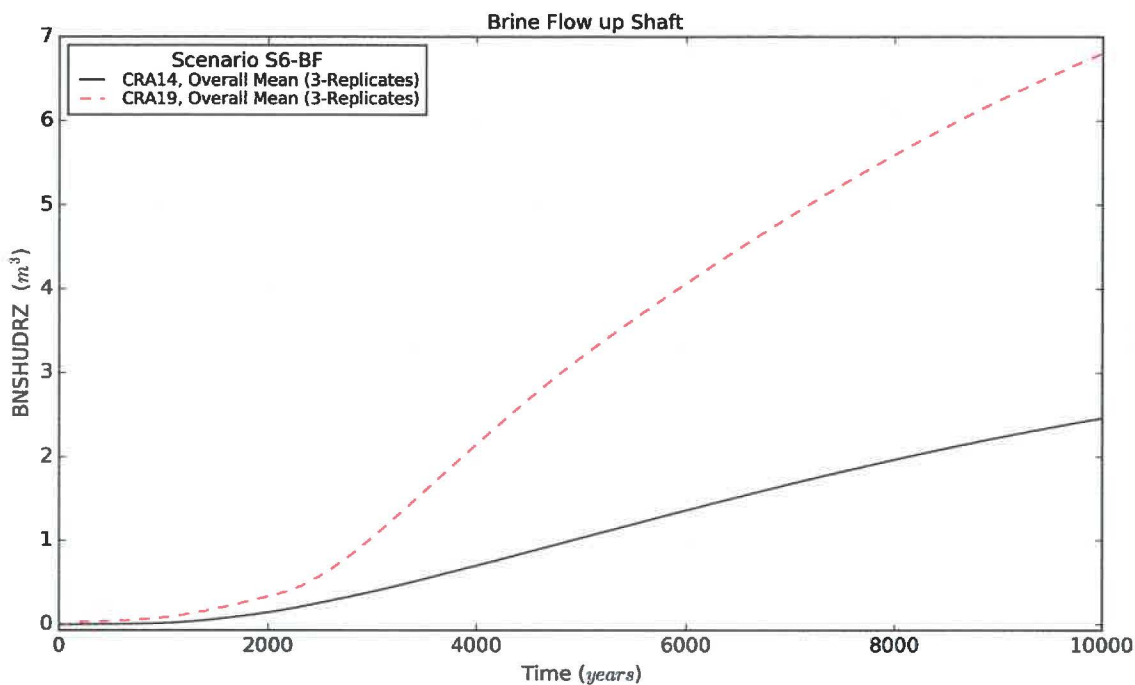


Figure 70 – Brine Flow Means up the Shaft, Scenario S6-BF

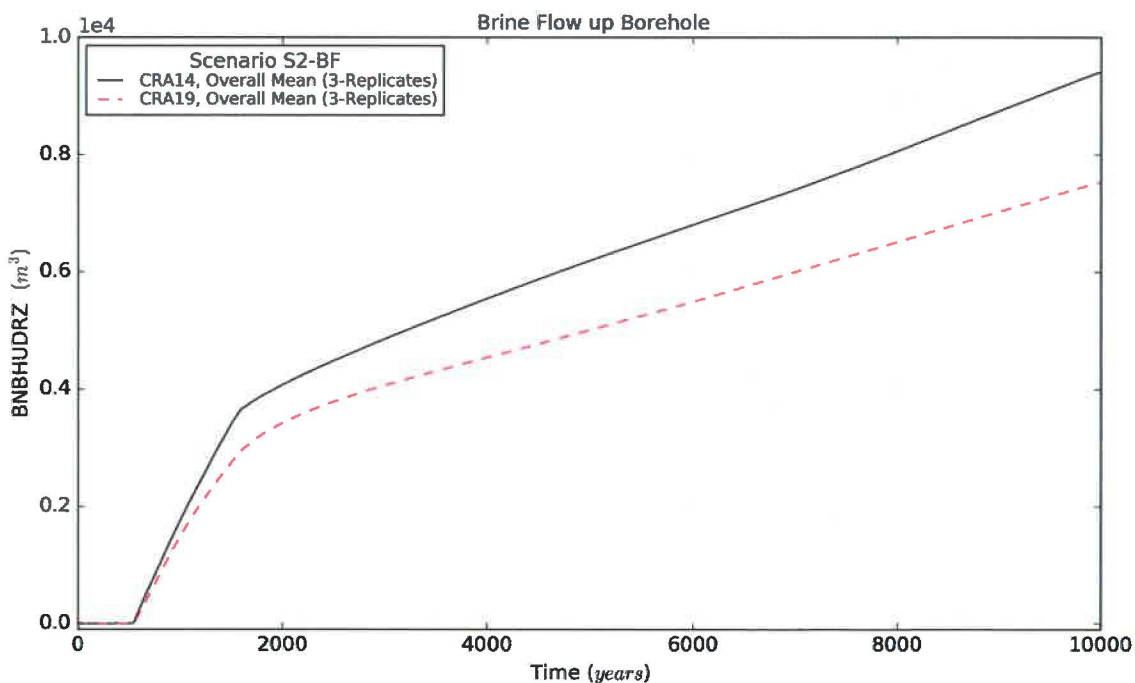


Figure 71 – Brine Flow Means up the Borehole, Scenario S2-BF

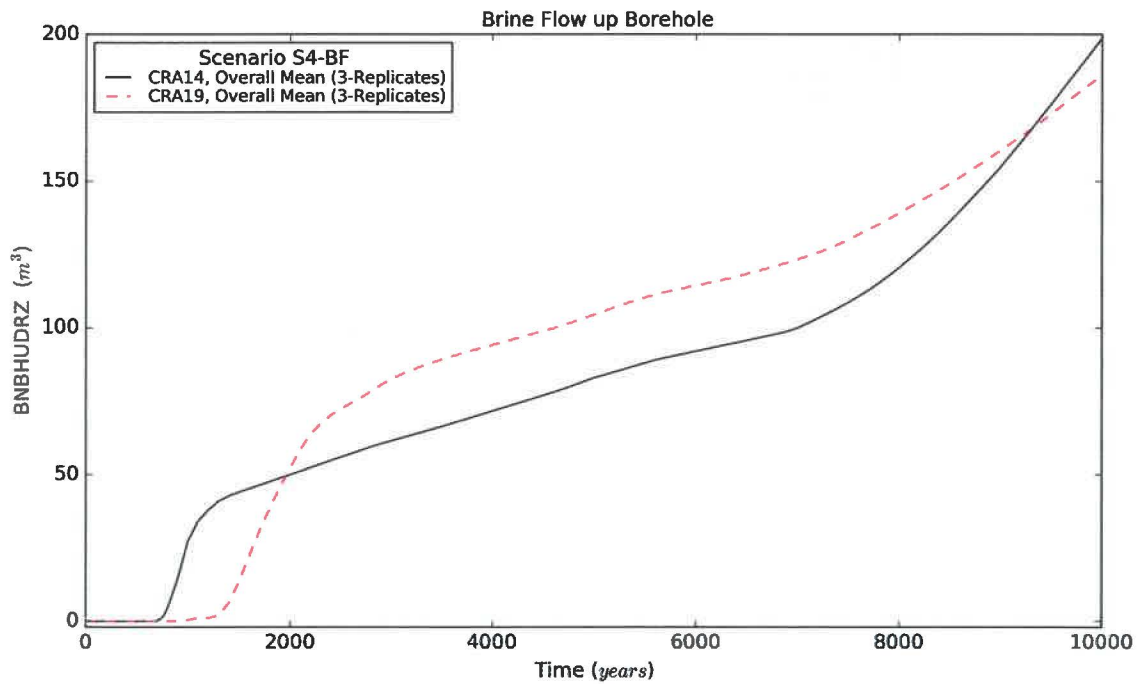


Figure 72 – Brine Flow Means up the Borehole, Scenario S4-BF

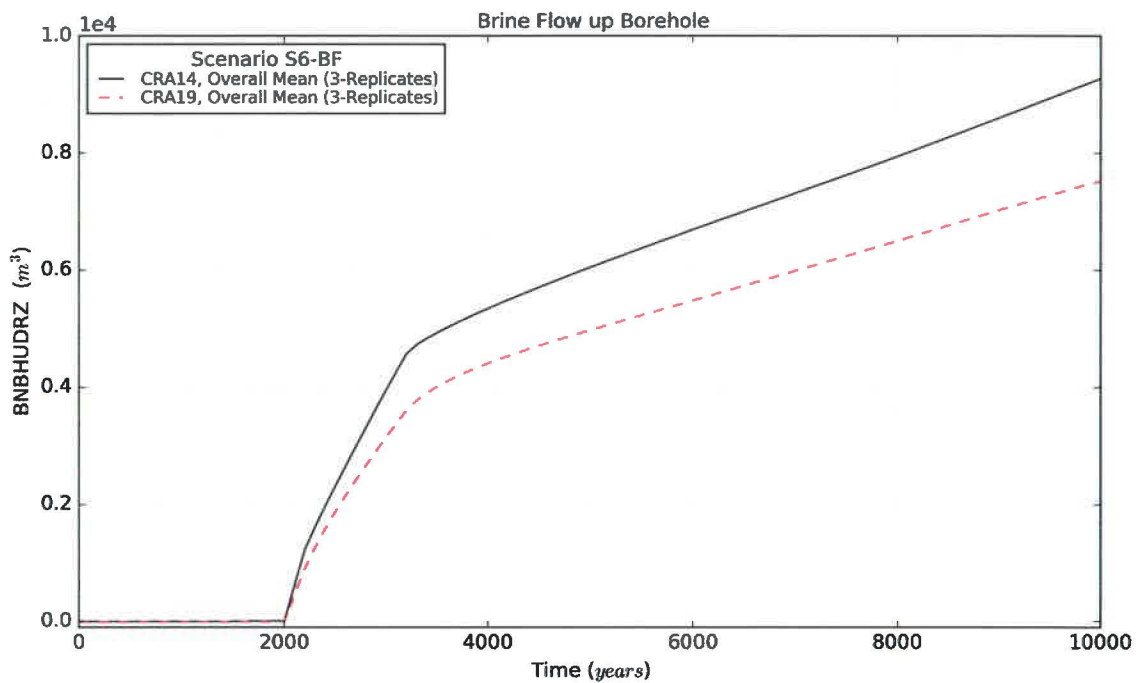


Figure 73 – Brine Flow Means up the Borehole, Scenario S6-BF

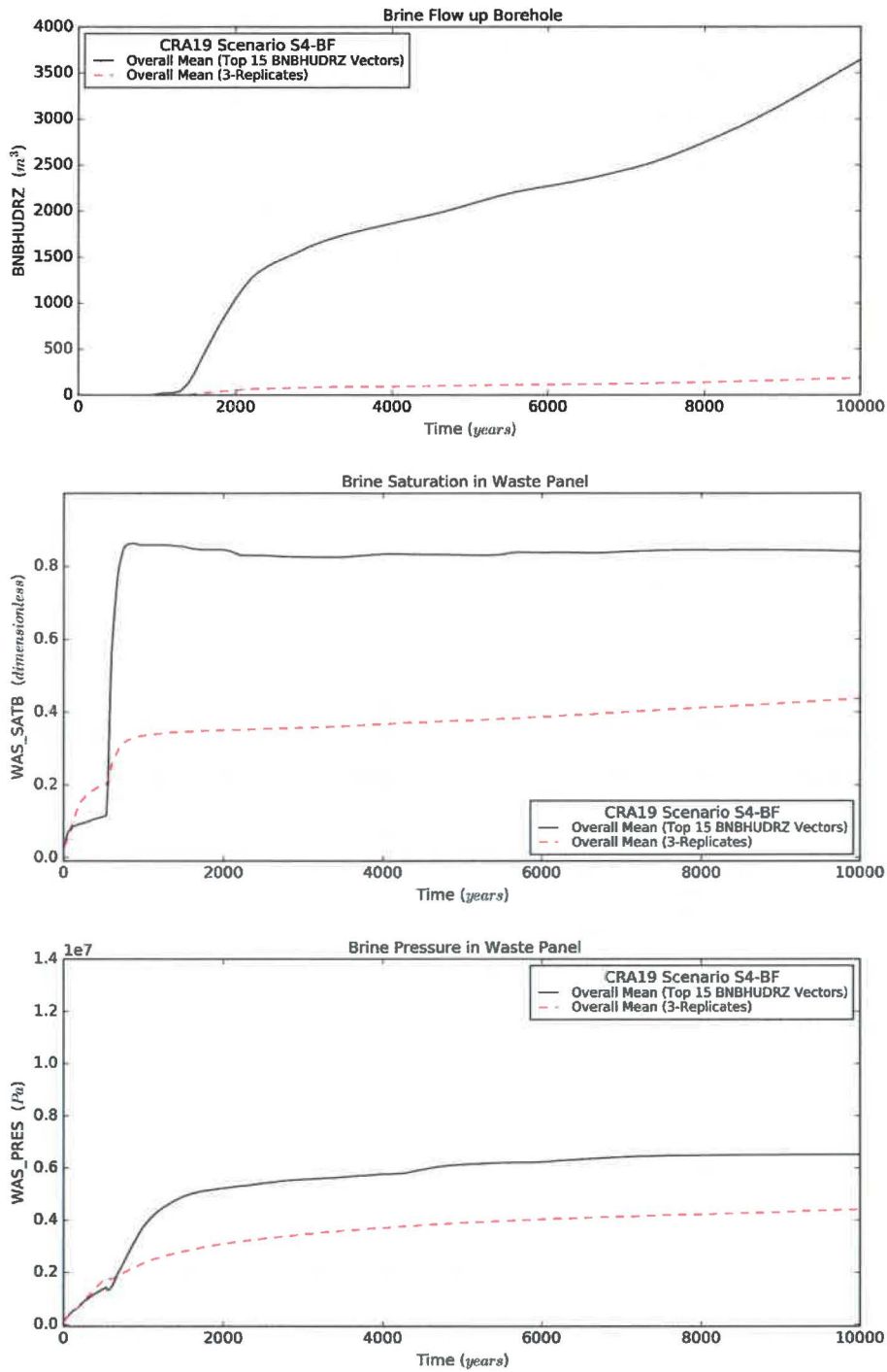


Figure 74 – CRA19 Brine Flow up the Borehole; Comparison of Brine Flow, Waste Panel Brine Saturation, and Pressure Overall Means to Top 15 Borehole Brine Flow Vector Means, Scenario S4-BF

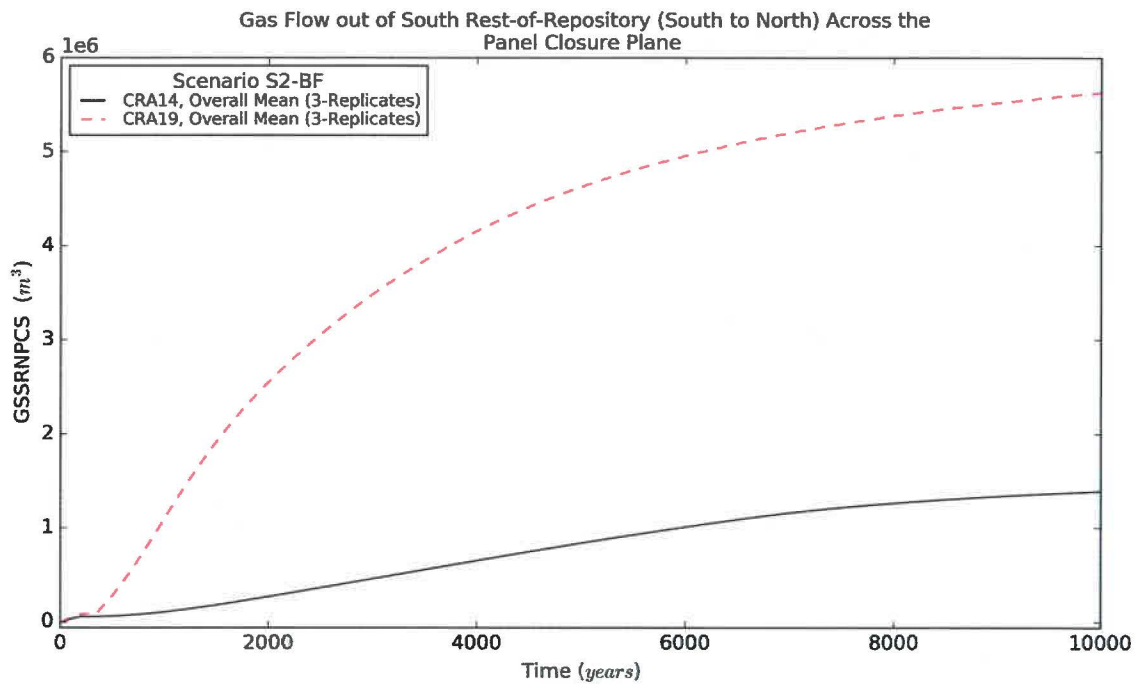


Figure 75 – Gas Flow Means out of South Rest-of-Repository (South to North) Across the Panel Closure Plane, Scenario S2-BF

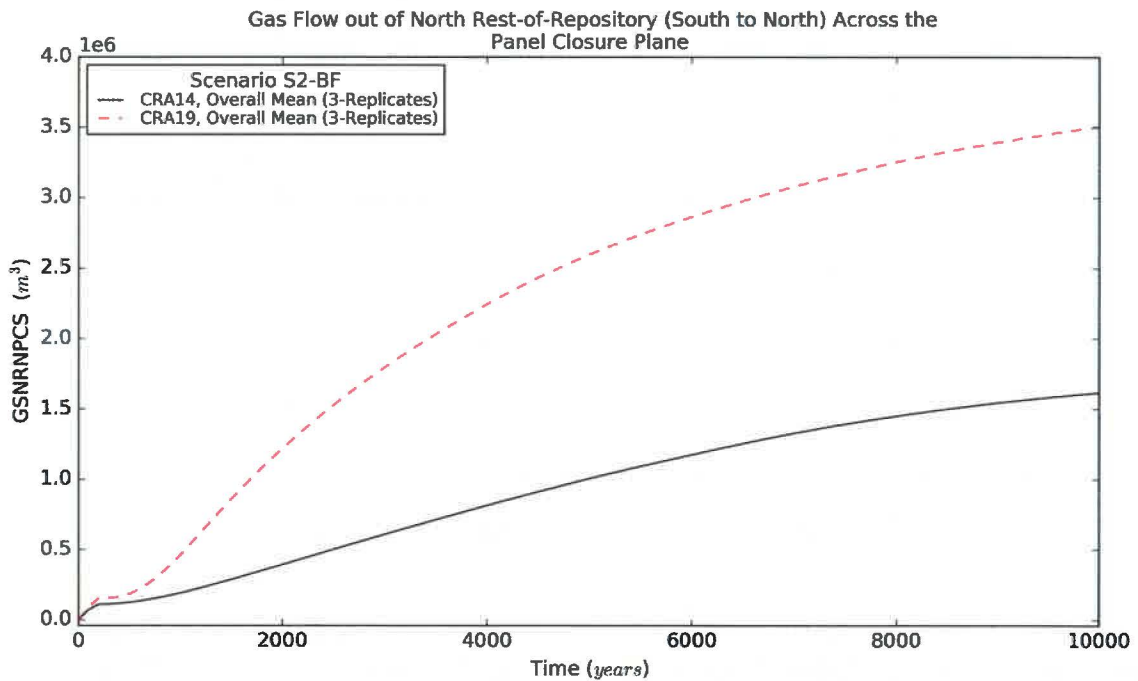


Figure 76 – Gas Flow Means out of North Rest-of-Repository (South to North) Across the Panel Closure Plane, Scenario S2-BF

Table 23 – Brine Flow Statistics on Overall Means for CRA14 and CRA19

Quantity (units)	Description	Scenario	Mean Value ¹		Maximum Value ²	
			CRA14	CRA19	CRA14	CRA19
BRNREPIC (m ³)	Brine Flow into Repository	S1-BF	2.52E+04	2.70E+04	2.98E+04	3.18E+04
		S2-BF	4.31E+04	1.00E+05	5.18E+04	1.12E+05
		S4-BF	2.69E+04	3.06E+04	3.24E+04	3.78E+04
		S6-BF	3.60E+04	6.00E+04	4.63E+04	7.58E+04
BNSHUDRZ (m ³)	Brine Flow up Shaft	S1-BF	9.94E-01	1.64E+00	2.18E+00	3.50E+00
		S2-BF	1.20E+00	4.76E+00	2.65E+00	8.90E+00
		S4-BF	9.07E-01	1.24E+00	1.98E+00	2.64E+00
		S6-BF	1.07E+00	3.09E+00	2.46E+00	6.81E+00
BNBHUDRZ (m ³)	Brine Flow up Borehole	S1-BF	-	-	-	-
		S2-BF	5.80E+03	4.72E+03	9.42E+03	7.54E+03
		S4-BF	8.51E+01	9.60E+01	1.99E+02	1.86E+02
		S6-BF	5.10E+03	4.17E+03	9.28E+03	7.53E+03

Notes:

- 1 Calculated as the function average (integrated) over the time interval (0-10,000 years) for the overall means (3 replicates)
- 2 Calculated as the function maximum over the time interval (0-10,000 years) for the overall means (3 replicates)

Table 24 – Brine Flow Statistics on Individual Vectors for CRA14 and CRA19

Quantity (units)	Description	Scenario	Maximum Value ³	
			CRA14	CRA19
BRNREPIC (m ³)	Brine Flow into Repository	S1-BF	1.39E+05	1.49E+05
		S2-BF	2.15E+05	2.79E+05
		S4-BF	1.39E+05	1.84E+05
		S6-BF	2.12E+05	2.55E+05
BNSHUDRZ (m ³)	Brine Flow up Shaft	S1-BF	2.47E+01	3.56E+01
		S2-BF	2.34E+01	4.31E+01
		S4-BF	2.21E+01	3.48E+01
		S6-BF	2.28E+01	3.80E+01
BNBHUDRZ (m ³)	Brine Flow up Borehole	S1-BF	-	-
		S2-BF	1.74E+05	1.49E+05
		S4-BF	5.53E+03	1.41E+04
		S6-BF	1.75E+05	1.61E+05

Notes:

- 3 Calculated as the function maximum over the time interval (0-10,000 years) for all replicates (300 vectors)

5.0 SUMMARY

Changes incorporated into the CRA-2019 PA include planned changes as well as parameter and implementation changes. Of the changes delineated in Section 1.1 as possibly having in impact on the Salado flow results, the following subset of changes are observed to be associated with the primary differences in the resultant waste area brine pressures and brine saturations or to be associated with processes that influence those results for CRA19 in comparison to CRA14:

- The lack of ROMPCS emplacement between Panels 3, 4, 5, 6, and 9, modeled as the southernmost panel closure area, which allows greater communication between the waste panel and the south rest-of-repository.
- Increase in the inundated steel corrosion rates and the addition of brine radiolysis which results in an increase in hydrogen gas generation.
- Addition of 5th shaft and associated access drift volume in the experimental area which increases the cross-sectional area of the shaft and increases void space in the experimental area.
- Updates to WIPP waste inventory parameters, including increased iron and cellulose mass, which contributes to increased associated corrosion and biodegradation gas generation.

Due to the primary importance with respect to downstream WIPP PA calculations, the resultant impacts and trends for brine pressures and brine saturation within the waste areas of the repository over the representative scenarios are summarized for CRA19 in comparison to CRA14. Additional consideration is given to the primary brine flow away from the repository toward the Culebra through the intrusion borehole.

For undisturbed repository conditions, the CRA19 changes yield an increase in the mean pressure calculated for repository waste areas as compared to the CRA14 over all time with the exception of the waste panel pressure which is increased early and then reduced below CRA14 values at later times. Although the expanded void space in the repository experimental area attenuates waste area pressures, the substantially increased total gas generation within the waste areas overcomes this void space and waste area brine pressures are generally increased for CRA19 in comparison to CRA14. The exception is a slight reduction in brine pressure at later times within the waste panel which is attributed to pressure equilibration through the abandoned southernmost panel closure with the south rest-of-repository. Due to the 1-degree Salado dip, the south rest-of-repository has historically lower pressures because of less gas generation in the presence of lower brine saturation in comparison to the waste panel. The equilibration between the two waste areas across the abandoned panel closure in CRA19 allows higher pressures in the waste panel to be more readily attenuated with northward flows into the south rest-of-repository. The CRA19 increased iron corrosion rates result in faster gas production due to iron corrosion (on average) along with increased cellulose mass that increases early time microbial gas generation. The addition of brine radiolysis in CRA19 not only increases hydrogen gas generation but also increases the consumption of brine to suppress the amount of free water available for gas production by iron corrosion and microbial degradation of cellulose at later

times. Because of increased gas generation and brine consumption within the waste areas, even under the influence of increased cumulative brine flow into the repository, brine saturations within all waste areas are reduced for CRA19 in comparison to CRA14.

For E1 and E2E1 intrusion scenarios, the flow of brine from the hypothetical Castile brine reservoir into the waste panel and into the south rest-of-repository across the abandoned panel closure results in substantially increased brine pressure, brine saturation, and gas generation for CRA19 within the south rest-of-repository. Influenced by the pressure equilibration between the waste panel and south rest-of-repository and associated brine and gas flows across the abandoned panel closure that are induced by the substantial increase in total gas generation in these areas, brine pressures within the waste panel are increased and brine saturation are slightly decreased for CRA19 in comparison to CRA14. Because an emplaced ROMPCS separates the south rest-of-repository from the north rest-of-repository, brine flow to the north is impeded more than gas flow and brine saturations are decreased for CRA19 as a result of enhanced brine consumption within the north rest-of-repository and gas flows from south to north. The increased gas flow from the south to the north and increased gas generation within the north rest-of-repository results in increased brine pressures within this area for CRA19 in comparison to CRA14. Cumulative brine inflows to the waste panel and the south rest-of-repository are substantially greater (on average) in CRA19 as compared to CRA14. This increased mean brine inflow yields a corresponding increase in the total gas generation within the waste areas for CRA19. Cumulative brine flows up the intrusion borehole are modestly increased for CRA19 as a result of the increased pressure and only slightly decreased brine saturation (over time) within the intruded waste panel.

Overall, the primary impacts of changes for CRA19 in comparison to CRA14 are substantially increased brine pressures for E1 and E2E1 intrusion scenarios that are influenced by increased total gas generation due to the availability of brine within the waste panel and south rest-of-repository that flows from the Castile brine reservoir, up the intrusion borehole, to the waste panel, and across the abandoned panel closure area to the south rest-of-repository.

6.0 REFERENCES

- Camphouse, R. 2014. Impact Assessment of an Additional WIPP Shaft Sandia National Laboratories, Carlsbad, NM. ERMS 562973.
- Clayton, D.J., S. Dunagan, J.W. Garner, A.E. Ismail, T.B. Kirchner, G.R. Kirkes, M.B. Nemer. 2008. Summary Report of the 2009 Compliance Recertification Application Performance Assessment. Sandia National Laboratories, Carlsbad, NM. ERMS 548862.
- Clayton, D.J., R.C. Camphouse, J.W. Garner, A.E. Ismail, T.B. Kirchner, K.L. Kuhlman, M.B. Nemer. 2010. Summary Report of the CRA-2009 Performance Assessment Baseline Calculation. Sandia National Laboratories, Carlsbad, NM. ERMS 553039.
- Clayton, D.J. 2013. Justification of Chemistry Parameters for Use in BRAGFLO for AP-164, Rev. 1. Sandia National Laboratories, Carlsbad, NM. ERMS 559466.
- Cotsworth, E. 2005. EPA Letter on Conducting the Performance Assessment Baseline Change (PABC) Verification Test. U.S. EPA, Office of Radiation and Indoor Air, Washington, D.C. ERMS 538858.
- Cotsworth, E. 2009. EPA Letter on CRA-2009 First Set of Completeness Comments. U.S. EPA, Office of Radiation and Indoor Air, Washington, D.C. ERMS 551444.
- Day, B. 2016. Operations and Experimental Area Sensitivity Study. Sandia National Laboratories, Carlsbad, NM. ERMS 565918.
- Day, B. 2018. Impact Analysis for BRAGFLO 6.03 Software Problem Report, SPR 18-002. Sandia National Laboratories. Carlsbad, NM. ERMS 570325.
- Day, B. 2019. Reassessment of Need and Parameter Justification for Modeling Gas Generation due to Radiolysis of Brine and Cellulose/Plastic/Rubber in WIPP for CRA-2019. Sandia National Laboratories, Carlsbad, NM. ERMS 570873.
- Day, B. and T. Zeitler. 2016. Panel Closure System Sensitivity Study. Sandia National Laboratories, Carlsbad, NM. ERMS 566725.
- Kicker, D. and T. Zeitler. 2013. Radionuclide Inventory Screening Analysis Report for the 2014 Compliance Recertification Application Performance Assessment. Sandia National Laboratories, Carlsbad, NM. ERMS 559257.
- Kicker, D. 2019. Radionuclide Inventory Screening Analysis for the 2019 Compliance Recertification Application Performance Assessment (CRA-2019 PA). Sandia National Laboratories, Carlsbad, NM. ERMS 571244.
- Kim, S. and M. Feng. 2019. Input Parameter Report for the 2019 Compliance Recertification Application Performance Assessment (CRA-2019 PA). Sandia National Laboratories, Carlsbad, NM. ERMS 571377.
- Kirchner, T., A. Gilkey, and J. Long. 2014. Summary Report on the Migration of the WIPP PA Codes from VMS to Solaris, AP-162 Revision 1. Sandia National Laboratories, Carlsbad, NM. ERMS 561757.

Analysis Package for Salado Flow in the 2019 Compliance Recertification Application
Performance Assessment (CRA-2019 PA)

Rev. 0, ERMS 571368

Kirchner, T., A. Gilkey, and J. Long. 2015. Addendum to the Summary Report on the Migration of the WIPP PA Codes from VMS to Solaris, AP-162. Sandia National Laboratories, Carlsbad, NM. ERMS 564675.

Leigh, C.D., J.F. Kanney, L.H. Brush, J.W. Garner, G.R. Kirkes, T. Lowry, M.B. Nemer, J.S. Stein, E.D. Vugrin, S. Wagner, and T.B. Kirchner. 2005. 2004 Compliance Recertification Application Performance Assessment Baseline Calculation, Revision 0. Sandia National Laboratories, Carlsbad, NM. ERMS 541521.

Long, J. 2013. Execution of Performance Assessment Codes for the CRA-2014 Performance Assessment. Sandia National Laboratories, Carlsbad, NM. ERMS 560016.

Long, J. 2019. Computational Code Execution and File Management for the 2019 Compliance Recertification Application Performance Assessment (CRA-2019 PA). Sandia National Laboratories, Carlsbad, NM. ERMS 571375.

MacKinnon, R.J., and G. Freeze. 1997a. Summary of EPA-Mandated Performance Assessment Verification Test (Replicate 1) and Comparison With the Compliance Certification Application Calculations, Revision 1. Sandia National Laboratories, Carlsbad, NM. ERMS 422595.

MacKinnon, R.J., and G. Freeze. 1997b. Summary of Uncertainty and Sensitivity Analysis Results for the EPA-Mandated Performance Assessment Verification Test, Rev. 1. Sandia National Laboratories, Carlsbad, NM. ERMS 420669.

MacKinnon, R.J., and G. Freeze. 1997c. Supplemental Summary of EPA-Mandated Performance Assessment Verification Test (All Replicates) and Comparison With the Compliance Certification Application Calculations, Revision 1. Sandia National Laboratories, Carlsbad, NM. ERMS 414880.

Nemer, M. B., J. S. Stein and W. Zelinski. 2005. Analysis Report for BRAGFLO Preliminary Modeling Results With New Gas Generation Rates Based Upon Recent Experimental Results. Sandia National Laboratories, Carlsbad, NM. ERMS 539437.

Reed, D.T., S. Okajima, L.H. Brush, and M.A. Molecke. 1993. Radiolytically Induced Gas Production in Plutonium-Spiked WIPP Brine. Materials Research Society Symposium Proceedings (pp. 431-38). Vol. 294. Warrendale, PA: Materials Research Society.

Roselle, G.T. 2013. Determination of Corrosion Rates from Iron/Lead Corrosion Experiments to be used for Gas Generation Calculations. Sandia National Laboratories, Carlsbad, NM. ERMS 559077.

Peake, T. 2018. Letter from T. Peake, Director of Center for Waste Management and Regulations, Environmental Protection Agency to M. Brown, Director of Office of Environmental Protection Department of the Department of Energy Carlsbad Field Office regarding resolution of outstanding issues for the CRA-2019 Performance Assessment, October 9, 2018. ERMS 570585.

Sandia National Laboratories (SNL). 1996. Summary Memo of Record, DR-3: Dynamic Closure of the North-End and Hallways, Memorandum from P. Vaughn, M. Lord, and R. MacKinnon to D.R. Anderson. ERMS 230794.

Analysis Package for Salado Flow in the 2019 Compliance Recertification Application
Performance Assessment (CRA-2019 PA)
Rev. 0, ERMS 571368

- Sarathi, R. 2019. Analysis Package for Actinide Mobilization and Salado Transport in the 2019 Compliance Recertification Application Performance Assessment (CRA-2019 PA). Sandia National Laboratories, Carlsbad, NM. ERMS 571371.
- U.S. Congress. 1992. WIPP Land Withdrawal Act, Public Law 102-579, 106 Stat. 4777, 1992; as amended by Public Law 104-201, 110 Stat. 2422, 1996.
- U.S. Department of Energy (DOE). 1996. Title 40 CFR Part 191 Compliance Certification Application for the Waste Isolation Pilot. U.S. Department of Energy Waste Isolation Pilot Plant, Carlsbad Area Office, Carlsbad, NM. DOE/CAO-1996-2184.
- U.S. Department of Energy (DOE). 2004. Title 40 CFR Part 191 Compliance Recertification Application for the Waste Isolation Pilot Plant, , 10 vols., U.S. Department of Energy Waste Isolation Pilot Plant, Carlsbad Area Office, Carlsbad, NM. DOE/WIPP 2004-3231.
- U.S. Department of Energy (DOE). 2015. Response to Environmental Protection Agency Letters Dated December 17, 2014 and February 27, 2015 Regarding the 2014 Compliance Recertification Application. U.S. Department of Energy, Waste Isolation Pilot Plant, Carlsbad Field Office. Carlsbad, NM. ERMS 563433.
- U.S. Department of Energy (DOE). 2016. WIPP UPDATE: October 14, 2016, Plans Call for Controlled Withdrawal from South End of Underground.
http://www.wipp.energy.gov/Special/WIPP%20Update%2010_14_16.pdf
- U.S. Department of Energy (DOE). 2017. Sandia Recommendation for Completion of Fully-Qualified RPC2 Calculations. Email from R. Patterson to P. Shoemaker dated February 7, 2017.
- U.S. Environmental Protection Agency (EPA). 1998. 40 CFR 194, Criteria for the Certification and Recertification of the Waste Isolation Pilot Plant's Compliance with the Disposal Regulations: Certification Decision: Final Rule, Federal Register. Vol. 63, 27354-27406.
- U.S. Environmental Protection Agency (EPA). 2006. 40 CFR 194, Criteria for the Certification and Recertification of the Waste Isolation Pilot Plant's Compliance with the Disposal Regulations: Certification Decision: Final Rule, Federal Register. Vol. 71, 18010-18021.
- U.S. Environmental Protection Agency (EPA). 2010. 40 CFR Part 194 Criteria for the Certification and Recertification of the Waste Isolation Pilot Plant's Compliance With the Disposal Regulations: Recertification Decision, Federal Register No. 222, Vol. 75, pp. 70584-70595, November 18, 2010.
- U.S. Environmental Protection Agency (EPA). 2017a. Criteria for the Certification and Recertification of the Waste Isolation Pilot Plant's Compliance with the Disposal Regulations; Recertification Decision. July 19, 2017. Office of Radiation and Indoor Air, Docket EPA-HQ-OAR-2014-0609-0079.
- U.S. Environmental Protection Agency (EPA). 2017b. Technical Support Document for Section 194.24, Evaluation of the Compliance Recertification Actinide Source Term, Gas Generation, Backfill Efficacy, Water Balance and Culebra Dolomite Distribution Coefficient Values. June 2017. Office of Radiation and Indoor Air, Docket EPA-HQ-OAR-2014-0609-0054.
- Van Soest, G.D. 2018. Performance Assessment Inventory Report – 2018. Los Alamos National Laboratory Carlsbad Operations. Carlsbad, NM. LA-UR-18-31882.

- Vaughn, P. 1996. WIPP Parameter Entry Form for SANTAROS: SAT_IBRN. Sandia National Laboratories. Carlsbad, NM. WPO 33552.
- WIPP PA. 2005. User's Manual for LHS Version 2.42 Document Version 2.42. Sandia National Laboratories. Carlsbad, NM. ERMS 538374.
- WIPP PA. 2018a. Requirements Document, Verification and Validation Plan, and Validation Document for BRAGFLO Version 7.00. Sandia National Laboratories. Carlsbad, NM. ERMS 570272.
- WIPP PA. 2018b. Requirements Document, Verification and Validation Plan, and Validation Document for PREBRAG Version 9.00. Sandia National Laboratories. Carlsbad, NM. ERMS 570251.
- Zeitler, T.R. and C. Hansen. 2015a. Cumulative Distribution for STEEL:CORRMCO2. Sandia National Laboratories, Carlsbad, NM. ERMS 565005.
- Zeitler, T.R. and C. Hansen. 2015b. Cumulative Distribution for STEEL:HUMCORR. Sandia National Laboratories, Carlsbad, NM. ERMS 565009.
- Zeitler, T.R. and C. Hansen. 2015c. Updated Calculation of the Cumulative Distribution for STEEL:HUMCORR. Sandia National Laboratories, Carlsbad, NM. ERMS 565108
- Zeitler, T.R. 2015d. Memo to Records: BRAGFLO calculations for updated northern-most ROMPCS representation. Sandia National Laboratories, Carlsbad, NM. ERMS 563875.
- Zeitler, T.R. and B. Day. 2016. CRA14_SEN4 Sensitivity Study, Rev. 1. Sandia National Laboratories. Carlsbad, NM. ERMS 567505.
- Zeitler, T.R., B. Day, J. Bethune, R. Sarathi, J. Long. 2017. Assessment of Abandoned Panel Closures in South End of Repository and Lack of Waste Emplacement in Panel 9. Sandia National Laboratories. Carlsbad, NM. ERMS 568459.
- Zeitler, T.R. 2018a. Cumulative Distribution for STEEL:CORRMCO2 for the CRA-2019 PA. Sandia National Laboratories. Carlsbad, NM. ERMS 570869.
- Zeitler, T.R. 2018b. Bounding Calculation of the Cumulative Distribution for STEEL:HUMCORR. Sandia National Laboratories. Carlsbad, NM. ERMS 569807.
- Zeitler, T.R. 2019a. Analysis Plan for the 2019 WIPP Compliance Recertification Application Performance Assessment. Sandia National Laboratories, Carlsbad, NM. ERMS 571150.
- Zeitler, T.R. 2019b. Calculation of Shaft and Experimental Area Dimensions for Use in the CRA-2019 PA. Sandia National Laboratories. Carlsbad, NM. ERMS 571045.
- Zeitler, T.R. 2019c. A Summary of EPA/DOE Defined Parameters to be Implemented in the CRA-2019 PA. Sandia National Laboratories. Carlsbad, NM. ERMS 570879.